



Unione Europea



La tua
Campania
cresce in
Europa



DI
C
Ma
PI

Dipartimento
di Ingegneria Chimica,
dei Materiali e della
Produzione Industriale
Università degli Studi
di Napoli Federico II



ISTITUTO ITALIANO DI TECNOLOGIA
CENTER FOR ADVANCED BIOMATERIALS FOR HEALTHCARE

Ph.D course in

Industrial Product and Process Engineering

Ph.D thesis – XXX Cycle

Entrapping Contrast Agent in Nanovesicles

Coordinator:

Prof. Giuseppe Mensitieri

Candidate

Franca De Sarno

Supervisors:

Prof. Paolo Antonio Netti

Eng. Enza Torino Ph.D.

TABLE OF CONTENT

<i>Abbreviations</i>	<i>i</i>
<i>Thesis abstract</i>	<i>iv</i>
<i>Intoduction</i>	<i>1</i>
1. <i>Diagnostic imaging in clinical practice</i>	2
1.1 <i>Magnetic Resonance Imaging (MRI)</i>	3
1.2 <i>Computed Tomography (CT)</i>	3
1.3 <i>Positron Emission Tomography (PET)</i>	4
1.4 <i>Single Photon Emission Computed Tomography (SPECT)</i>	4
2. <i>Imaging and future trends</i>	5
3. <i>MRI and Contrast Agents</i>	6
4. <i>Next generation of CAs</i>	8
4.1 <i>Nanomedicine and nanocarriers for diagnostic applications</i>	9
4.2 <i>Polymer Nanoparticles</i>	10
4.3 <i>Block Copolymers</i>	15
5. <i>Liposomes</i>	21
6. <i>Aim of work</i>	27
Chapter I - Impact of water dynamics on relaxometric properties of Gd- DTPA	29
1. <i>Introduction</i>	30
2. <i>Experimental Section</i>	32
2.1 <i>Materials</i>	32
2.2 <i>Isothermal Titration Calorimetry</i>	33
2.3 <i>NMR</i>	33

2.4	<i>Differential Scanning Calorimetry</i>	34
2.5	<i>Time-Domain Relaxometry</i>	34
3.	<i>Results and Discussion</i>	35
3.1	<i>Diffusive mixing time in Hydrodynamic Flow Focusing approach</i> ...	35
3.2	<i>NMR study of DTPA interactions and water mobility in polymer solution</i>	39
3.3	<i>Water dynamics within hydrated polymer matrix containing Gd-DTPA</i>	43
3.4	<i>Relaxation times, rates and relaxivity of the polymer matrix</i>	45
4.	<i>Theory of the gadolinium mesh formation</i>	48
5.	<i>Conclusion</i>	50
CHAPTER II - Hyaluronic Acid Nanoparticles: water-mediated nanostructures for enhanced MRI		52
1.	<i>Introduction</i>	53
2.	<i>Experimental Section</i>	57
2.1	<i>Materials</i>	57
2.2	<i>Emulsion preparation</i>	57
2.3	<i>Temporal emulsion stability determination</i>	58
2.4	<i>Preparation of DVS-crosslinked nanoparticles</i>	58
2.5	<i>Loading of HA NPS with Contrast agents</i>	60
2.6	<i>Collection of the nanoparticles</i>	60
2.7	<i>Characterization of the nanoparticles</i>	60
2.8	<i>Determination of Gadolinium loading by ICP-MS</i>	61
2.9	<i>MRI Testing</i>	61
2.10	<i>NMR dispersion measurements</i>	61
2.11	<i>In vivo tests and cytotoxicity evaluation of HA-based Nanoparticles</i>	61

3. Results and Discussion.....	63
3.1 Case study: production of polymer particles based on Hydrodentcity.....	63
3.2 Study of emulsion stability.....	64
3.3 Preparation of DVS-crosslinked nanoparticles with and without CA.....	66
3.4 Purification and characterization of HA-NPs.....	68
3.5 Relaxivity studies.....	70
3.6 Modeling of NMR dispersion: NMRD profile.....	72
3.7 In vivo analysis and cytotoxicity evaluation of HA NPs.....	74
4. Conclusion.....	78
CHAPTER III - Functionalized HA NPs: the case study of a B-cell lymphoma.....	79
1. Introduction.....	80
2. Experimental Section.....	82
2.1 Materials.....	82
2.2 Functionalization of HA NPs.....	83
2.2.1 Quantification of carboxyl groups on the surface of crosslinked HA NPs.....	83
2.2.2 Direct conjugation of HA NPs.....	84
2.2.3 Indirect conjugation streptavidin-biotin-peptide.....	84
2.2.4 Bicinchoninic Acid Assay.....	84
2.2.5 Cell Lines.....	85
2.2.6 PEGylation.....	85
3. Results and Discussion.....	86
3.1 Functionalization of HA NPs.....	86
3.1.1 Quantification of carboxyl groups on the surface of crosslinked HA NPs.....	86

3.1.2 Direct conjugation with peptide pA20-36 and pA20-S.....	87
3.1.3 Indirect conjugation with peptide pA20-36.....	87
3.1.4 PEGylation.....	89
4. Conclusion.....	93
CHAPTER IV - Emerging use of nanoparticles in diagnosis of atherosclerosis disease.....	94
1. Introduction.....	95
2. Advances in targeting strategies for nanoparticles in atherosclerosis imaging.....	96
2.1 Superparamagnetic Iron Oxide Nanoparticles (SPIONs).....	97
2.2 Polymeric Nanoparticles.....	100
2.3 Micelles.....	101
2.4 Liposomes.....	102
2.5 Dendrimers.....	103
3. Conclusion.....	104
CHAPTER V - Application of HA NPs in atherosclerosis field: preliminary results.....	106
1. Introduction.....	107
2. Experimental design.....	108
3. Experimental section.....	113
3.1 Materials Superparamagnetic Iron Oxide Nanoparticles (SPIONs).....	113
3.2 Electron Microscopy analysis.....	113
3.3 Nanoparticles investigation.....	114
4. Results and discussion.....	114
5. Conclusion.....	119
Main conclusions and future perspectives.....	120
References.....	123

<i>Publications along three years</i>	141
<i>Communications to Congress/Conferences</i>	143
<i>Project Activities</i>	144
<i>Collaborations</i>	144
<i>Other Activities</i>	144

Abbreviations

CA: contrast agent;

cHANPs: crosslinked hyaluronic acid nanoparticles;

DOSY: diffusion-ordered nmr spectroscopy;

DSC: differential scanning calorimetry;

DVS: divinyl sulphone;

EE: encapsulation efficacy;

EMA: european medicines agency;

FDA: food and drug administration;

Gd: gadolinium;

Gd-DTPA: diethylenetriaminepentaacetic acid gadolinium(iii) dihydrogen salt hydrate;

HA: hyaluronic acid;

HA NPs: hyaluronic acid nanoparticles;

HLB: hydrophilic-lipophilic balance;

HyCoS: hybrid core-shell;

ICP-MS: inductively coupled plasma mass spectrometry;

IR: inversion recovery;

ITC: isothermal titration calorimetry;

LC: loading capability;

MLS: multiple light scattering;

MRI: magnetic resonance imaging;

NaOH: sodium hydroxyde pellets;

NMR: nuclear magnetic resonance;

NMRD: nuclear magnetic relaxation dispersion;

NPs: nanoparticles;

NSF: nephrogenic systemic fibrosis;

P_C: continuous phase;

P_D: dispersed phase;

PET: positron emission tomography;

S80: sorbitan monooleate (span® 80);

SBM: solomon-bloembergen-morgan;

SEM: scanning electron microscopy;

SR: saturation recovery;

T85: polyoxyethylenesorbitan trioleate (tween® 85);

TEM: transmission electron microscopy;

W/O: water in oil.

Thesis Abstract

Cancer and cardiovascular diseases are silent killers which cause million deaths worldwide every year and this number is expected to triple by 2035.

Current diagnostic techniques cannot easily, safely, and effectively detect these human body lesions in the early stage, nor can they characterize the lesion features.

In this context, the biological application of nanoparticles is a rapidly developing area of nanotechnology that raises new possibilities in the diagnosis and treatment of pathologies. Recently, rational design of a new class of contrast agents (CAs), based on biopolymers (hydrogels), have received considerable attention in Magnetic Resonance Imaging (MRI) diagnostic field. Several strategies have been adopted to improve relaxivity without chemical modification of the commercial CAs, however, understanding the MRI enhancement mechanism remains a challenge. Here, in order to develop a safe and more efficient MRI CA for imaging applications, the basic principles ruling biopolymer-CAs interactions are investigated to better understand their influence on the relaxometric properties of the CA by adopting a multidisciplinary experimental approach. In addition, the effect of the hydration of the hydrogel structure on the relaxometric properties, called Hydrodentivity, is used to develop Gadolinium-based polymer nanovectors with improved MRI relaxation time. The experimental results indicate that the

entrapment of metal chelates in hydrogel nanostructures offers a versatile platform for developing different high performing CAs for diseases diagnosis.

Introduction

1. Diagnostic imaging in clinical practice

Historically, our understanding of the different pathologies has been mainly based on postmortem examinations of human body or analysis of resected surgical specimens from patients. In recent years, there have been many advances in the pathogenesis and diagnosis of diseases and nowadays, imaging technology allows to look directly inside the human body¹.

Imaging science is a dynamic field and, for more than 50 years, the purpose of scientists is to provide a non-invasively approach to visualize anatomical details using different energy forms. Initially, imaging innovation was primarily driven by technical advances in order to improve image quality and have led to greater use imaging as an important tool at all stages of the pathological process, from prevention to post-treatment follow-up. In current clinical practice, in fact, several imaging modalities, invasive and noninvasive, are available to provide structural and functional information to clinicians about tissue and organ physiology. Of these, only Computed Tomography (CT), Magnetic Resonance Imaging (MRI), Single-photon Emission Computed Tomography (SPECT) and Positron Emission Tomography (PET) are capable of providing 3D data of pathologies anywhere in the human body². Undoubtedly, available structural and functional imaging techniques have improved diagnostic accuracy, but the choice and applicability of each imaging technique depend not only on its diagnostic efficacy, but also on the type of questions being asked. In addition, these diagnostic modalities do not inform clearly on the cellular and molecular processes that drive the development of specific pathologies and each of the imaging techniques has advantages and limitations in terms of radiation exposure, reproducibility, sensitivity, resolution and costs.

The main benefits, limitations and risks associated with four different types of imaging techniques are reported below.

1.1 Magnetic Resonance Imaging (MRI)

MRI is a non-invasive imaging modality that able to acquire 3D tomographical information at high spatial and temporal resolution in whole tissue samples (i.e. human soft tissues, animals). In contrast to the other medical imaging methods, which expose patients to ionizing radiation, MRI uses strong non-ionizing electromagnetic fields in the radio frequency range, offers an excellent spatial resolution, is operator independent and provides 3D data^{3,4}. It is mainly used for analysis of heart, brain, and nervous system. Owing to its higher intrinsic soft-tissue contrast, MRI has distinct advantages for the detection of distant metastases, especially in the skeleton, the brain, soft tissues, and the liver. Compared to other imaging techniques (i.e., nuclear medicine techniques), it shows low sensitivity and long acquisition time. Moreover, MRI's susceptibility to artifacts of motion and organ pulsation means that it has certain limitations for the detection of specific pathologies.

During MRI scans, it is often required the use of contrast media, also called contrast agents (CAs), chemical substances injected into the body, in order to improve the quality of the MRI analysis and obtain more accurately report on abnormality present.

1.2 Computed Tomography (CT)

This diagnostic technique uses X-ray to provide cross-sectional, 3D images of internal organs, bone, soft tissue and blood vessels. It provides a high temporal and spatial resolution and allows to view anatomical details and identify a wide range of disorders including carcinomas (lung, liver, kidney, and pancreas), vascular disease, pulmonary embolism, skeletal abnormalities, and children-specific conditions, such as congenital malformations (heart, kidneys and blood vessels)^{5,6}. CT scan can also have a role in the determination of surgeries and it can be performed with or without administration

of contrast agents (CAs). Currently, the technical limits of CT is represented by poor soft tissue contrast. In addition, unlike MRI, CT exposes patients to high radiation dose

and the iodinated CAs utilized for enhancing a specific part of an organ. The radiation dose depends on multiple factors (i.e. volume scanned, patient build, scanning time and desired resolution)⁵ and creates ions and hydroxyl radicals in the body that interact with DNA critically damaging chromosomes. Furthermore, the intravascular administration of these agents involves allergic or toxic reactions for patients⁷.

1.3 Positron Emission Tomography (PET)

Unlike CT or MRI, which show anatomic detail, Positron Emission Tomography (PET) is a nuclear imaging technique and provides quantitative in vivo assessment of physiological and biological phenomena. This modality necessitates the injection of a small quantity of radioisotopes used as tracers⁸. PET agents provide a better functional assessment of diseases than tracers used in current nuclear imaging modalities and one of the most used PET agents, for understanding the pathological stages of vascular lesion in vivo, is 2-deoxy-2-¹⁸F-fluoro-D-glucose (¹⁸F-FDG), a synthetic molecule that competes with glucose for uptake into metabolically active cells (ie. inflammatory cells), but is not metabolized⁹. The advantage of PET over other imaging modalities, such as SPECT (Single Photon Emission Computed Tomography), is represented by high spatial resolution and contrast resolution and superior sensitivity that allow detection of picomolar tracer concentrations in the arteries¹⁰. Unfortunately, limited spatial resolution (~ 2 mm) means that images must be coregistered with CT or MRI for precise anatomical localization of ¹⁸F-FDG uptake.

1.4 Single Photon Emission Computed Tomography (SPECT)

Single Photon Emission Computed Tomography (SPECT) is a non-invasive nuclear imaging technique that provides tomographic images of the distribution of intravenous

radiolabeled molecules (radioactive tracers) to detect and track overtime molecular changes in the central nervous, cardiovascular, respiratory, and skeletal systems with a high degree of confidence¹¹.

The radiotracers used in SPECT applications have long half-lives (from a few hours to a few days) and emit gamma rays. On the basis of specific application being investigated, different type of radiotracers can be used: Technetium-99m (^{99m}Tc, T1/2 = 6.0 h), Indium-111 (¹¹¹In, T1/2 = 67.3 h), Iodine-123 (¹²³I, T1/2=13.3 h) and Thallium-201(²⁰¹Tl, T1/2 = 72.9 h)¹².

Unlike PET, SPECT does not require higher infrastructure cost, but PET scans offer a higher spatial resolution and accuracy than SPECT scans (spatial resolution: 10 mm). Despite these limitations, SPECT represents the modality of choice in cardiac field.

1.5 Imaging and future trends

The significant improvements in image quality and speed have evolved directly from technological advances in the design and construction of new and more efficient machines for diagnosis, but spatial resolution represents the main limitation for almost of imaging modalities, while sensitivity is limited by radiation dose or other safety considerations.

Nowadays, imaging focus has been moved to contrast agents/probes/biomarkers that target specific biological processes. Continuing developments in molecular biology and nanotechnology, however, have expanded the area of imaging applications with the aim of providing a diagnose diseases earlier (before symptoms are obvious in preclinical stages) and more precisely. Moreover, additional structural and functional information to clinicians about the site of interest allow delivering the right treatment to the patient at the right time.

In this context, MRI technology plays a key role and represents the unique technique for molecular imaging applications that combines excellent soft tissue discrimination, high spatial resolution, outstanding signal to noise ratio and short imaging times

without the use of ionizing radiation. Nevertheless, this imaging modality is limited by its low sensitivity and requires the use of CAs to display clearly the site of interest.

Next sections highlight the latest knowledge about the role of CAs in MRI applications and future research directions based on nanotechnology approaches in diseases diagnosis.

2. MRI and Contrast Agents

In order to improve the sensitivity of MRI by increasing the contrast of the target from the background, intravenous administration of diagnostic pharmaceutical compounds, as known as contrast agents (CAs), is often required during MRI scans. MRI CA are generally categorized as T1 (longitudinal relaxation time) and T2 (transverse relaxation time) CA based on their magnetic properties and relaxation mechanisms. Gadolinium (Gd^{3+}) chelates are effective for increasing T1 relaxation rate ($1/T1$) and commonly used as T1 CA, generating a positive image contrast. Superparamagnetic iron oxide nanoparticles (SPIONs) are more effective for increasing T2 relaxation rate ($1/T2$) and commonly used as T2 CA, producing negative image contrast. To date, the majority of MRI CA used in clinical practice are Gd^{3+} chelates, with over 10 million contrast-enhanced MRI scans on an annual basis, because of their high paramagnetism, favorable properties in term of relaxation enhancement, relatively high stability, and inertness in the body¹³. They include non-specific extracellular CAs and organ-specific CAs, mostly liver-specific CAs. Gadolinium chelates are the most widely used extracellular as non-specific contrast agents¹⁴.

Gd is a powerful paramagnetic ion with seven unpaired electrons and influences the relaxation of nearby water protons. Free ion Gd^{3+} is acutely toxic in vivo owing to its tendency to precipitate and be deposited in tissues (primarily in the liver), which prolongs its half-life¹⁵⁻¹⁷; the binding to a chelate complex makes the ion chemically inert. After chelation, the rate of renal excretion of the Gd complex is increased several times compared with free Gd^{18} . These agents differ in a number of properties (magnetic properties and biodistribution), some of which may significantly impact

their clinical utility, particularly for specific applications¹⁹. In addition, they can be classified into four main categories according to their biochemical structure (macrocyclic or linear) and to their charge (ionic or non-ionic)²⁰. Despite differences among the chelating molecules, they appear to have remarkably similar diagnostic efficacies and safety profiles¹⁴.

Currently, seven Gadolinium based contrast agents (GBCAs) are approved for clinical use in the international market by the U.S. Food and Drug Administration (FDA): gadopentetate dimeglumine (gadolinium diethylene triamine pentaacetic acid (Gd-DTPA), Magnevist®; gadodiamide (gadolinium diethylene triamine penta-acetic acid bis-methylamide (GD-DTPA-BMA), OmniScan®; Gadoteridol (Gadolinium-1,4,7- tris (carboxymethyl)-10-(2' hydroxypropyl)-1, 4, 7 -10-tetraazacyclododecane (Gd-HPD03A)), ProHance®; gadoterate meglumine (gadolinium-tetraazacyclododecane tetra acetic acid (Gd-DOTA), Dotarem®; gadobenate dimeglumine, gadoversetamide, (OptiMARK, Covidien, Dublin, Ireland); gadobutrol²¹.

They work by altering the intrinsic longitudinal (T1) relaxation times of the water protons in the various soft tissues where the agents distribute²². These agents are characterized by the relaxivity (r_1 , for T1 contrast agents) which is defined as the change in relaxation rate ($R_1 = 1/T_1$ in units of s^{-1}) of solvent water protons upon addition of CA, normalized to the concentration of contrast agent ($[CA]$ in units of mM)²³. This effect includes inner-sphere (from water molecules directly coordinated to the Gd) and outer-sphere contributions (from nearby, H-bonded waters) and it is described by the Solomon-Bloembergen-Morgan (SBM)²⁴ equation. Thus, high relaxivity of a CA is critical for effective contrast-enhanced MRI and it is not a constant, but depends on various parameters such as applied field, temperature, the hydration state of the molecule and the molecular size.

Current MRI agents require injection of gram quantities of Gd in order to obtain satisfactory contrast in the resulting image. For clinical use, the recommended dose for GBCAs is typically 0.1–0.3 mmol/kg¹⁴. Potential advantages of using Gd chelates at higher doses include better lesion enhancement, delineation and detectability of cancer pathology. With such large doses required for reasonable image enhancement, current

contrast agents are limited to targeting sites where they can be expected to accumulate in high concentrations, such as in the bloodstream. In addition, their effectiveness remains limited owing to nephrotoxic effects, lack of tissue specificity, low relaxivity and short circulation half-lives. These agents have historically been considered safe, well tolerated when used at recommended dosing levels and linked to the occurrence of nephrogenic systemic fibrosis (NSF) in renal impaired patients²⁵⁻²⁷, but, recently, McDonald and coworkers have reported results about progressive Gd deposition in the brain, bone and kidneys after repeated intravenous administration of CAs^{28, 29}. As a result, the Food and Drug Administration (FDA) has alarmed the medical community and has recommended healthcare professionals to limit the use of Gd-based CAs unless necessary and to report any possible related side effects. Also the European Medicines Agency (EMA) confirms recommendations to restrict the use of some linear Gd agents used in MRI body scans and to suspend the authorisations of others.

3. Next generation of CAs

Despite the valuable role of the CAs for MRI, these latest results confirm the need to have a biocompatible system able to boost a clinical relevant Gd-chelate without its chemical modification.

Ideally, the next generation agents will be site-specific; much higher relaxivities will be required to account for the decrease in concentration that accompanies increased tissue specificity.

There have been significant efforts to design and develop novel GBCAs with high relaxivity, low toxicity and specific site binding. The relaxivity of the diagnostic pharmaceutical compounds can be increased by proper chemical modification. According to SBM theory, it is needed to design a ligand that will enable the complex to have a greater number of inner-sphere water molecules (q); an optimally short water residence life time (τ_m); and a slow tumbling rate (τ_r) while maintaining sufficient thermodynamic stability. Indeed, it has been demonstrated that the relaxivity of a Gd complex will increase upon slowing down its molecular tumbling (increasing its

molecular weight) insofar as its water residence time is close to optimal. Considering the aforementioned properties, current commercial CAs have several disadvantages. They have only one coordinated water molecule and fast tumbling rates due to their small size³⁰. In addition, the toxicity of Gd³⁺ can be reduced by increasing the agents' thermodynamic and kinetic stability, as well as optimizing their pharmacokinetic properties. Moreover, the increasing knowledge in the field of genomic and biology provides an opportunity for designing site-specific CAs. According to these parameters and by exploiting the versatile properties of nano- and bio-materials several nanostructured CAs with enhanced relaxivity have been investigated.

4. Nanomedicine and nanocarriers for diagnostic applications

Nanotechnology is defined as the use of materials and structures with novel properties and functions obtained from their size which ranges from 1 to 100 nm. Nanomedicine is the medical application of nanotechnology and it is a science based on the design and development of therapeutics and/or diagnostic vectors on the nanoscale³¹.

The main goal of nanomedicine is to delivery agents in a specific and efficient way to the site of interest. In general, this can be achieved by different ways of administration, such as oral, nasal, transdermal, and intravenous.

Factors that determine nanomaterial design and characterization include size and shape, blood half-life, controlled drug release and active targeting of nanovectors³². In addition, the efficacy of the pharmaceutical compound can be improved and side effects reduced by encapsulation or association to some type of nanovector. Indeed, through advances made in nanotechnology and materials science, researchers are now creating a new generation of CAs that are capable of providing more sensitive and specific informations. In fact, nanoscale manipulation in combination with traditional diagnostic methods, provides new sensitive, specific, reproducible and cost effective methods for diagnosis of different types of pathology.

Extensive libraries of nanostructures, composed of an assortment of different sizes, shapes, and materials, and with various chemical and surface properties, have already been constructed. The field of nanotechnology is under constant and rapid growth and new additions continue to supplement these libraries. Several nanocarriers have been approved for clinical use and they are currently used to diagnosis various types of cancers³³. Furthermore, there are several formulations, which are now in various stages of clinical trials³⁴.

Clinical aspects related to the use of nano- and biomaterials such as polymer nanoparticles, block copolymers structures and liposomes for MRI applications are reported below. In addition, taking into account that multimodal imaging techniques have a huge impact on the early diagnosis, the design of novel nanocarriers with multimodal imaging characteristics is also of great interest and requires the integration in a single system of complementary imaging functionalities. The main examples of nanovectors which combine MRI with other diagnostic techniques, such as Optical Imaging and Positron Emission Tomography (PET), are set out with a particular focus on nanoparticle-based multimodal PET/MRI probes³⁵.

4.1 Polymer Nanoparticles

Nanostructured materials have been shown to have some advantages over conventional CAs. In this field, Polymeric Nanoparticles (PNPs) have attracted considerable interest over the last years due to their properties that can be modulated depending on the particular application³⁶. Advantages of PNPs as nanovectors include controlled release, the ability to combine therapy and imaging (theranostics) in just one particle, protection of active molecules and its specific targeting, facilitating improvements in the therapeutic index³⁷.

Several hydrophilic polymers, such as Hyaluronic Acid (HA), Chitosan (CS) and Dextran are widely used to manufacture PNPs for medical applications. Among them HA and its derivatives have been investigated for the development of several carrier systems for cancer diagnosis, staging and therapy³⁸. HA salts have also been used in

combination with CS for drug delivery and diagnostic applications. In this context, Chen and coworkers³⁹ report a very interesting example of nanotheranostic system in which disease diagnosis and therapy are combined. This nanocarrier has a yolk-shell structure with a radioluminescent yolk based on Gd₂O₃:Eu nanospheres, an up conversion luminescent in a silica shell, and a coating constituted by HA/CS combination for pH-triggered drug release. The deposition of the polymeric combination HA/CS is performed in layer-by-layer manner by alternating addition of the particles in HA and CS solutions. The resulting system is also able to act as dual T1/T2 MRI agents. Mitoxantrone (MTX), selected as anticancer model drug, is loaded in the empty area between the core and the shell. The *in vitro* MTX release from the nanocarrier is studied in PBS (pH 7.4) and in acidic conditions (pH 5.0) and, interestingly, a marked difference is noted. The drug release occurs with a faster kinetic in acidic conditions and it may be favorable in cancer therapy, taking into account that in tumors and in endosomes an acidic environment is present. The usefulness of the combination HA/CS is also well documented for different bio-applications³⁸. Particularly marked results have been achieved by Courant et al.⁴⁰. Their goal is to develop a new and straightforward synthesis of high-relaxivity Gd-NPs for MRI applications, with optimized nanoparticle production characteristics, Gd-loading, and relaxivity at the same time. They choose to encapsulate a low-risk CA: gadolinium-tetraazacyclododecanetetraacetic acid (also known as Gd-DOTA). Because of its hydrophilic nature, the encapsulation of Gd-DOTA is made in a hydrophilic polymer matrix. For biocompatibility reasons, CH and HA are chosen as polymer matrix. A spectacular boost in relaxation rate is found in Gd-DOTA-loaded PNPs. Furthermore, recently, Torino et al.⁴¹ have coupled a flow focused nanoprecipitation to an efficient crosslinking reaction based on Divinyl Sulfone (DVS) to entrap the relevant clinical gadolinium-diethylenetriaminepentaacetic acid (also known as Gd-DTPA) in crosslinked Hyaluronic Acid Nanoparticles (cHANPs) able to increase its relaxometric properties without the chemical modification of the chelate. Authors hypothesize that Gd-chelate modifies the affinity of the polymer solution shifting the supersaturation to a low degree and leads to a slow heterogeneous nucleation followed

by the growth of produced nuclei into large or aggregated particles. These specific interactions induce flow perturbation, causing an uncontrolled size variation and formation of aggregated morphologies. Subsequently, the macrocyclic molecules have been firmly entrapped within the hydrogel matrix, using a crosslinking reaction simultaneously occurring with the nanoprecipitation. Investigations related to the addition of the DVS in the middle channels or into the side channels have attributed to the hydrogel nanoparticles some peculiar properties responsible for the modulation of the release behaviour and swelling properties. *In vitro* MRI results prove that using the flexible platform it is possible to take advantages from the strong interference detected by the presence of Gd-DTPA producing Gd-entrapped NPs with enhanced MRI properties. This observation is crucial to lead potentially to a significant reduction of administration dosage on clinical usage of T1 contrast agents and to gain advantages in the imaging modalities based on nanotechnologies. Indeed, the nanoparticles (NPs) are widely used for the improvement of imaging techniques and all the tunability features reported for this system can potentially reduce limitation linked to a fast clearance from the bloodstream and low detection due to the dependence on the concentration. The proposed approaches aim to overcome some drawbacks of the traditional procedures for the production of NPs such as high polydispersity, expensive and time-consuming purification/recovery steps. Furthermore, results present the effective strategy to dose all species and to control property the entrapment of CAs within the hydrogel nanostructures that influences MRI performances in the signal intensity and, potentially, the tissue specificity. Then, the same authors propose a high versatile microfluidic platform to design, in a one-step strategy, PEGylated cHANPs entrapping a magnetic resonance imaging CA and a dye for multimodal imaging applications⁴². Clinically relevant biomaterials are shaped in the form of spherical NPs through a microfluidic flow focusing approach. A comparison between post processing and simultaneous PEGylation is reported to evaluate the potentiality of the chemical decoration of the cHANPs in microfluidics. An accurate control of the NPs in terms of size, PEGylation and loading is obtained. Furthermore, *in vitro* cell viability is reported and their ability to boost the magnetic resonance imaging signal up to 6 times is also

confirmed. The proposed microfluidic approach reveals its ability to overcome several limitations of the traditional processes and to become an easy-to-use platform for imaging applications⁴². All these results drive to the conclusions that the hydration of the hydrogel structure can be used to control the relaxometric properties of Gd-DTPA. In particular, this concept is explained for the first time by Torino et al.⁴³ and called Hydrodenticity. The ability to tune the hydrogel structure is proved through a microfluidic flow-focusing approach able to produce cHANPs, analyzed regarding the crosslink density and mesh size, and connected to the characteristic correlation times of the Gd-DTPA. Hydrodenticity explains the boosting (12-times) of the Gd-DTPA relaxivity by tuning hydrogel structural parameters, potentially enabling the reduction of the administration dosage as approved for clinical use^{43,44}.

To date, ¹H MRI has been widely used in clinical diagnosis, but in recent years, researchers have focused on exploring alternative MRI atoms. Among them, the ¹⁹F atom, as the most promising imaging nucleus, owns several unique features such as 100% natural isotopic abundance, low background ¹⁹F in the human body, relatively high sensitivity (83% of protons) and a broad range of chemical shifts. Given that the ¹⁹F element present in the human body exists in bones and teeth, low doses of fluorinated agents are required for performing ¹⁹F MRI⁴⁵.

It has been proved that structure of a fluorinated agent is of crucial importance for achieving satisfactory MRI performance. Preferably, a ¹⁹F MRI agent shall display a high fluorine content, high signal-to-noise resonance spectrum, short T1 and long T2. To this end, various types of ¹⁹F MRI agents have been developed and manufactured in the form of delivery vectors for MRI. For example, Wang et al.⁴⁶ prepare ¹⁹F moiety loaded nanocomposites with an organic fluorescent core via a facile strategy by encapsulating organic dyes with oleylamine-functionalized polysuccinimide and 1H,1H,2H,2H-perfluorodecyltriethoxysilane (PDTES). The aggregation of organic fluorescent dyes in the core results in significant fluorescence for optical imaging, while the ¹⁹F moieties on PDTES allow for simultaneous ¹⁹F MRI. Moreover, the nanocomposites exhibit high water dispersibility and excellent biocompatibility. These

properties make them promising for both cell imaging and *in vivo* imaging applications.

Among other biomaterials, silica nanostructures have earned a key role in the MRI field. Indeed, in contrast to many other nanomaterials, silica NPs do not acquire any special property from their sub-micrometer size, except for the corresponding increase in surface area. What makes silica NPs fascinating from a nanotechnology point of view is their well-defined and tunable structures (i.e., size, morphology and porosity) and surface chemistry. By introducing new functional groups via well-established siloxane chemistry, it is possible to modify the silica surface to impart new properties to the particles, such as diagnostic and therapeutic capabilities. Moreover, silica NPs are effectively “transparent” in the sense that they do not absorb light in the near-infrared (NIR), visible and ultraviolet regions, or interfere with magnetic fields. In addition, silica NPs are inexpensive, easy to prepare, relatively chemically inert, biocompatible, and water dispersible. A fundamental use of silica particles has been reported by Decuzzi et al.⁴⁷. In their work, they demonstrate enhanced efficiency of Gd-based CAs (Gd-CAs) by confining them within the nanoporous structure of intravascularly-injectable Silicon Micro Particles (SiMPs). Enhancement in efficiency is shown for three different Gd-CAs: Magnevist (MAG), a clinically-used Gd³⁺ polyaminocarboxylate complex, and two carbon nanostructure-based lipophilic agents, Gadofullerenes (GFs) and Gadonanotubes (GNTs). The GFs have a single Gd³⁺ ion encapsulated by a spherical fullerene cage of ~0.7 nm in diameter. The external fullerene cage, which prevents the leakage of the Gd³⁺ ions, can be chemically functionalized to provide solubility and biocompatibility. Even after functionalization, the GFs exist as aggregates in solution. The GNTs are nanoscale carbon capsules (derived from full-length single-walled carbon nanotubes) with a length of 20-80 nm and a diameter of about 1.4 nm, which are internally loaded with Gd³⁺ ion clusters. Within the GNTs, the Gd³⁺ ions are present in the form of clusters (<10 Gd³⁺ ions per cluster), and each GNT contains approximately 50 to 100 Gd³⁺ ions. The Gd³⁺ clusters are stable and the Gd³⁺ ions do not leak from the nanocapsules under physiological conditions. Because of the hydrophobic nature of their external carbon sheath, the

GNTs exist in the form of bundles. In this work, a homogeneous dispersion of GNTs (debundled GNTs) is prepared using Na0/THF reduction.

As assessed in the introduction, multimodal imaging is becoming the new perspective into the fields of clinical and preclinical imaging, and nanomedicine represents a valid field of application to support its development. Here, it is report a successful example, developed by the author of this chapter, to combine boosted MRI with Optical Imaging or PET. This is the only case available providing multimodal imaging with improved relaxometric properties and without the chemical modification of the chelate. In particular, core-shell polymeric NPs are obtained, which can be encapsulated with both Gd-DTPA and a dye for Dual Imaging applications through a complex coacervation that exploits an innovative double crosslinking to improve the stability of the nanostructure overcoming the interference of the Gd-DTPA in the coacervation process⁴⁸. Furthermore, the adjustment of the process parameters, the coacervation and chemical reaction kinetic promote the interpolation of the hydrophobic core with the hydrophilic shell, controlling the water exchange and, consequently, the relaxation rate T1, enhancing the MRI signal at reduced concentration compared to the relevant clinical CAs. Finally, process conditions able to develop a pH-sensitive behavior of the Hybrid Core-Shell (HyCoS) NPs have been identified.

Further investigations are required to highlight the benefits and the drawbacks of this behavior and to consider the system as an effective and safe platform for theranostic nanomedicine. Further developments of this project have been the upgrade of the designed nanosystem to the trimodal applications and *in vivo* tests. In particular, a study of HyCoS NPs with the Fluorodeoxyglucose (¹⁸F-FDG) is planned for PET-MRI applications⁴⁹.

4.2 Block Copolymers

Polymers containing a mixture of repeat units are known as copolymers and they occupy an extensive research area and they are well known in, size, and chemical composition⁵⁰. For this reason the interest in the synthesis and characterization of

copolymers the biomaterials field thanks to their ability to generate nanostructures particularly in aqueous solution by varying their architecture is increased enormously in the last years thanks also to advances in polymer chemistry. Therefore, the synthetic nature of copolymers allows the design of interfaces containing various biochemically active functional groups. Among them, Block Copolymers (BCPs) are a specific type of copolymer system such that each monomer is homopolymerized to create chemically distinct domains.

A broad range of functional BCPs with tailored properties and organic and also inorganic components are now accessible especially for pharmaceutical or diagnostic applications^{51,52}.

An increased number of reports on the synthesis, structures, properties and applications of copolymers have been published in the last years⁵³. A vast majority of di- and tri-block copolymers are used for the creation of nanosystems loaded with imaging agents, not only to protect these agents from degradation or inactivation *in vivo* but also to optimize dosage and efficacy. These molecules can be physically encapsulated into polymer assemblies or covalently conjugated onto polymer chains. Moreover, as known, the polymer carriers with surface bioconjugation is the key to prolong the bioavailability of the encapsulated active molecules.

Particularly remarkable are the data reported by Xiao et al.⁵⁴ about a new Gadolinium(III)-copolymer (ACL-A2-DOTA-Gd), developed as a potential liver MRI contrast agent. ACL-A2-DOTA-Gd consists of a poly (aspartic acid-co-leucine) unit bound with Gd-DOTA via the linkage of ethylenediamine. *In vitro* experiments show that new complex is biodegradability, biocompatibility and its relaxivity is 2.4 times higher than the clinical Gd-DOTA. *In vivo* MRI study and biodistribution in rats confirm that Gadolinium(III)-copolymers are mainly accumulated in the liver with a long time-window.

Hou et al. ⁵⁵, instead, report a novel approach to synthesize poly(ethylene glycol) (PEG)-based Gd-NPs with small size (7 nm) and high relaxivity. They construct a pentablock copolymer through two sequential atom transfer radical polymerization (ATRP) reactions. The nanostructure consists of a Gd chelates-conjugated block in the

center and PEG-terminated segments at both ends. In this way, the interactions of Gd chelates with proteins are shielded by the hydrated PEG segments. *In vitro* and *in vivo* studies demonstrate that the relaxivity is 20 times higher than commercial CA.

Then, Cao and coworkers⁵⁶ synthesize a new type of triblock polymeric micelle based on biocompatible poly(glycerol) (PG) and poly(caprolactone) (PCL) for tumor-targeted MRI *in vivo*. Gadolinium chelates (such as Gd-DOTA) and folic acid (FA) molecules are conjugated to PG block through efficient click chemistry reaction and the final structure is T-micelle (PCL-PG-PCL-g-DOTA(Gd)+FA) of 250 nm. T-micelles exhibit a higher longitudinal relaxivity (r_1) and show significant targeting specificity to tumor cells. The capability of T-micelle as an MRI CA for contrasting tumor tissue *in vivo* is evaluated *in vivo* on tumour-bearing mice at different time points. The results indicate that FA functionalized T-micelle could provide efficient contrast effect at the tumor region through targeting specificity.

Luo et al.⁵⁷, have successfully synthesized an amphiphilic poly(aminoethyl ethylene phosphate)/poly(L-lactide) (PAEEP-PLLA) copolymer by ring-opening polymerization reaction, which contains hydrophobic PLLA and hydrophilic PAEEP segments with good biocompatibility and biodegradability. Oleylamine-coated Fe_3O_4 magnetic nanoparticles (OAM-MNPs) are encapsulated in the PAEEP-PLLA copolymer nanoparticles, while the molecules of lactoferrin (Lf) are conjugated for glioma tumor targeting. The results indicate strong, long-lasting, tumor targeting, and contrast-enhanced MRI ability of Lf-MPAEEP-PLLA-NPs owing to the selectively accumulation in brain glioma tissue.

Another interesting strategy for the development of new contrast reagents is the synthesis of amphiphilic Gadolinium(III) complexes that can form spontaneously micelles. Jeong and colleagues⁵⁸ synthesize biocompatible amphiphilic derivatives of DOTA with hydrophobic alkyl chains, whose gadolinium(III) are incorporated into DOTA of micelles via ethylenediamine. To prepare the micelle-formed MRI contrast agent with Gd, hydrophilic (mPEG) and hydrophobic moieties (hexadecylamine) are conjugated with the PHEA backbone. PEG chains, being exposed to the external aqueous phase. The final structure (PHEA-mPEG-C16-ED-DOTA-Gd) has an average

diameter of 180 nm and can be used for the detection of liver lesion. *In vitro* experiments show that this nanovector give better imaging contrast than commercial contrast agent at low concentration of Gadolinium. Therefore, when solution of PHEA-mPEG-C16-ED-DOTA-Gd is intravenously injected into a rabbit, the T1-weighted image of the liver in an animal model shows prolonged intravascular duration time of about 30 min.

With the rapid development of polymer synthetic and nano-techniques, stimuli-responsive block copolymers and corresponding assemblies are created one after another and used for targeted delivery of drugs and imaging/contrast agents to tumor sites. These vehicles are able to react to internal environmental changes, such as temperature, ionic strength, light, pH level, pressure, and so on or external stimuli (light and electromagnetic field) exhibiting reversible or irreversible changes in chemical structures and physical properties⁵⁹.

In particular, the measurement of pH *in vivo* has received considerable attention because, in presence of solid tumors, it provides the potential not only for early detection and diagnosis of tumors but also for monitoring the efficacy of the treatment plan used to combat the disease⁶⁰. The non-invasive measurement of pH is based on MRI. Gao and coworkers⁶¹ are one of the first groups to prepare a stimuli-responsive BCPs by encapsulation of iron oxide NPs in a pH-responsive diblock copolymer, consisting of poly(ethylene oxide) (PEO) as the hydrophilic, biocompatible segment and a poly(β -amino ester) (PAE) as the pH-sensitive segment. When the pH is low (<7.0), the transverse relaxivity (r_2) of the imaging agent increases due to the release of the iron oxide nanoparticles from the core of the micelles. Subsequently, Okada et al.⁶², develop a different approach to prepare a pH-responsive system by attaching Gd-chelates to a poly(methacrylic acid) (PMAA). MRI *in vitro* studies indicate that the relaxivity of the contrast agent increases of two times when the environmental pH is acid. Also Zhu et al.⁶³. design a pH-responsive MRI CA that demonstrates significant changes in term of relaxivity upon changes in the environmental pH at physiological relevant values. Recently, to enhance the stability of polymeric micelles, Hu et al.⁶⁴ report the fabrication of cross-linked micellar structure, which covalently labelled with

DOTA(Gd) and green-emitting fluorophores within pH-responsive cores, serving as a dual-modality MR/fluorescence imaging agents. The acidic pH-triggered turn-on and enhancement of signal intensities for both imaging modalities are declared. Compared with non-cross-linked diblock precursor, this system shows better MR and fluorescence imaging performance due to structural stability. Subsequently, the same group develops a novel theranostic polyprodrug platform with synergistic imaging/chemotherapy capability consisting of hyperbranched cores conjugated with reduction-activatable prodrugs (an anticancer agent) and MRI CA (Gd complex), and hydrophilic coronas functionalized with guanidine residues⁶⁵. The hyperbranched cores avoid the potential interactions between anticancer agent and blood components and serve as the embedding matrix for MR contrast agents to weaken MR background signals. Upon cellular internalization, the synergistic turn-on of therapeutic potency and enhanced diagnostic imaging in response to tumor milieu are achieved.

Mouffouk et al.⁶⁶, for example, report the development of a smart CA composed of pH-sensitive micelles containing a hydrophobic Gd(III) complex with the aim of specifically detecting cancer by MRI. This vector (35–40 nm) consists of pH-sensitive polymeric micelles formed by self-assembly of a diblock copolymer poly(ethyleneglycol-*b*-trimethylsilyl methacrylate) (PEG-*b*-PTMSMA), loaded with the hydrophobic complex tetraaquodichloro(4,4'-di-*t*-butyl-2,2'-bipyridine) Gadolinium(III) chloride (tBuBipyGd) and decorated with a specific monoclonal antibody (mAb) against the human MUC1 protein, which is more expressed in many epithelial cancers and a specific targeting vector in preclinical and clinical trials. This system is able to amplify the MRI signal chemically and at the same time has the ability to remain silent during circulation; in fact, the CA remained in the “off state,” being activated only upon micelle disruption in an acidic medium represented by tumour microenvironment. In fact, the extracellular pH of most tumor tissues is weakly acidic (pH 6.5), which is lower than that of normal tissues (pH 7.2) and this discrepancy is usually used as the trigger factor. Finally, the conjugation of a specific biomolecule to smart agents increases significantly their affinity toward cancer cells.

Other stimuli-responsive BCPs are extensively studied. Tsai et al.⁶⁷, for example, develop a core-shell structure composed by poly(HEMA-co-histidine)-g-PLA and diblock copolymer PEG-PLA with functional moiety. The inner core of poly(HEMA-co-histidine)-g-PLA exhibits pH stimulate to enable intracellular drug delivery, while the outer shell PEG-b-PLA with functional moiety Cy5.5 for biodistribution diagnosis and folate for cancer specific targeting. The nanospheres has an average diameter of 200 nm. From drug release study, a change in pH destroy the inner core to lead a significant drug release from mixed micelles. Cellular uptake of folate-micelles is found to be higher than that of non-folate-micelles. *In vivo* study reveal that specific targeting of folate-micelles exhibit cancer targeting and efficiency expression on tumor growth, indicating that multifunctional micelles prepared from poly(HEA-co-histidine)-g-PLA and folate-PEG-PLA have great potential in cancer chemotherapy and diagnosis.

Concomitantly, additional and promising technologies in nanomedicine are currently under investigation such as multimodal imaging, which combines two or more diagnostic strategies into one procedure and nanotheranostics, which integrates both therapeutic and diagnostic capabilities into one single nanoplatform.

Locatelli et al.⁶⁸, for example, report a nanocarrier system for dual PET/MRI imaging. In this case hydrophilic superparamagnetic maghemite NPs are synthesized and coated with a lipophilic organic ligand and the entrapped into polymeric NPs made of biodegradable poly(D,L-lactide-co-glycolide)-block-poly(ethylene glycol) copolymer (PLGA-b-PEG-COOH). Moreover, the surface of NPs show active sites (COOH) that allow a modification with 2,2'-(7-(4-((2-aminoethyl) amino)-1-carboxy-4-oxobutyl)-1,4,7-triazonane-1,4-diyl) diacetic acid (NODA) to chelate ⁶⁸Ga for PET imaging. Zhang and coworker⁶⁹, instead, realize a copolymer-based single-photon emission computed tomography/magnetic resonance (SPECT/MR) dual-modality imaging agent that can be labeled with technetium-99m (^{99m}Tc) and Gd simultaneously. The copolymer P(VLA-co-VNI-co-V2DTPA) (pVLND2) is synthesized by radical copolymerization reaction and based on asialoglycoprotein receptor (ASGPR) targeting agent for hepatic tissue.

An example of theranostic polymer platform is developed by Porsch et al.⁷⁰. In this work, they report the use of natural isotope ¹⁹F as an efficient alternative to the conventional imaging contrast agents, because this nucleus is not intrinsic to the body, thus enabling MRI images with great spatial selectivity against a zero background and synthesize fluorinated NPs loaded with doxorubicin (Dox). The NPs are formed by self-assembly of amphiphilic BCPs with fluorinated elements incorporated in the hydrophilic corona and anticancer drug in the hydrophobic core. Experimental data show that the nanovector has a controllable drug release kinetics, are detectable by ¹⁹F-MRI and toxic for breast cancer cells.

Recently, Koziolova and colleagues⁷¹ evaluate the influence of molecular weight and dispersity of N-(2-hydroxypropyl)methacrylamide (HPMA) copolymer conjugates with Dox on their biodistribution is studied using two complementary imaging methods PET and Fluorescence Imaging (FI). The HPMA copolymers are synthesized by RAFT polymerization and functionalized with a chelator for further radiolabelling with Zirconium-89 (⁸⁹Zr; t_{1/2} = 78.4 h) prior to *in vivo* and *ex vivo* studies. PET/Optical Imaging studies indicate that dispersity and molecular weight of the HPMA polymer carriers have a significant influence on the *in vivo* fate of the polymer conjugates and thanks to presence of anticancer drug bound show higher cytotoxicity and cellular uptake *in vitro*.

4.3 Liposomes

Liposomes are structures composed of hydrophobic head groups and hydrophilic tail groups. They can be prepared by adding lipids in organic solution, which is slowly evaporated to produce a thin film. The film is then hydrated with a desired aqueous buffer and sonicated. Liposomes are generally nano-scaled structures and can be further size refined by passage through physical membrane pores of known size (extrusion). Liposomes are typically characterised by their size, shape and lamellarity. They may be composed of a single bilayer (unilamellar), a few bilayers (oligolamellar), or multiple bilayers (multilamellar). Due to their aqueous cavity and “tunable” bilayer,

liposomes have traditionally been used as drug delivery vehicles, encapsulating water-soluble drugs within the aqueous cavity in order to improve drug pharmacokinetics⁷². Zou et al.⁷³ for example, report an amphiphilic MRI-traceable liposome NPs encapsulating Gd-DOTA for *in vivo* inner ear visualization through MRI. They design these multifunctional NPs through the film hydration method that allows the encapsulation of Gd-DOTA inside the hydrophilic core of the NPs. They observe acceptable relaxivity values allowing visible signal characteristics for MRI. *In vivo* studies demonstrate that these systems are efficiently taken up by the inner ear after both transtympanic and intracochlear injection. The latter shows better NPs distribution throughout the inner ear, including the cochlea and vestibule, and induced stronger MRI signals on T1-weighted images.

Bui et al.⁷⁴ produce lipid NPs containing phospholipids that express Gd-chelate or DTPA by incorporating DTPA-PE into the lipid core of the NPs and then adding Gd³⁺ to preformed NPs (for binding to Gd³⁺ as Gd-DTPA-PE chelate). They also add 10-mole percentage of lipid conjugated to mPEG-PE to lipid nanoparticles in order to increase the bound water on the lipid nanoparticle surface, thereby increasing the MRI contrast. In this case, the following nanoparticle system shows a higher longitudinal relaxivity (33-fold) than the current FDA approved Gd-chelated CAs. In addition, intravenous administration of these Gd-LNP at only 3% of the recommended clinical Gd dose produce MRI signal-to-noise ratios of greater than 300 times in all vasculatures.

Kamaly and colleagues⁷² synthesize a bimodal imaging liposome for cell labeling and tumour imaging. The lipid molecules are able to bear both fluorophore and CA on the same structure, thereby representing a useful probe for both MRI and fluorescence microscopy utility. Very briefly, they conjugate a rhodamine moiety onto a DOTA-bearing C-18 dialkyl lipid and complex Gd into the molecule to obtain the bimodal lipid Gd DOTA Rhoda DSA 1. The lipid is used to label IGROV-1 human ovarian carcinoma cells and to image xenograft tumours in mice. The new paramagnetic and fluorescent lipid proved to be a valuable probe to obtain anatomical information, through MRI, and liposome biodistribution, through *ex vivo* fluorescence microscopy.

Kono et al.⁷⁵ synthesize multi-functional pegylated liposomes having both highly thermosensitive polymers and newly synthesized Gd-chelate-attached dendron lipid (G3-DL-DOTA-Gd) with a compact conformation. The multifunctional liposomes show temperature-responsive drug release and MR imaging functions. In particular, authors load liposomes with Dox and tested the stability of the nanostructures, showing that liposomes are able to retain Dox below physiological temperature but release it immediately above 40°C. As far as the MRI properties, the developed liposomes exhibit the ability to shorten the longitudinal relaxation time with a relaxivity ($5.5 \text{ mM}^{-1} \text{ s}^{-1}$) higher than that of free Gd-DOTA ($4.6 \text{ mM}^{-1} \text{ s}^{-1}$).

In addition, Na and co-worker⁷⁶ report dual functional liposomes co-encapsulating Dox and Gd as therapeutic and diagnostic carriers. They measure MR relaxivity and cellular uptake showing that the liposomes can entrap 3.6 mM of Dox and 1.9 mM of Gd. Although the low relaxivity ($5.5 \text{ mM}^{-1} \text{ s}^{-1}$) compared to that of MRbester[®] due to limited water diffusion across the liposome membrane, the surface charge induced good cellular uptake, allowing a higher accumulation of Gd into cells than MRbester[®]. Additionally, Dox is more easily internalized to the nucleus compared to Doxil[®].

Li et al.⁷⁷, instead, prepare fluorescent and paramagnetic liposomes for early tumor diagnosis by incorporating a RGD-coupled-lipo-peptide, synthesized using a cyclic RGD peptide headgroup coupled to palmitic acid anchors via a KGG tripeptide spacer, into lipid bilayers. As far as the paramagnetic liposomes, they adopted the thin film hydration method and hydrated the lipid film with commercial Gd-DTPA as MRI contrast agent. *In vivo* MRI scanning demonstrate that the signal enhancement in tumor after injection of RGD-targeted liposomes is significantly higher than non-targeted liposomes and pure Gd-DTPA. In addition, biodistribution study also show specific tumor targeting of RGD-targeted paramagnetic liposomes *in vivo*, proving them an effective means for noninvasive diagnosis of early tumor.

Liao et al.⁷⁸ design a core-shell NPs system composed of a PLGA core and a paramagnetic liposome shell for simultaneous MRI and targeted therapeutics. They encapsulate Dox within biocompatible and FDA-approved PLGA NPs, and DTPA-Gd is conjugated to the amphiphilic octadecyl-quaternized lysine-modified chitosan

(OQLCS). The paramagnetic liposome shell is based on Gd-DTPA-conjugated OQLCS (Gd-DTPA-OQLCS), folate-conjugated OQLCS (FA-OQLCS), and PEGylated OQLCS (PEG-OQLCS). Briefly, the carboxyl groups of DTPA used as a chelating agent are combined with the amino groups of OQLCS. Then Gd is incorporated into the complex. As a result, the NPs show paramagnetic properties with an approximately 3-fold enhancement in the longitudinal relaxivity ($r_1 = 14.381 \text{ mM}^{-1}\text{s}^{-1}$) compared to the commercial Gd-DTPA complex and exceptional antitumor effects without systemic toxicity.

Another remarkable example as reported by Gianolio et al.⁷⁹. They prepare pH-responsive Gd-DO3A-loaded liposomes which maintain the pH responsiveness of the unbound paramagnetic complex, and their relaxivities are markedly affected by the magnetic field strength, exhibiting a steep change in the relaxivity in the pH range 5-7.5. Moreover, they provide a ratiometric method for measurement of the pH based on a comparison of the relaxation effects at different magnetic fields, offering an alternative tool for accessing measurement of the pH without prior knowledge of the concentration of the paramagnetic agent.

Subsequently, Hossann et al.⁸⁰ investigate formulations of 6 clinically approved CAs encapsulated into thermosensitive liposomes (TLs):

- (1) Gd-DTPA (Magnograf[®]) from Marotrust GmbH, Jena, Germany;
- (2) Gd-BOPTA (Multihance[®]) from Bracco Imaging Deutschland GmbH (Konstanz, Germany);
- (3) Gd-DOTA (Dotarem[®]) from Guerbet GmbH (Sulzbach/Taunus, Germany);
- (4) Gd-BT-DO3A (Gadovist[™]) from Bayer Vital GmbH (Leverkusen, Germany);
- (5) Gd-DTPA-BMA (Omniscan[™]) from GE Healthcare Buchler GmbH & Co. KG (Braunschweig, Germany);
- (6) Gd-HP-DO3A (Prohance[®]) from Bracco Imaging Deutschland GmbH (Konstanz, Germany).

They observe that Omniscan™ and Prohance® are the most promising candidates to be encapsulated into DPPG2-TSL. In particular, Prohance® allows the highest loading capability (256 mM) due to the lowest osmolality and yielded the highest relaxivity. Omniscan™ is the only formulation that could be stored at 4°C for weeks. The other CAs induce phospholipid hydrolysis, which results in unwanted CA leakage, and therefore reduce the shelf life of TSL. Nevertheless, Omniscan™ is associated with nephrogenic systemic fibrosis (NSF)⁸¹.

The Human Serum Albumin (HSA) and Immunglobulin G (IgG) contribute to the increase of MRI signal at 30°C by increasing Pd. A high concentration of encapsulated CA is a prerequisite to achieve a sufficiently high Δr_1 during heat triggered CA release combined with a low r_1 at 37°C. Hence, the optimal CA is characterized by a non-ionic structure and a low contribution to osmolality.

Cheng et al.⁸², instead, encapsulate Gd within a nanometer-sized stabilized porous liposome in order to increase the Gd relaxivity thanks to the porous structure, enabling a fast water exchange rate. A further increase in relaxivity (up to 9.9 mM⁻¹s⁻¹) is achieved by attaching large molecular weight dextran to the Gd moiety (Gd-DOTA) prior to encapsulation.

Others authors report further interesting strategies for the development of new liposome-complexes. Park and coworker⁸³ develop nanohybrid liposomes coated with amphiphilic hyaluronic acid-ceramide for targeted delivery of anticancer drug and *in vivo* cancer imaging. Dox, an anticancer drug, and Magnevist, a Gd-based CA for MRI, are loaded into this nanohybrid liposomal formulation. They find that *in vitro* release and *in vivo* clearance of Dox as well as cellular uptake from the nanohybrid liposome is enhanced than that from conventional liposome, thanks to the prolonged circulation of the nanohybrid liposome in the blood stream and to the HA-CD44 receptor interactions.

Another example is reported by Smith and Kong⁸⁴. In this case, it is evaluated the stability of liposomes with Gd-loaded in presence of serum. The authors assemble crosslinkable liposomes composed of diyne-containing lipids, conjugate the liposome surface to DTPA-chitosan-g-C18 and then crosslink the liposome via UV irradiation.

The particles are mixed with Gd to enhance the quality of MRI contrast. They demonstrate that the crosslinking strategy after the adsorption of the polymer fastener allows stabilizing the thermodynamically favorable association between liposome and DTPA-chitosan-g-C18. In the end, they observe that CS-coated crosslinked liposomes are more effective than non-crosslinked liposomes in terms of stability, showing reduced liposome degradation and chitosan desorption.

Concomitant, Gu et al.⁸⁵ develop novel Gd-loaded liposomes guided by GBI-10 aptamer for enhanced tumor MRI. They conjugate GBI-10, as targeting ligand, onto the liposome surface and the so obtained system shows an accumulation of Gd at the periphery of C6 glioma cells, where the targeting extracellular matrix protein tenascin-C is overexpressed. This novel design strategy, obtained by simply replacing the aptamers with other kinds of aptamers, can be applied to a variety of target cells with high efficiency and specificity.

Silva et al.⁸⁶ synthesize and incorporate complexes of Gd with aliphatic chain ligands of N-alkyl-N-methylglucamine series into liposomes in order to enhance MRI contrast. The presence of two aliphatic chains is conceived to reduce the local rotational motion of the Gd-complexes after incorporation in the liposomal bilayer. They show that the incorporation into liposomes is accompanied by an increase of the vesicle zeta potential and in relaxation effectiveness (r_1 up to $15 \text{ mM}^{-1}\text{s}^{-1}$) compared to commercial Gd-DTPA, presumably because of the slower molecular rotation due to the elevated molecular weight and incorporation in liposomes.

Xiao et al.⁸⁷ report liposomes loaded with Sorafenib (SF) and commercial Gd-based CA (Gd-DTPA) for theranostic applications. Thin film hydration method is used to prepare liposomes exhibiting spherical shapes or ellipsoidal shapes, uniform particle size distribution (around 180 nm), negative zeta potential, high encapsulation efficiency and drug loading. As far as the longitudinal relaxivity, they achieve a value of $3.2 \text{ mM}^{-1}\text{s}^{-1}$, slightly lower than the commercial CA ($4.5 \text{ mM}^{-1}\text{s}^{-1}$) and the MRI test show longer imaging time and higher signal enhancement at the tumor tissue. Furthermore, they demonstrate *in vivo* antitumor efficacy of the developed SF/Gd-liposomes on hepatocellular carcinoma (HCC) in mice. To sum up, the authors show

that SF/Gd liposomes could be promising nano-carriers for MRI-guided *in vivo* visualization of the delivery and HCC treatment.

In the end, Tian et al. synthesize Gd-DTPA-loaded mannosylated liposomes (M-Gd-NL) and test their ability to target macrophages in Acute Pancreatitis (AP) and discriminate between mild and severe AP. Lipid film-based method is used to synthesize DSPE-PEG2000-Man liposomes encapsulating DPPE-DTPA-Gd, with size around 100 nm. *In vitro* tests show efficient bind and readily release of Gd-DTPA into macrophages, resulting in enhanced MRI ability. Indeed, M-Gd-NL show a longitudinal relaxivity 1.8-1.9 higher than Gd-DTPA, as a consequence of the embedding of DPPE-DTPA-Gd into the bilayer of liposomes, which slowed down the tumbling motion of Gd complexes. As far as the safety profile, M-Gd-NL do not show any severe organ toxicity in rats, thus proving to be promising nanocarriers for clinical use and for the early detection of AP.

5. *Aim of work*

The large variety of systems now available in the nanometric scale represents a clear advantage in diagnostic and therapy of some of the most challenging human pathologies. In this context, the following thesis project has been focused on the design and synthesis of new CAs for MRI applications.

Initially, the basic principles ruling biopolymer-CA interactions are clearly highlighted in the perspective of their influence on the relaxometric properties of the CA by adopting a multidisciplinary experimental approach. HA⁸⁸ is used as a model polymer because of its biocompatibility and high hydrophilicity.

In this theoretical framework, the peculiar effect of Hydrodenticity on the polymer conformation and the formation of the stable water compartments responsible for the enhancement of the MRI signal is introduced and discussed. Then, the acquired knowledge about polymer-CA systems to apply the concept of Hydrodenticity to the design of Gd-based polymer NPs with enhanced relaxometric properties. Thus, the development of the nanomaterial drug carriers, based on biopolymer nanoparticles,

physically and chemically characterizations of interactions between hydrophilic biopolymers and Gd-based CAs, and possible medical applications (lymphoma and atherosclerosis diseases) are reported here.

CHAPTER I

Impact of water dynamics on relaxometric properties of Gd-DTPA.

1. Introduction

Recently, rational design of a new class of CAs, based on biopolymers (hydrogels), have received considerable attention in MRI diagnostic field and several strategies have been adopted to improve relaxivity without chemical modification of the commercial CAs. As reported by Port et al.⁸⁹, rigidification of Gd-based CAs would be favourable to an increase in the relaxivity of the metal chelate since the presence of the ligand around the Gd ion induces a shortening of the residence lifetime of the inner-sphere water molecules (τ_M)⁸⁹⁻⁹¹. In addition, they hypothesized that the presence of a rigid coordination cage of a chelate should limit its intramolecular conformational motions, which distorts the ligand field at the metal centre due to solvent molecules collisions, thus influencing the electronic relaxation times (τ_{S1} and τ_{S2})⁸⁹. To assess the rigidification strategy, Port synthesized a constrained derivative of Gd-PCTA12, Gd-cyclo-PCTA12, in which one ethylene bridge connecting two nitrogen atoms of the triamine block is replaced by a cyclohexylene bridge, and the impact of rigidification was studied by comparing the physicochemical and relaxometric properties of both gadolinium MRI contrast agents, Gd-PCTA12 and Gd-cyclo-PCTA12.

Other experimental approaches studied by Decuzzi et al.^{47, 92, 93} proved that geometrical confinement could limit the mobility of water molecules and thereby enhance the relaxation response of Gd-based CAs without its chemical modification. In particular, they observed that nanometric pores of silica microparticles increase the rotational correlation time (τ_R) of Gd-DTPA (inner-sphere effect), which cannot tumble freely being adsorbed on the walls of the 100 nm pores. At the same time, it also increases the diffusion correlation time (τ_D) for water molecules (outer-sphere effect), which are geometrically confined and forced to interact longer with Gd-DTPA adsorbed to the inner pore surface⁹³. Through the confinement strategy, a poor increment of the relaxivity can be obtained without modifying the chemical structure of the CA.

As advancement of the geometrical confinement, in some more recent works, Courant et al.⁴⁰ and Callewaert et al.⁹⁴, showed that biocompatible hydrophilic hydrogels can

be exploited to produce high water content nanoparticles (NPs) encapsulating the metal chelate. Inside the hydrogel, which creates a favourable aqueous environment for Gd-based CAs^{88, 95-97}, the rotational motion of the encapsulated CA (Gd-DOTP, Gd-DOTA and Gd-DTPA) is restricted and its magnetic properties are amplified.

In our recently published works^{98, 99}, we have initially analysed the impact that hydrophilic biopolymer networks have on the relaxivity of Gd-based CAs and explained the role of the water in the interaction between polymers and metal chelates. This concept, called “*Hydrodentivity*”, has been the subject of further investigations as reported by Russo et al.⁴³. In a still previous work published by Russo and co-worker⁴¹, crosslinked Hyaluronic Acid NanoParticles (cHANPs) containing a Gd chelate (Gd-DTPA), are synthesized through a microfluidic platform that allows a high degree of control over particle synthesis, enabling the production of monodisperse particles as small as 35 nm for MRI applications. The relaxivity (r_1) achieved with the cHANPs is 12-times higher than Gd-DTPA. Within cHANPs, the properties of *Hydrodentivity* can be modulated to obtain desired mesh size, crosslink density, hydrophilicity and loading capability, as reported by Russo et al.^{42, 43}. Moreover, they proved that an increase of the crosslinking degree of biopolymer can induce the enhancement of relaxivity by restricting molecular tumbling while maintaining the switching property¹⁰⁰ and allowing easy access of water throughout the structure, which is a key feature in MRI CAs. The possibility to adopt a unique platform to tune the hydrogel structural parameters and, consequently, increase the relaxivity of a metal chelate without any chemical modification, could have a great impact on the clinical outcome. In fact, thanks to their improved relaxometric properties, cHANPs could ensure a brighter contrast with a lower amount of metal chelate, thus enabling the potential reduction of the administration dosage as approved for clinical use.

In a further work¹⁰¹, we reported an efficient way to produce Hybrid Core-Shell (HyCoS) NPs composed of a Chitosan core and a shell of HA with improved relaxometric properties (up to 5-times than the commercial CA). Subsequently, the same nanosystem is used to develop a new nanoprobe for simultaneous Positron

Emission Tomography (PET)/MRI acquisitions as reported in our more recent publication¹⁰².

Based on the above reported works, it has been finally demonstrated that the polymer architecture affects some characteristic parameters of the metal chelate and tunes its relaxometric properties^{40, 43, 92, 103-105}. Moreover, it is clear that crosslinked biopolymers can have a significant role to overcome the limitations of clinically relevant CAs without their chemical modification and as a compound in the design of advanced nanostructures with improved safety profile and switchable relaxometric properties. Indeed, it is known that the functional properties as well as the swelling behaviour of hydrogels are influenced by the hydration degree, which can be likely modulated by changing the chemical composition of the system¹⁰⁶⁻¹¹².

Here, we aim to highlight the basic principles ruling biopolymer-CA interactions in the perspective of their influence on the relaxometric properties of the CA by adopting a multidisciplinary experimental approach. HA⁸⁸ is used as a model polymer because of its biocompatibility and high hydrophilicity. We characterize, physically and chemically, the interactions between hydrophilic biopolymers and Gd-based CAs. In this theoretical framework, the peculiar effect of *Hydrodenticity* on the polymer conformation and the formation of the stable water compartments responsible for the enhancement of the MRI signal is introduced and discussed.

2. Experimental Section

2.1 Materials

All chemicals used are of analytical reagent grade quality and are employed as received. Divinyl sulfone (DVS, 118.15 Da), Diethylenetriaminepentaacetic acid gadolinium(III) dihydrogen salt hydrate (Gd-DTPA, 547.57 Da) and Sodium hydroxide pellets (NaOH).

Sodium Hyaluronate, with an average molecular weight of 850 kDa (purity 99%; Hyasis® 850P) and 42 kDa, is respectively supplied by Novozymes Biopharma and Bohus Biotech (Sweden) as dry powder and used without purification.

Magnevist[®] (Bracco Imaging, Italy), a contrast agent commercially available, is used in this study. The water is purified by distillation, deionization, and reverse osmosis (Milli-Q Plus) and systematically used for sample preparation, purification and analysis. All experiments are repeated in triplicate and conducted at room temperature, 25°C.

2.2 Isothermal Titration Calorimetry

Titration experiments are performed by using a Nano ITC Low Volume calorimeter (TA Instruments). CA and polymer are prepared in double-distilled filtered water without any additives. The sample cell (700 μ L) and the syringe (50 μ L) are filled with aqueous solutions of HA and Gd-DTPA respectively. Syringe Gd-DTPA concentration is fixed at 1.5 mM, while different HA concentrations in the sample cell are tested, ranging from 0.3 to 0.7% w/v. The measurements are performed at 25 °C and at fixed stirring rate of 200 rpm. Fifty Injections, each of 1 μ L of Gd-DTPA, are delivered in intervals of 500 s. The concentration of polymer is expressed as the mass of the repeat unit (unit mol/L).

Data analysis and processing to provide ITC and enthalpy change (ΔH) profiles is carried out using the NanoAnalyze (TA instruments) and the OriginPro software.

2.3 NMR

¹H NMR spectra are recorded at 25 °C with Varian Agilent NMR spectrometer operating at 600 MHz to observe chemical interactions between polymer and chelating agent (DTPA). The NMR samples consisted of water solution of HA-DTPA at different molar ratios (HA/DTPA ranging from 0 to 0.5), with 10% v/v D₂O.

Diffusion-ordered NMR Spectroscopy (DOSY) are also performed and the z-gradient strengths (Gz) is varied in 20 steps from 500 to 32500 G/cm (maximum strength). The gradient pulse duration (δ) and the diffusion delay (Δ) are kept constant, 2 ms for δ and ranging from 7 to 1000 ms for Δ . After Fourier transformation and baseline correction, DOSY spectra are processed and analysed using Varian software VNMRJ (Varian by Agilent Technologies, Italy) in order to obtain the values of water self-diffusion coefficient.

2.4 Differential Scanning Calorimetry

For all measurements the HA/water solution ($M_w = 42$ kDa) is used. The aqueous solutions are prepared in a concentration range of polymer 0.3–0.7% w/v. Next, Gd-DTPA is added as CA at different molar ratio HA/Gd-DTPA (from 1:0.25 to 1:3) and stirred for 12 h. The hydrated polymer samples, with and without CA, are sealed at room temperature in a Tzero hermetic pans prior to analysis. DSC measurements are performed in a TA Instruments' Q20TM calorimeter on samples between 5 and 10 mg. The samples are cooled down from 25°C to -50°C followed by heating scan up to 25°C. The same heating and cooling rate are 10°C/min for all runs. Samples are tested in triplicate to ensure reproducibility. For DSC and ITC measurements, we used low molecular weight HA (42 kDa) to highlight better the energetic contributions of different components without exceeding the maximum scale of the instruments.

2.5 Time-Domain Relaxometry

The spin-lattice relaxation times (T_1) are measured in a Bruker Minispec (mq 60) bench-top relaxometer operating at 60 MHz for protons (magnetic field strength: 1.41 T). Measurements are taken at 37°C, and before NMR measurements, the tube is placed into the NMR probe for about 15 min for thermal equilibration. Experiments are made using water solutions of Gd-DTPA (from 0 to 0.1 mM) and HA (0.3, 0.5 and 0.7% w/v) crosslinked with DVS (DVS/HA weight percentage ratio equal to 1:8). T_1 values are determined by both saturation (SR) and inversion recovery (IR) pulse sequences. The relaxation recovery curves are fitted using a multi-exponential model. Relaxivities, r_1 , are calculated from the slope of the regression line of $1/T_1$ [s^{-1}] versus concentration [mM] with a least-squares method.

3. Results and Discussion

3.1 Diffusive mixing time in Hydrodynamic Flow Focusing approach

The polymer conformation can be modified by the affinity with the solvent solution^{113, 114}. Furthermore, the addition of a solute can still induce a change in the polymer conformation. In our previous work, we proved that the relaxivity of CAs can be modulated combining them with macromolecules or polymers⁹⁸. Therefore, the understanding of the interaction between polymers and CAs in aqueous solution could be critical to tune the relaxometric properties of CAs. We aim to show how the presence of the Gd-DTPA in the aqueous solution can influence the behaviour of the polymer matrix and, on the other side, how these adjustments of the polymer conformation can govern the characteristic correlation times of the Gd-DTPA^{41, 43, 98}.

To investigate thermodynamic interactions between polymer and contrast agent, HA and Gd-DTPA respectively, are selected to be tested by Isothermal Titration Calorimetry (ITC). We aim to take advantage of the molecular interactions that are accompanied by some level of heat exchange between the interacting system and its surrounding medium; indeed, these interactions can be evaluated, at constant temperature, through the ITC. Basic principles of this technique have been widely discussed elsewhere^{115, 116}

Titration experiments are conducted injecting a solution of Gd-DTPA in the ITC cell containing the polymer solution. Different HA concentrations, ranging from 0.3 to 0.7% w/v, are tested and more representative results are reported in Figure 1 (peaks above the baseline represent exothermic phenomena while peaks below the baseline represent endothermic phenomena). It is clear that significant enthalpy variations are obtained in the titration experiments (Figure 1A-C) and can be associated with the water-mediated interaction between the Gd-chelate and the polymer, which induces changes in polymer chains' conformation. Since Figure 1A-C show ITC thermograms varying the HA concentration in the sample cell, a wide range of Gd-DTPA/HA molar ratios is examined and the relative energetic contribution and enthalpy values are calculated by integrating peaks of the experimental curves and are reported in Figure

1D. Simple dilution of Gd-DTPA in water (Figure 1 bis) exhibits only small constant exothermic peaks over the whole experiment.

In Figure 1, it is worth noting that the energetic contribution decreases as the Gd-DTPA/HA molar ratio increases; thus, the higher is the concentration of HA in the sample cell, the higher is the Gd-DTPA concentration needed to observe endothermic peaks. It can also be observed that the endothermic contribution exceeds the exothermic one at the recurrent Gd-DTPA/HA ratio approximately equal to 0.5 through all the experiments at different HA concentrations in the sample cell. It means that a specific energetic contribution is needed to induce the adjustment of the polymer conformation. Then, when the Gd-DTPA/HA molar ratio equals 0.5, the endothermic peaks start slightly increasing until reaching a plateau, which corresponds to the thermodynamic equilibrium established within the ternary system (polymer-CA-water). The measured energetic variation reflects the conformational changes of polymer chains due to the presence of the CA in solution and leads to the formation of stable sub-domains in which a balanced exchange of water molecules occurs between the polymer, the CA and the bulk.

The attainment of this thermodynamic equilibrium derives from a water-mediated interaction occurring between HA and Gd-DTPA. As both hydrophilic components, HA and Gd-DTPA interact with the water by forming hydrogen bonds and by coordinating water molecules. This competitive behaviour generates a measurable heat that reflects the change in polymer chains conformation and the exchange of bound water molecules with the bulk, thereby, bringing the system to a more stable configuration. In our previous paper⁴³, we preliminary showed how this equilibrium is able to affect the relaxometric properties of the system, as an effect of the new concept of *Hydrodentivity*, which will be further explained in the following paragraphs.

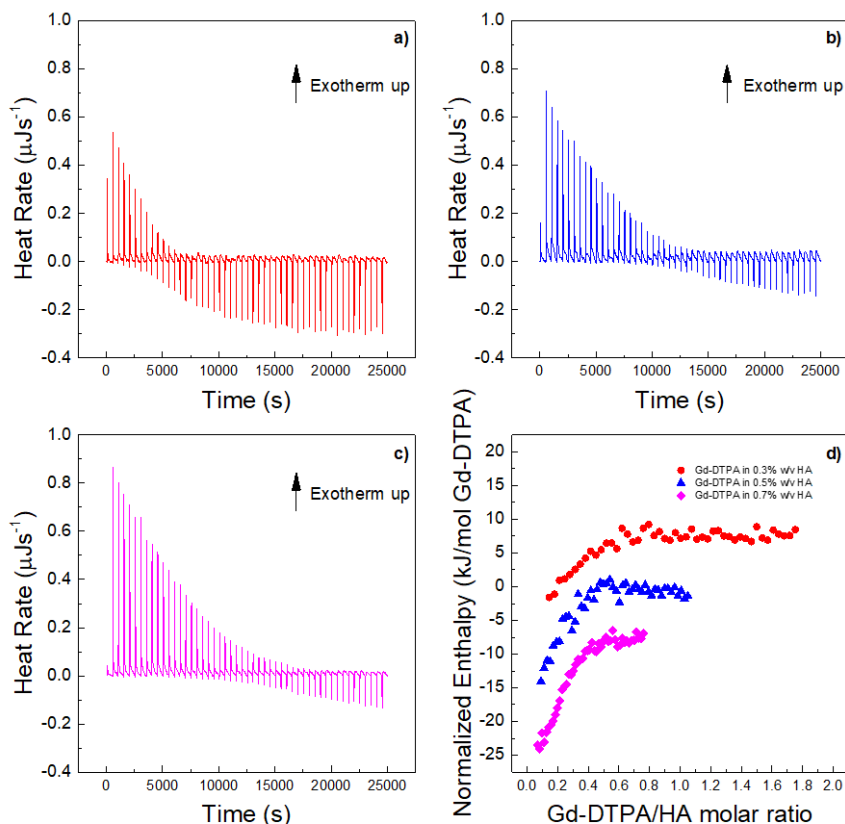


Figure 1. Titration curves of Gd-DTPA into aqueous polymer solutions at 25 °C. Calorimetric traces (heat flow against time) for (a) 0.3% w/v HA, (b) 0.5% w/v HA and (c) 0.7% w/v HA. In (d) it is reported the normalized enthalpy vs Gd-DTPA/HA molar ratio for Gd-DTPA in 0.3% w/v HA (red circles), in 0.5% w/v HA (blue triangles) and in 0.7% w/v HA (magenta diamonds). The curves were shifted vertically for clarity; y-offset were set at 2 (red circles), 0 (blue triangles) and -10 (magenta diamonds).

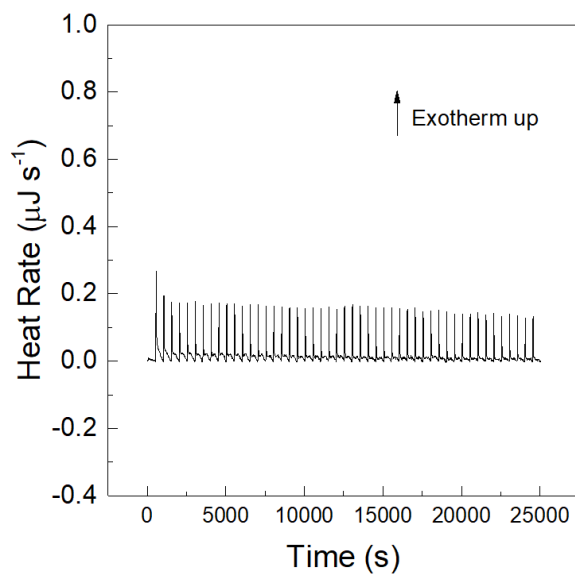


Figure 1 bis. Titration curve of Gd-DTPA solution injected into water at 25 °C.

3.2 NMR study of DTPA interactions and water mobility in polymer solution

Since previous ITC measurements reported by Gouin et al.¹¹⁷ have shown no binding energy between free Gd^{3+} ions and HA, we hypothesize that polymer conformational changes are mainly induced by the presence of the chelating macromolecule, DTPA. NMR spectroscopy is used to confirm this hypothesis. NMR spectra are calculated for HA and DTPA solutions. We use only the DTPA without the metal ion since we are mostly interested in examining interactions between the polymer and the chelating macromolecule.

Considering the spectra of the only DTPA and HA (Figure 2A-B), whose characteristic peaks are circled in blue and red respectively, the observations of DTPA/HA solutions at different molar ratios are reported (Figure 2C-I). The molar ratio ranges from 2 to 100 and is obtained by decreasing the HA concentration from 150 to 10 μM .

In Figure 2, it can be observed that the characteristic DTPA peak at 3.50 ppm (s, 2 H, CH_2-COOH) is influenced by the presence of HA in solution. In fact, it seems to shift and reduce its intensity far more than the other peaks by increasing the HA concentration. As an example, the shift is evident by comparing Figure 2I, where the DTPA peak is highlighted in blue, with Figure 2C, where the signal is dramatically reduced.

It results that an interaction between the two components of the system exists and generates changes in the NMR spectrum of the solution.

Through NMR-DOSY, instead, we investigate how the presence of both HA and Gd-DTPA can affect the mobility of water molecules.

Figure 3 shows the normalized time-dependent self-diffusion coefficient of water in both polymer solutions (Figure 3A) and polymer-CA solutions (Figure 3B). For short diffusion delays, the measured self-diffusion coefficient D is nearly equal to the free self-diffusion coefficient D_0 of water at 25°C ($2.5 \cdot 10^{-9} \text{ m}^2/\text{s}$), since the molecules travel over a short distance and only few of them feel the surrounding macromolecules. As the diffusion time increases, more water molecules go through these restrictions and the self-diffusion coefficient reaches a plateau value.

We can hypothesize that the presence of Gd-DTPA compete with those HA-molecular sites beared by water molecules and that are responsible for polymer hydration and hydrogel formation. As highlighted with ITC results, the polymer conformation can be modified by the presence of Gd-DTPA, which could interplay with the water molecules and with the formation of hydrogen bonding. NMR-DOSY measurements are carried out to assess these hypothesized changes in water mobility. It can be observed that, in the case of the ternary system, the diffusivity of water beyond decreases, suggesting that the polymer-CA combination affects the water mobility more than the polymer itself.

Figure 3A clearly shows that the water diffusion behaviour is affected by the polymer concentration. In particular, the diffusion coefficient decreases at increasing polymer concentration. Besides, Figure 3B shows the additional contribution of the CA to the water mobility. In fact, the presence of Gd-DTPA, even at relatively low concentrations (5 - 30 μM), can further reduce the value of the water self-diffusion coefficient for both short and long diffusion times.

It is worth noting that low Gd-DTPA concentrations are chosen (Figure 3B) because Gd-DTPA is highly paramagnetic and it can interfere with NMR measurements^{118, 119}, while the HA concentrations (0.1 - 3% w/v) are slightly higher than those used in the ITC experiments to highlight and make more evident the differences in diffusion behaviour between samples. In particular, as illustrated in Figure 3B, a fixed polymer concentration of 1% w/v is selected to show the effect of CA on the diffusion of water molecules.

A data comparison between ITC and NMR spectra confirms the hypothesized fundamental properties behind the concept of *Hydrodentivity*: the ability of Gd-DTPA to induce changes in polymer conformation and in water mobility.

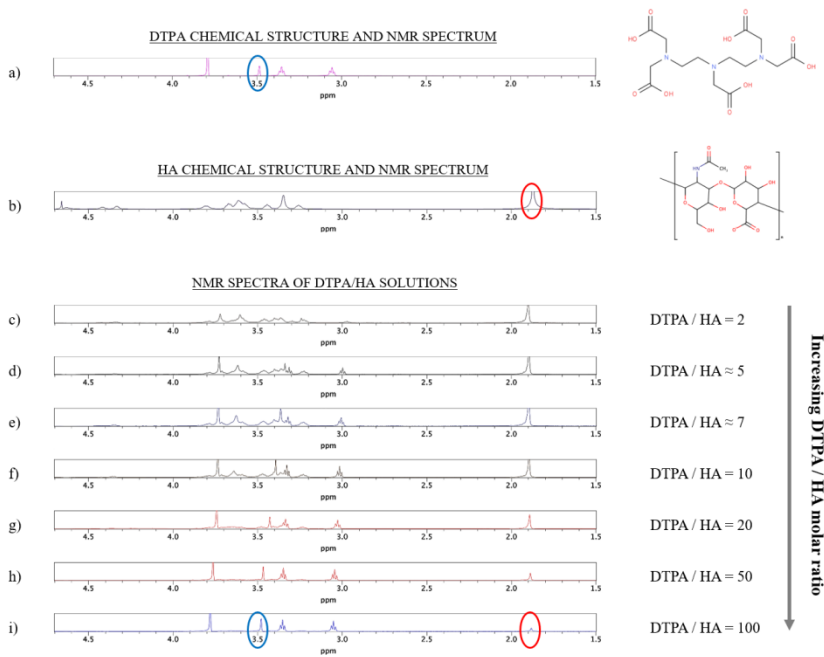


Figure 2. (a) ^1H NMR spectrum and chemical structure of DTPA; (b) ^1H NMR spectrum and chemical structure of DTPA; (c – i) ^1H NMR spectra of DTPA/HA solutions at different molar ratios, from DTPA/HA = 2 to DTPA/HA = 100. Characteristic peaks of DTPA and HA are highlighted in blue and red respectively.

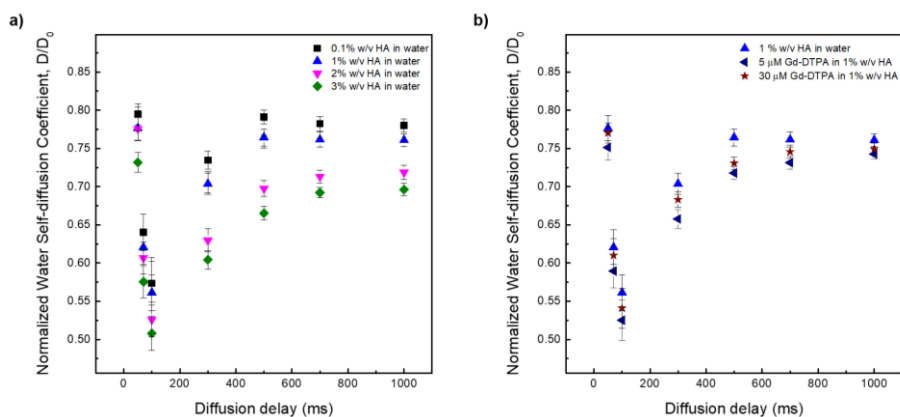


Figure 3. (a) Normalized time dependent water self-diffusion coefficient in 0.1% w/v HA (squares), 1% w/v HA (triangles), 2% w/v HA (flipped triangles), 3% w/v HA (diamonds). (b) Normalized time dependent water self-diffusion coefficient in 1% w/v HA (triangles), 5 μM Gd-DTPA in 1% w/v HA (flipped triangles) and 30 μM Gd-DTPA in 1% w/v HA (stars).

3.3 Water dynamics within hydrated polymer matrix containing Gd-DTPA

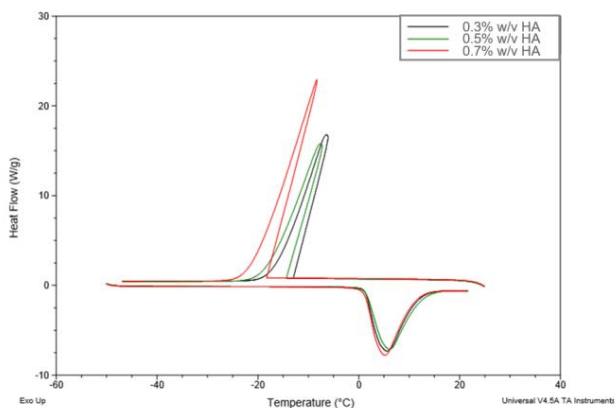
To analyse further the role of water mobility in the *Hydrodenticity*, a study of the dynamics and behaviour of water molecules is needed. Within hydrated polymer matrices (hydrogels), containing metal chelates, water molecules mediate polymer-CA interactions and, therefore, play a dual role: on one hand, the amount of absorbed water^{120, 121} and its interaction with the hydrogel structure affects the chain motion of the hydrophilic polymer; on the other, the mobility of water molecules in the polymer matrix is responsible for the relaxometric properties of the CA.

We investigate the water dynamics in water-HA systems, with and without Gd-DTPA, using the Differential Scanning Calorimetry (DSC). We focus on the thermal effects that the polymer (Figure 4A) and the CA (Figure 4B) have on the water dynamics. According to the literature, indeed, the crystallization of water changes with the polymer concentration and with the hydration degree¹¹¹.

In Figure 4, thermograms of water-polymer systems at different HA concentrations (0.3 - 0.7% w/v) are displayed. We can observe that, during the cooling phase, the crystallization peaks shift to lower temperatures and lower enthalpy values. As expected, the enthalpy, given as the peak area, reaches its maximum value at the highest HA concentration (0.7% w/v).

Figure 4B shows a comparison of melting (T_m) and crystallization (T_c) temperatures between HA solutions with and without Gd-DTPA (concentration range: 60 - 200 μ M). It can be noted that the transition properties remained unaffected in presence of the CA, suggesting that the influence of the polymer on the thermal behaviour of water is predominant with respect to the CA at the selected concentration.

a)



b)

Sample	Concentration	T _c (°C)	ΔH (J/g)	T _m (°C)	ΔH (J/g)
Gd-DTPA	60 μM	-7.47	218.7	5.37	249
	100 μM	-8.36	245.0	6.52	255
	140 μM	-8.00	239.7	5.36	266
	200 μM	-9.27	238.6	5.17	269.9
HA	0.3% w/v	-6.40	243	5.62	260.8
	0.5% w/v	-7.72	248.4	6.05	253.3
	0.7% w/v	-8.31	239.2	5.21	270
HA + Gd-DTPA	0.3% w/v + 60 μM	-9.73	229.1	7.94	255.1
	0.5% w/v + 100 μM	-7.88	244.9	6.47	273.0
	0.7% w/v + 140 μM	-6.24	254.5	5.02	259.0

en

Figure 4. (a) DSC thermograms of HA at different concentrations (0.3, 0.5 and 0.7% w/v). (b) Melting (T_m) and crystallization (T_c) temperatures for free Gd-DTPA in water and HA solutions with and without CA.

represent a threshold for the maximum effect of the hydrogel on the Gd-DTPA relaxation mechanism.

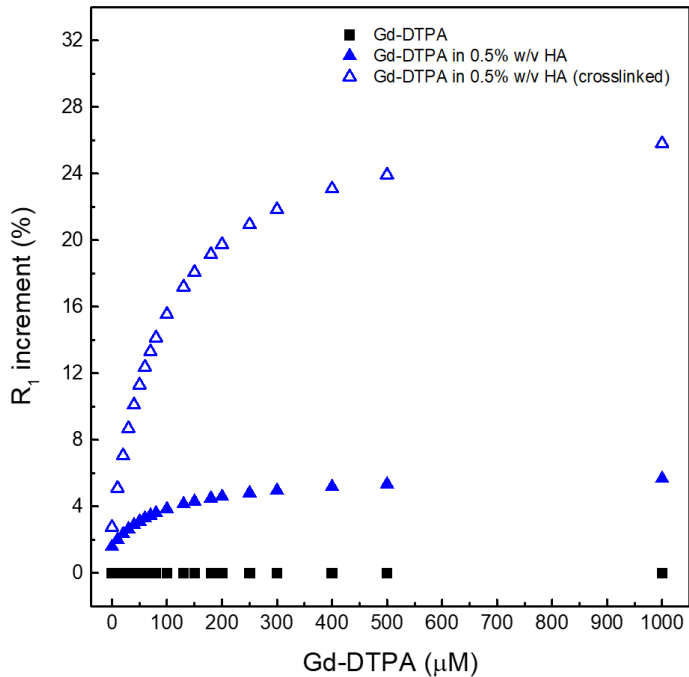


Figure 5. Increment in longitudinal relaxation rate, R_1 , at different contrast agent concentrations (from 0 to 1 mM) for: free Gd-DTPA in water (black squares); Gd-DTPA in 0.5% w/v HA solution (blue filled triangles); Gd-DTPA in 0.5% w/v HA crosslinked with DVS (blue empty triangles). The R_1 increment is calculated in percentage with respect to the corresponding R_1 of Gd-DTPA in water. A fast increment in R_1 is observed until a Gd-DTPA concentration equal to 300 μM . For higher Gd-DTPA concentrations, the R_1 increment reaches a plateau.

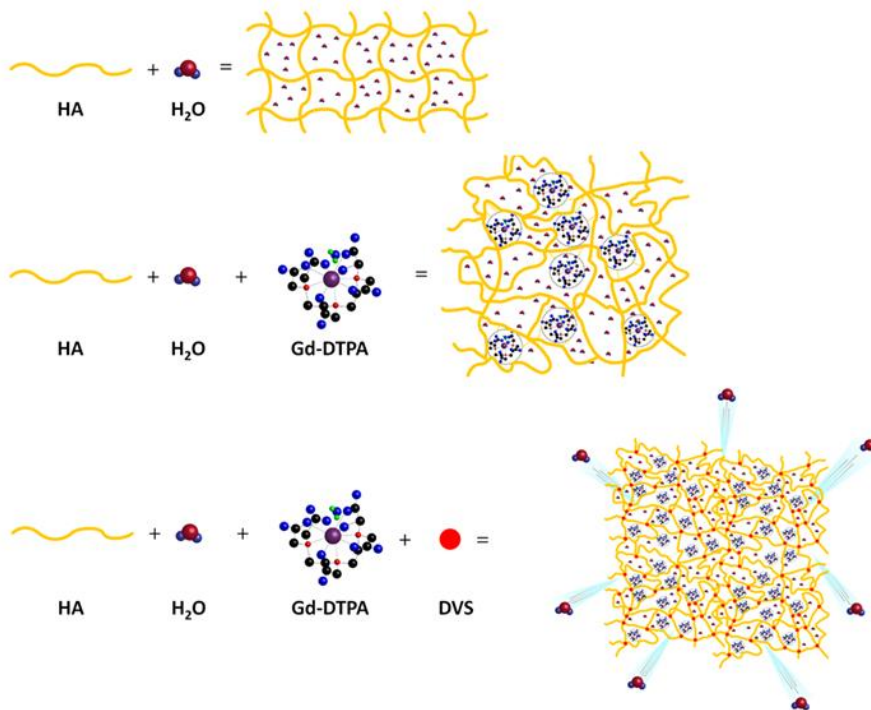


Figure 6. Formation mechanism affects hydrogel network structure: schematic representation of: formation of a hydrogel of hyaluronic acid in water (top); complex HA-Gd-DTPA structure (middle); crosslinked hydrogel network containing the contrast agent (bottom).

Figure 6 displays a schematic representation of the hydrogel network formation, even in presence of the crosslinking agent, and its influence on the polymer conformation. We hypothesize that the boosting of Gd-DTPA relaxivity in a hydrogel matrix is due to a proper complexation between the polymer and the CA in solution, mediated by the water and further amplified by the addition of a crosslinker. It is confirmed that the reached equilibrium among osmotic pressure and elastodynamic forces of the polymer meshes and hydration degree of the CA in the matrix are able to tune finely the relaxometric properties of the metal chelates in the ternary system. The overall ensemble of these phenomena is defined as *Hydrodentivity*⁴³.

4. Theory of the gado-mesh formation

This work reports the use of polymer hydrogels for boosting the relaxivity of clinical relevant CAs.

Results show that a spontaneous complexation exists between HA and Gd-DTPA due to thermodynamic interactions as demonstrated by both calorimetric and NMR measurements. It is already known that, in an aqueous polymer solution, solvent affinity can alter polymer conformation by inducing a local solvation of the structure that influences the number of available conformations of the polymer chains. Moreover, the introduction of another soluble ionic component, such as Gd-DTPA, in the system can induce further changes in polymer conformation, detectable via diverse thermodynamic approaches¹²²⁻¹²⁵. Based on our findings, we prove for the first time that these conformational changes, induced by the metal chelate, contribute to an increase in CA's relaxivity.

In order to tune the MRI enhancement, we exploit the versatile structural characteristics of HA. In fact, the high porosity of the hydrogel, which shows a mesh-like structure, is controlled by varying the density of covalent crosslinking^{126, 127}. Moreover, the presence of negatively charged groups and the degree of crosslinking

influence water adsorption capacity and, thus, the relaxometric properties of the ternary system¹⁰⁶.

Therefore, the presence of the hydrogel matrix can greatly amplify the magnetic properties of the encapsulated Gd-DTPA, suggesting a strong outer-sphere and second-sphere contribution to the relaxivity.

Based on these observations, we hypothesize that increased relaxivity is mainly related to the creation of water domains or clusters (water compartments) around the CA within the polymer matrix. In fact, biopolymer systems contain intermolecular cavities that can be considered as molecular nano-domains in which various self-assembly processes can be implemented in principle¹²⁸. The formation of peculiar structures within these cavities can be associated with thermodynamic transitions and it is a characteristic of many metallopolymeric systems^{129, 130}.

The sub-nanostructures, here defined “Gado-meshes”, are generated from a three-way interaction between HA, Gd-DTPA and water. The entrapment of the CA inside the hydrophilic matrix of HA results in a reduction of the rotational tumbling rate, due to an increase of the effective viscosity of the aqueous solution into the hydrogel matrix. At the same time, multiple CA-water interaction pathways occur between the exchangeable protons of the water molecules coordinated by the CA and the other water molecules freely moving within the hydrogel mesh or bonded to the polymer chains^{93, 105, 131}.

Our “Gado-mesh” consists of highly relaxing Gd-water compartments spontaneously generated within the hydrogel matrix by the combination of these multiple physico-chemical interactions. The so created nanostructure is composed of different water layers departing from the polymer chains that surround the Gd-molecules. It is known, in fact, that hydrated polysaccharides, such as HA, are characterized by the presence of multiple water layers, contiguous regions of variable water density within a polyelectrolyte solution¹³², differing in their physical properties depending on the distance from the polysaccharide chain¹³³. The hydration process of HA generates: the “bound water layer”, which is the water fractions closely associated with the polymer matrix; the “unbound water layer”, made by the water molecules which are not directly

interacting with the polymer; and the “free water layer”, which resembles dynamics of pure water. In addition, the developed polymer network can be dependent not only on the water layers organization but also on other solute species, such as Gd-DTPA, altering the bound water layer with non-negligible effect on the HA conformation and dynamic ¹³⁴. In the “Gado-mesh”, Gd-DTPA has a competitive behaviour with the respect of HA, similar to the cation shielding of the HA due to the presence of salts ¹³⁵, and interposes itself between the water molecules around the HA, altering the bound water layer and generating water compartments with high MRI enhancing properties. The “Gado-mesh” influences the τ_R , τ_D and τ_M times through the action of the *Hydrodentivity*, whose effect is magnified by the crosslinking. *Hydrodentivity*, hence, refers to the status of the hydrated Gd-DTPA with the coordination water subjected to osmotic pressure deriving from elastodynamics equilibrium of swollen gels ^{43, 136-141}. We hypothesize that the attainment of this equilibrium is reached when the normal energetic stability of the meshes is compromised by the presence of the Gd-DTPA and evolves to a new spontaneous equilibrium involving the formation of nanocompartments, so called “Gado-Meshes”, in which water is in an abnormal aggregate state that influences the relaxivity. Water molecules in the hydrogel matrix that are subjected to the effect of *Hydrodentivity*, are able to change their water dynamics and can mediate the hydrogel conformation and the physical and relaxometric properties of the metal chelate.

5. Conclusion

The properties of *Hydrodentivity* and its application to the nanomedicine field is reported. The explanation of this concept take place through several key aspects underlying biopolymer-CA's interactions mediated by the water. A multidisciplinary approach is used: changes in polymer conformation and thermodynamic interactions of CAs and polymers in aqueous solutions are detected by isothermal calorimetric (ITC) measurements and later, these interactions are investigated at molecular level using NMR to better understand the involved the phenomena. Water molecular dynamics of

these systems is also studied by means of Differential Scanning Calorimetry (DSC). In order to observe relaxometric properties variations, it is monitored the MRI enhancement of the examined structures over all the experiments.

The study of polymer-CA solutions reveals that thermodynamic interactions between biopolymers and CAs could be used to improve MRI Gd-based CA efficiency.

In conclusion, this work proves that a new generation of more efficient CAs can be developed by exploiting the affinity between CAs and biopolymers. It can be done using biocompatible and clinical relevant CAs without their chemical modification as approved in the clinical practice.

CHAPTER II

Hyaluronic Acid Nanoparticles: water-mediated nanostructures for enhanced MRI

1. Introduction

Conventional drug preparations suffer from certain limitations like high dose and low availability, instability, and so on. As indicated in introduction section, an ideal nanocarrier for drug delivery applications should fit the following profile: biodegradable and biocompatible, able to recognize the target site, optimal biophysico-chemical properties for drug loading, long circulation time, favorable therapeutic index and amenable to cost-effective scale-up for commercialization. The incorporation of these properties in one nanocarrier is the primary objective of nanomedicine³¹.

In recent years, the scientific research has focused on biopolymers, biomolecules that are produced by living organisms (green plants, animals, bacteria and fungi)¹⁴². Characteristics such as biocompatibility, biodegradation and non-cytotoxicity make these material excellent candidates to be used in biomedical applications, in particular, to the development of therapeutic and diagnostic carriers.

The main biopolymers used in biomedical field are collagen, chitin, chitosan (CS) and hyaluronic acid (HA)¹⁴³.

HA, in particular, has been extensively investigated in drug delivery applications, especially with the aim to treat cancer^{88, 144}. As is well known, this is a biocompatible, biodegradable, non-toxic and non-inflammatory linear polysaccharide with high molecular weight made of repeating disaccharide units of D-glucuronic acid and N-acetylglucosamine linked by $\beta(1,4)$ and $\beta(1,3)$ glucosidic bonds^{88, 145}. In physiological condition, it is widely distributed in extracellular matrix in the form of a sodium hyaluronate and shows negative charge¹⁴⁵. In addition, due to its high capacity in retaining water, HA-based hydrogels are promising materials not only for tissue engineering but also nanomedicine¹⁴⁶. Its short lifetime, however, necessitates chemical modifications and physical processing to improve its stability and maintain native biological functions^{147, 148}. Physically crosslinked hydrogels have the advantages of forming hydrogels without the addition of crosslinking agents, but they also have limitations in terms of pore size, chemical functionalization, and degradation time. Chemical crosslinking, instead, allows to realize a 3D-network with desirable

mechanical properties based on the nature of the chemical reagents and controllable degradation time¹⁴⁹. An example of chemical crosslinking agent is represented by divinyl sulfone (DVS), which reacts with hydroxyl group on the backbone of HA to create intramolecular and intermolecular network¹⁵⁰⁻¹⁵².

Thus, chemically crosslinked networks have permanent junctions and these modifications can be introduced to provide a biomaterial with the desired functional properties¹⁴⁵. In addition, the use of these biopolymers on nanoscale size allows further to optimize their properties depending on the specific application. In the end, in order to achieve the properties of interest, the mode of preparation plays a vital role and different techniques are currently available for HA-based micro- and nano- particles production. Among them, emulsification process has been greatly exploring¹⁵³. Many products based on emulsions are widely used in pharmaceutical field as precursors to prepare carriers for diagnostic and drug delivery applications. Several scientific works report particles based on HA, prepared by water-in-oil (W/O) emulsion process, where the reaction take place within the aqueous droplets (containing HA) that are dispersed in a continuous organic phase with the aid of oil-soluble surfactants¹⁵⁴.

Yun and colleagues, for example, produce HA crosslinked microspheres (5–20 μm) for gene delivery application using a W/O microemulsion system as template, DVS as the crosslinker and an isooctane as continuous phase^{155, 156}.

Different hydrophilic HA NPs, instead, have been obtained using a diamine, 2,2'(ethylenedioxy)bis(ethylamine), for cross-linking of the HA linear chains^{157, 158}.

In addition, also radical polymerization of HA (methacrylate groups are added to HA to obtain HA-glycidyl methacrylate conjugates) in an inverse emulsion of water in hexanes is made¹⁵⁹. Then crosslinked HA particles (200–500 nm) are prepared dispersing the aqueous solution of thiolated HA in hexanes containing a surfactant mixture composed by different emulsifiers, such as Span 65, Span 80, and Tween 80. In this case, the resulting particles are loaded with siRNA and selectively endocytosed by cells expressing CD44 receptors on the surface. The release of siRNA in intracellular environment allow to silence the target genes¹⁶⁰.

Further nanogels based on HA have been obtained by photochemical crosslinking of polymer confined in nanoemulsion¹⁶¹. HA chains, containing polymerizable methacrylate groups, are confined within W/O emulsion where the water droplets act as nanoreactors of the photopolymerization process mediated by UV. Subsequently, intravenous docetaxel (DCT) delivery have been realized by Cho et al.¹⁶². In this case, HA conjugated with ceramide and Pluronic 85 (P85) give self-assembled nanoparticles (140 nm). In particular, P85 is added to provide stability to the micellar structure¹⁶³, in fact, this copolymer is known for its low micellization and solubilization capacity to hydrophobic drugs. Thus, this type of delivery system depends on the copolymer type¹⁶². However, taking into account that the residues of oil and surfactant are prohibited for medical treatment and, often it is difficult to completely remove these components from the final product, production processes without the use of oil and surfactant are performed by Fakhari and colleagues¹⁶⁴. They synthesize crosslinked HA NPs via carbodiimide chemistry. In this case, EDC activates carboxyl groups available on HA and provides reactive intermediates (O-acylisourea derivatives) that react with two primary amines of adipic acid dihydrazide, forming a peptide bond resulting in the neighboring HA chains being chemically cross-linked.

Then, two sequential additions of acetone are performed to break the strong hydrogen bonding between HA chains and HA-water molecules to release carboxyl groups for the cross-linking reaction is reached. After the consumption of carboxyl groups by adipic acid dihydrazide, the cross-linked HA polymer chains become less soluble (hydrophilic) inducing transformation from coils to globules.

As described in the Chapter I, several scientific works have been demonstrated that the polymer architecture affects some characteristic parameters of the metal chelate and tunes its relaxometric properties^{40, 43, 92, 103-105}. In fact, rational design of a new class of CAs, based on biopolymers (hydrogels), have received considerable attention in MRI diagnostic field and several strategies have been adopted to improve relaxivity without chemical modification of the commercial CAs.

Moreover, it is clear that crosslinked biopolymers can have a significant role to overcome the limitations of clinically relevant CAs without their chemical

modification and as a compound in the design of advanced nanostructures with improved safety profile and switchable relaxometric properties. Indeed, it is known that the functional properties as well as the swelling behaviour of hydrogels are influenced by the hydration degree, which can be likely modulated by changing the chemical composition of the system¹⁰⁶⁻¹¹².

In this context, HA⁸⁸ is chosen and used as a model polymer because of its biocompatibility and high hydrophilicity and, the acquired knowledge about polymer-CA interaction (see Chapter I) is applied to the concept of *Hydrodenticity* in order to obtain Gd-based polymer NPs with enhanced relaxometric properties.

Here, it is reported a method based on single emulsion system (w/o) which has been developed to prepare HA-based NPs with a well-defined structure for MRI applications. The polymer chains are confined in the aqueous droplets of a water-in-oil nanoemulsion and crosslinked by chemical reactive (DVS) in the droplets as nanoreactors. The control of emulsion size distribution and stability are obtained by a careful choice of the emulsion composition and emulsification process. The conditions of the crosslinking reaction are modulated by changing the concentration, time of reaction and modality of addition of the DVS. The properties of the resulting NPs are analyzed using a combination of chemical-physical technique.

2. Experimental Section

2.1 Materials

All chemicals used are of analytical reagent grade quality and are employed as received. Sorbitan monooleate (Span[®] 80) (S80), Polyoxyethylenesorbitan trioleate (Tween[®] 85) (T85), Mineral oil (light oil, 0.8 gr/cm at 25°C), Divinyl sulfone (DVS, 118.15 Da), Diethylenetriaminepentaacetic acid gadolinium(III) dihydrogen salt hydrate (Gd-DTPA, 547.57 Da), Sodium hydroxide pellets (NaOH), Acetone and Ethanol are purchased from Sigma Aldrich Chemical (Italy). Sodium Hyaluronate, with an average molecular weight of 850 kDa (purity 99%; Hyasis[®] 850P) and 42 kDa, is respectively supplied by Novozymes Biopharma and Bohus Biotech (Sweden) as dry powder and used without purification.

Magnevist[®] (Bracco Imaging, Italy), a contrast agent commercially available, is used in this study. The water is purified by distillation, deionization, and reverse osmosis (Milli-Q Plus) and systematically used for sample preparation, purification and analysis. All experiments are repeated in triplicate and conducted at room temperature, 25°C.

2.2 Emulsion preparation

The emulsions are prepared at different water to oil (W/O) ratio (10/90 and 20/80 v/v). Mineral oil is used as oil phase (or continuous phase, P_C) and W/O emulsions are made by varying the concentration of surfactants for the P_C and water phase (or dispersed phase, P_D) and the concentration of NaOH (from 0 to 0.2 M) for the P_D in order to obtain emulsion systems. In particular, a pair of non-ionic surfactants, Span-80 (S80) and Tween-85 (T85), are used to prepare mixtures with a range from 4.3 to 7.65 of HLB values. Depending on the initial HLB to be used, mixtures of S80 and T85 are pre-dissolved in the appropriate S80/T85 mass ratios (from 50/50 to 75/25) in P_C and P_D, respectively. P_D containing T85 and NaOH, is added dropwise to P_C and W/O emulsions are prepared using a high-shear homogenizer (Silverson L5M-A, Silverson

Machines Ltd, Waterside, UK). Homogenization of the Emulsion is performed from 5000 to 7000 rpm for 10 min at room temperature (25°C).

2.3 Temporal emulsion stability determination

The stability of emulsions is evaluated, at regular time intervals, by visual observation, measuring the height of the phase separated by creaming in centimeters as a function of the time. In addition, an optical characterization of emulsion stability made is using a Turbiscan (Turbiscan LabThermo) by static multiple light scattering (MLS), sending a light beam from an electroluminescent diode ($\lambda=880$ nm) through a cylindrical glass cell containing the sample. The emulsion sample without dilution is placed in a cylindrical glass cell and two synchronous optical sensors receive the light transmitted through the sample (180° from the incident light) and the light backscattered by the droplets in the sample (45° from the incident light). The optical reading head scans the height of the sample in the cell (about 40 mm), by acquiring transmission and backscattering data every 40 μm . Transmitted and backscattered light are monitored as a function of time and cell height for a period of 24 hours at an interval of 30 min at 25°C.

2.4 Preparation of DVS-crosslinked nanoparticles

Based on these preliminary results, P_D/P_C ratio in all samples is set at 10/90 v/v. In particular, for the preparation of cross-linked NPs, HA powder ($M_w = 850$ kDa) is dissolved at different concentrations (from 0.1 to 0.5% w/v) under alkalyn condition (NaOH ranging from 0 to 0.2 M) by vigorous stirring at room temperature for 4 hours until a homogenous solution is obtained. Mineral oil and S80 (from 0.5 to 2% w/v) are separately mixed by stirring. P_D is added drop-wise in the P_C without stirring and all the components are completely mixed by homogenization at various times (5-15 minutes) and speeds (5000 - 7000 rpm). Then, the cross-linking agent (DVS) is added to the final emulsion (40 ml), which is kept in agitation on a laboratory tube rotator for 24 hours in order to obtain a homogeneous DVS distribution in the P_D . To test DVS activity, various conditions of crosslinking reaction are explored: (1) at different DVS concentrations (from 0.01 to 0.5% v/v); (2) at three starting times of reaction

(beginning, during and post homogenization) and (3) at different temperatures (4 and 25°C).

The best experimental conditions for production of crosslinked HA-NPs are reported in Table 1.

Pd / Pc ^{a)}	HA ^{b)} [% w/v]	NaOH [M]	DVS ^{c)} [% v/v]	Span-80 [% w/v]
10 / 90	0.1	0	0.045	1
		0.1		
		0.2		
	0.25	0		
		0.1		
		0.2		
	0.5	0		
		0.1		
		0.2		

^{a)} Pd is the volume of the disperse phase, Pc is the volume of the continuous phase; ^{b)} Hyaluronic Acid; ^{c)} Divinyl Sulfone

Table 1. Experimental conditions for production of HA-NPs

2.5 Loading of HA NPS with Contrast agents

After identifying the protocol to obtain NPs, Gd-DTPA is chosen as CA and mixed in the P_D before homogenization. Gd-loaded HA NPs (HA-Gd NPs) are prepared using different HA/CA mass ratios (1:1, 1:2 and 1:5). DVS are added post homogenization to the batch at room temperature using the same procedure reported above.

2.6 Collection of the nanoparticles

Recovery of the NPs and their separation from W/O emulsion system is made using dialysis and/or ultracentrifugation. For dialysis method, the obtained emulsion is placed in a pre-washed cellulose membrane tubing (Spectra/Por[®] Dialysis Tubing, cut-off of 25 kDa). Organic impurities (Mineral oil and S80) are removed dialyzing first against solvents as acetone and/or ethanol, and gradually against water. Dialyzing solutions are changed at regular time intervals. In the case of ultracentrifugation, 1 ml of the emulsion is added to 5 ml of ethanol and mixed for 2 hours. Then, this mix is centrifuged with an ultracentrifuge (Beckman-Coulter OPTIMA MAX-XP) at 55000 rpm for 20 min at 15°C. The resulting pellet is washed twice and resuspended in MilliQ water. The second step of ultracentrifugation (70000 rpm, 10 min, 15°C) is applied to the pellet in order to obtain purified NPs.

2.7 Characterization of the nanoparticles

The chemical modifications of polymer by DVS are identified by infrared spectroscopy (Thermo). The characteristic peaks for DVS are: 1310 cm⁻¹ (S=O asymmetric stretching vibrations), 1130 cm⁻¹ (S=O symmetric stretching vibrations) and 794 cm⁻¹ (S-C stretching vibrations) and through the ether bond at 1255 cm⁻¹ (C-O-C stretching vibrations).

To determine size distribution of NPs, dynamic light scattering (DLS) are performed using a Zetasizer S-90 1000 HS (Malvern Instruments, UK).

All samples are diluted (1:10) with deionized water to prevent the effects of multiple scattering. The measurement temperature is set at 25°C. The morphology and size of NPs are investigated using a ULTRA PLUS field emission Scanning Electron microscope (FE-SEM Carl Zeiss, Oberkochen, Germany) and a Transmission Electron

microscopy (TEM, TECNAI). In the first case, the samples are coated with gold (7 nm).

2.8 Determination of Gadolinium loading by ICP-MS

The quantitative determination of loaded Gd in HA NPs is assessed by ICP-MS (NexION 350, Perkin Elmer) without any previous digestion processes. For all examinations, purified NP suspensions are used. The non-encapsulated Gd-complexes are separated from the NPs by high speed centrifugation (55000 rpm, 20 min, 15 °C).

2.9 MRI Testing

To explore the potential of Gd-loaded HA NPs as MRI contrast agent, MRI in vitro test is performed at two different magnetic fields, 1.5 T and 3 T MR (Philips Achieva) using Sense Head 8 coil. The T1-weighted MR images of HA NPs, unloaded and loaded with Gd-DTPA at different concentrations using an inversion recovery sequence are measured with the following parameters: TR = 2500 ms; TE = 12 ms; TI = 50, 100, 200, 400, 800, 1100, 1800 ms; FOV= 180x146 mm; slice thickness = 4 mm, acquisition matrix = 360x292.

The signal intensity of the samples is measured on the obtained T1-weighted MR images and compared to Gd-DTPA.

2.10 NMR dispersion measurements

The proton $1/T_1$ NMRD profiles are measured using a fast-field-cycling Stellar SmarTracer relaxometer over a continuum of magnetic field strengths from 0.00024 to 0.25 T (which correspond to 0.01 - 10 MHz proton Larmor frequencies). The uncertainty of these measurements is less than 1%. Additional data points in the range 15 - 70 MHz are obtained using a Stellar Relaxometer and a Bruker WP80 NMR electromagnet adapted to variable-field measurements (15 - 80 MHz proton Larmor frequency).

2.11 In vivo tests and cytotoxicity evaluation of HA-based Nanoparticles

After excluding the toxicity in vitro, animal experiments are carried out and, a total of 9 mice (body weight about 20 g, C57 - Balb/c mice model) are used. Unloaded and

loaded HA NPs are prepared using physiological saline solution and Magnevist® is used as control. In each solution, the final Gd concentration is the same.

The NPs formulations (final volume: 200 µl) are injected into the tail veins of mice. All studies are performed with mice under general anesthesia, obtained with an intraperitoneal injection of tribromoethanol solution at a final concentration of 12.5 mg/mL and administered at a dose of about 250 mg/kg. Once anesthetized, mice were prepared for venous cannulation by bathing the whole tail in tap water warmed at 39 °C to obtain proper vasodilation. A lab-made catheter, consisting of a 30 G needle mounted on a polyethylene tube, is delicately advanced in one of the lateral caudal veins, until blood could be seen in the tube. Hence, two-three drops of surgical glue were spilled on the needle /tail interface area and let dry. The tube is flushed with 20 µL of a heparinized solution and the tip of the tube is closed to avoid further bleeding. The mice are then positioned on magnetic compatible bedding within a head coil and the baseline acquisition was performed. Then, 200 µL of the CA solution are slowly injected, following any eventual reaction of the mouse or any change in the respiratory pattern. Acquisition are performed every 10 minutes till one hour post injection, and then after 3, 6, 8 and 24 hr.

Images are taken using the PET/MRI 3T Siemens instrumentation applying an Inversion Recovery (IR) sequence (*VOF= 100x75 mm; slice thickness=1.2 mm without GAP, contiguous slice, acquisition matrix=192x144; Averages: 6; Turbo spin-echo; Sequence duration: 10 minutes -36 seconds; Signal to Noise Ratio: 1; Spatial Resolution: 0.5 x 0.5; TR: 550; TE: 11*). A basal acquisition has been conducted for all subjects before the injection protocol. The DICOM files of each acquisition were stored on an external unit. The files were imported in dedicated software for imaging analysis (OsiriX© Lite, Pixmeo SARL, Bernex, Switzerland). A circular region of interest (ROI) of about 2 mm² is drawn and then saved, to be used in the analysis of all images. The anatomic areas studied are: renal cortices and medullas, the urinary bladder, the salivary glands. The mean intensity obtained for each organ (IO) is normalized to the mean muscle intensity (IM) applying the formula: $IO_{norm} = IO/IM$,

and the result was used to calculate the percentage of contrast enhancement (% CE) according to Corbin et al.¹⁹⁰ $\% \text{ CE} = (I_{\text{post}} - I_{\text{pre}}) / I_{\text{pre}} * 100$.

After the MRI scans, in order to analyze the quantitative distribution of the HA NPs in vivo, the mice are sacrificed at different time points (2 hr, 4 hr, 24 hr, 48 hr and 40 days) after injection. The blood, heart, spleen, lungs and liver are collected and immediately washed twice with physiological saline solution. Experiments have been repeated in triplicate. Quantitative analysis has been made by digesting and homogenizing the organ with nitric acid at 100°C for at least 3 hr. Later, NPS are resuspended in a solution of deionized (DI) water at a concentration of 150,000 particles/mL. All data are collected and processed using the Syngistix Nano Application Module.

3. Results and Discussion

3.1 Case study: production of polymer particles based on Hydrodenticity

Recent recommendations from Food and Drug Administration (FDA) and European Medicine Agency (EMA) about the Gd deposition in the brain and other tissues have highlighted the importance to design polymer biocompatible NPs with enhanced relaxivity without chemical modification of the clinical relevant CAs^{28, 165}. Thus, crosslinked NPs formed by HA, a biodegradable, biocompatible, non-toxic, non-immunogenic and non-inflammatory linear polysaccharide¹⁶⁶, could represent a successful candidate among nanovectors for MRI applications³⁸. Indeed, in the last decades, it is undisputed the growing research interest toward the therapeutic action of HA and in developing new diagnostic tools based on this polymer³⁸. In this work, starting from the above-presented results, we aim to apply the *Hydrodenticity* in the design of biocompatible hydrogel nanostructures to obtain improved relaxometric properties. We propose a concrete example of the concept of *Hydrodenticity* applied to the production of crosslinked HA NPs for MRI, loaded with Gd-DTPA. An emulsion-based method is used to obtain stable W/O nanoemulsions as templates.

3.2 Study of emulsion stability

Stable W/O emulsions are prepared by stirring appropriate amounts of oil phase (Mineral oil) and aqueous phase containing different concentrations of Span-80 (S80) or S80 with Tween-85 (S80/T85). The pH, ranging from 12 to 14 is adjusted by adding appropriate amounts of NaOH from a stock solution (0.2 M). Further details are reported in the Materials and Method Section. As expected, in the absence of any surfactant, W/O emulsions prepared in the same conditions split very rapidly in two phases due to their unfavourable thermo-dynamic state. Visual comparison, turbidimetry and backscattering are successfully used to study emulsion stability (Figure 7 and 8) ¹⁶⁷.

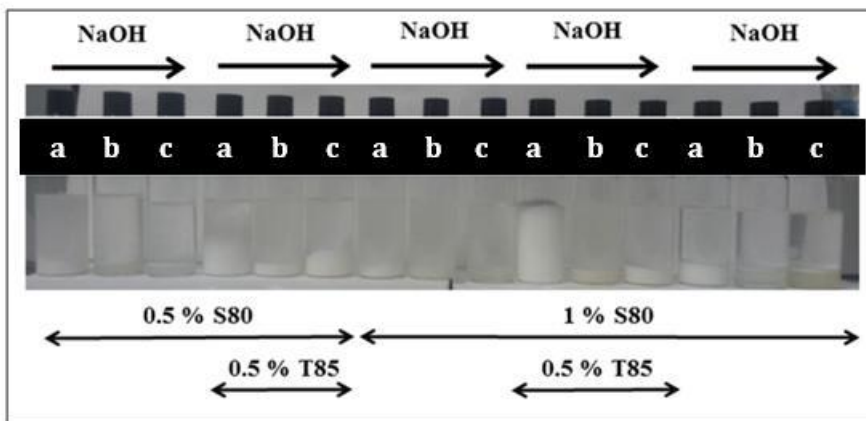


Figure 7. Photographic image of the appearance of emulsions at 25 °C by the effect of increasing concentration of surfactants and NaOH [(a) 0 M; (b) 0.1 M; (c) 0.2 M] on stability of W/O (10/90 and 20/80) emulsion after 12 h.

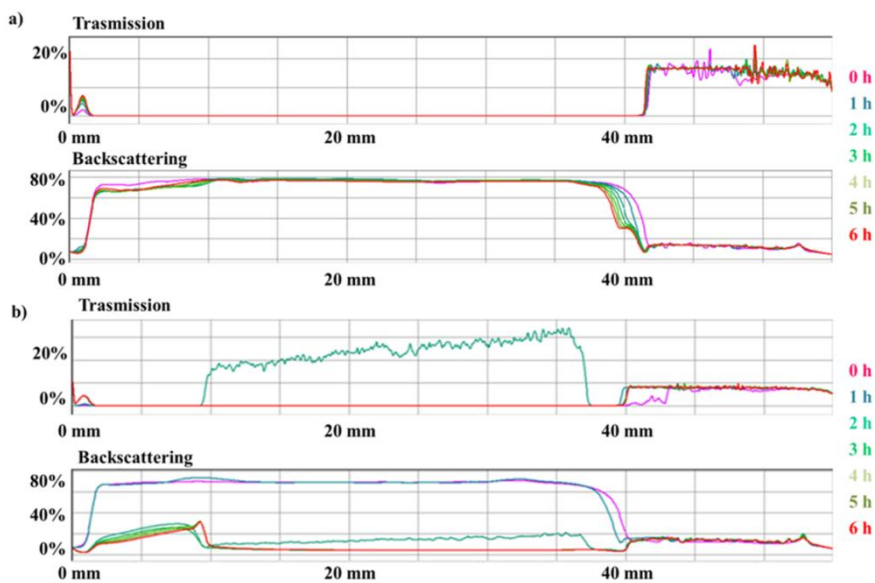


Figure 8. Transmission and backscattering spectra of W/O (10/90) emulsion (total volume, 20 ml; 5000 rpm, 10 min) with 1% w/v of S80 without (a) and with (b) 0.2 M NaOH.

Comparing emulsions obtained at different W/O ratio, 10:90 and 20:80, but at same concentration of surfactant, the stability is more extended for emulsions with lower water content. In particular, a formulation 10/90 W/O volume ratio containing S80 (1% w/v) and T85 (0.5 % w/v) resulted the more stable. However, even though the stability of the emulsion is crucial to reduce polydispersity, an alkaline environment (addition of NaOH) is necessary for the crosslinking reaction to take place. Indeed, Balazs and Leshchiner¹⁶⁸ showed that the crosslinking reaction starts shortly after addition of DVS (5 - 10 min) and, that, 1 hour is sufficient for the completion of the reaction.^{169, 170} On the basis of these requirements, to conduct the experimental campaign, we select the formulation with S80 (1% w/v) and NaOH (0.2 M) as the optimal trade-off to obtain an emulsion stable for at least 3 hours (Figure 7 and 8), enough for the DVS to react.

3.3 Preparation of DVS-crosslinked nanoparticles with and without CA

The exploitation of the best process conditions to design biocompatible nanostructures based on *Hydrodentivity* and control their relaxation parameters for MRI application is reported. In particular, the effect of the homogenization, HA concentration and the role of the crosslinking reaction is analysed. Different experimental parameters and conditions are tested and details are reported in the Materials and Methods section. A preliminary mixing is performed at 5000 or 7000 rpm for 10 min, by keeping constant the temperature at 25 °C. A 5000 rpm speed is preferred to avoid and uncontrolled increasing of the temperature.

After the homogenization, a crosslinking reaction is performed at high pH values (12 - 14) and creates sulfonyl bis-ethyl linkages between the hydroxyl groups of HA¹⁷¹. This crosslinking method has the advantage of occurring at room temperature, which limits the degradation of HA in alkaline solutions. Even though the starting material DVS is highly reactive and toxic, the biocompatibility of the HA-DVS hydrogels are confirmed by histological analysis¹⁷².

In our protocol, a study of the modalities of injection of the crosslinking agent at different steps of the homogenization process has shown that only when DVS is added after the homogenization step spherical NPs are obtained. On the contrary, when the

addition of the crosslinker is performed at any time point during the homogenization phase, a shear stress behavior of the polymer phase, interfering with the formation of that particles, is observed (Figure 9).

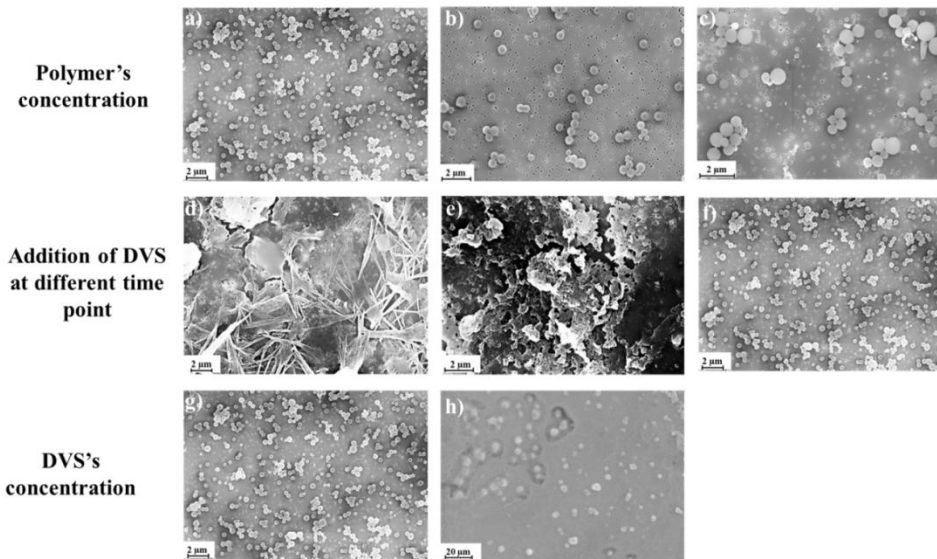


Figure 9. Optimization of HA NPs synthesis. SEM images of crosslinked nanoparticles (0.5% w/v HA; 18 μ L (0.045% v/v) of DVS; 40 mL of W/O (10/90) emulsion; 5000 rpm, 10 min, RT, using high-shear homogenizer) under various conditions: **HA's concentration**, (a) 0,5% w/v; (b) 0,25% w/v and (c) 0,1% w/v. **Start of reaction**, (d) during, (e) end and (f) after homogenization. **DVS's concentration**: (g) 18 μ L and (h) 200 μ L (0.5% v/v).

The best experimental condition for production of crosslinked NPs is reached at 0.045% v/v DVS (Table 1).

Based on these results and using the same process conditions, loaded NPs are obtained by adding the CA in the water phase of the emulsion. Among several FDA approved CAs, we have chosen to encapsulate a Gd chelated, Gd-DTPA (9.13 mM).

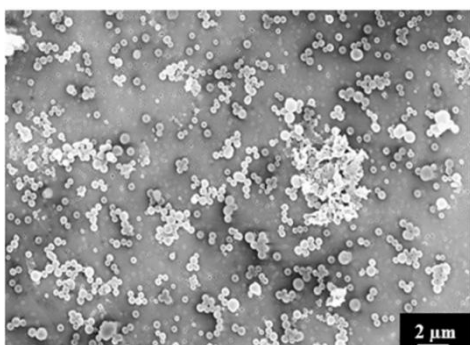
3.4 Purification and characterization of HA-NPs

Ultracentrifugation (UC) and dialysis are performed to purify HA NPs. Dynamic Light Scattering (DLS) measurements are made on aqueous dilute NP suspension (1:10). The smaller NPs' size without CA (217.57 ± 34.65 nm) is obtained at 0.25% w/v of HA solution. At higher polymer concentration (0.5% w/v) particle size is higher (401.67 ± 77.65 nm), while the formulation with 0.1% w/v HA shows a reverse phenomenon with larger particles (760.15 ± 86 nm), probably due to less stability of the nuclei that tend to coalesce. When Gd-DTPA is added to the process, the particle size at HA 0.25% w/v is slightly increased (258.77 ± 15.65 nm) for the same process conditions. After purification, NPs are investigated by electron microscopy techniques (SEM and TEM). The morphology of the NPs observed revealed that the particles are spherical in shape and monodisperse (Figure 10).

In addition, to confirm that the crosslinking reaction is successfully completed, IR analysis are performed. The chemical modifications of HA are identified in IR spectra of the HA NPs by the presence of characteristic peaks for DVS that appear between 1384 and 1280 cm^{-1} , which are attributed to the sulfone group ($\nu\text{SO}_2=1350, 1310 \text{ cm}^{-1}$).

Loading Capability (LC) and Encapsulation Efficiency (EE) is determined through ICP-MS by comparing the theoretical amount initially used to prepare the particles and the Gd encapsulated in the system after ultracentrifugation. The higher encapsulation results for 0.25 % w/v HA (1:2 w/w HA/Gd-DTPA ratio). Results show that probably ionic nature of Gd-DTPA impacts on its encapsulation. The zeta potential value of the 0.25% HA-NPs, with and without CA, indicate that they had a negatively charged surface (-37.4 ± 1.34 mV and -31.8 ± 0.88 mV, respectively), due to the carboxylic group of HA.

a)



b)

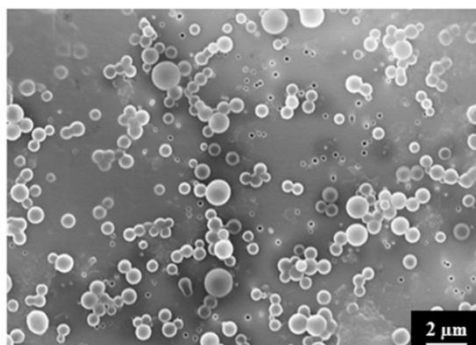


Figure 10. SEM images of crosslinked HA nanoparticles (0.5% w/v of HA; 1% w/v of S80; 0.045% v/v of DVS) without (a) and with (b) contrast agent.

3.5 Relaxivity studies

T1 and T2 measurements at 60 MHz (1.5 Tesla) and 120 MHz (3 Tesla): Relaxivity and relaxation times are measured for both unloaded and loaded NPs and compared with free Gd-DTPA solution. Measurements are performed on a 120 MHz (3 Tesla) MRI system and on a 60 MHz (1.5 T) benchtop relaxometer.

Relaxivity results obtained at 120 MHz are presented on a per millimolar Gd basis in Figure 11a and show a maximum r_1 of 33.3 s-1mM⁻¹ (i.e. 10 times higher compared to free Gd-DTPA). Even though all the proposed formulations of Gd-DTPA-loaded HA nanostructures show an increase of the r_1 signal, as reported in Figure 11a, the highest boosting of the relaxivity is provided by the NPs obtained using the formulation at 0.25% HA and 1:2 w/w HA/Gd-DTPA (Figure 11 A-C).

T1 relaxation time distributions at 37°C and 60 MHz are investigated for loaded and unloaded NPs (HA at 0.25% w/v) as well as for free Gd-DTPA solution (Figure 11 D). Compared to the 200 μM free Gd-DTPA solution, which shows a broad distribution around 1000 ms, NPs loaded with 200 μM Gd-DTPA exhibit an excellent T1 distribution with a sharp peak centered below 500 ms. Gd concentration within loaded NPs was determined through Inductively Coupled Plasma Mass Spectrometry (ICP-MS).

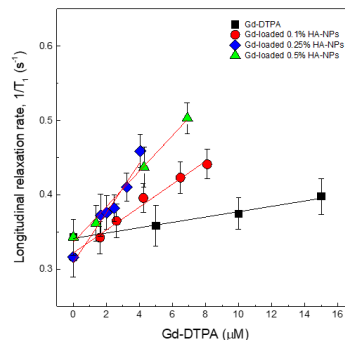
Loaded NPs perform far better even compared to the unloaded ones, whose distribution appears to be broad and centered around 2800 ms.

It is worth mentioning that, compared to T1 distribution for bulk water (3600 ms), unloaded NPs' distribution shows that a slight contribution to the longitudinal relaxivity is ascribable to the crosslinked polymer nanostructure, which is able by itself to tune the water mobility for a non-nanostructured material. The contribution, therefore, to the overall relaxivity is further enhanced in the ternary system, thanks to the water-mediated interaction between the polymer and metal chelate.

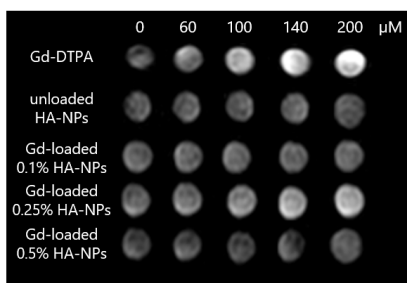
a)

Sample	r_1 [mM ⁻¹ s ⁻¹]
Gd-DTPA	3.59 ± 0.27
Gd-loaded 0.1% HA-NPs	15.4 ± 1.081
Gd-loaded 0.25% HA-NPs	33.3 ± 3.908
Gd-loaded 0.5% HA-NPs	23.9 ± 1.296

b)



c)



d)

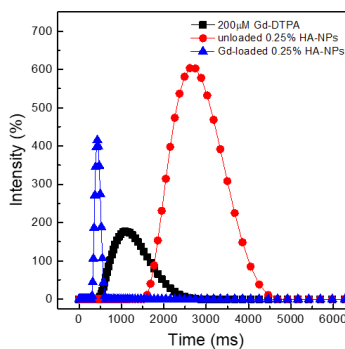


Figure 11. (a) Relaxivity values r_1 determined at magnetic field strengths of 3T for different set of HA-NPs with respect to free Gd-DTPA in water. (b) Longitudinal relaxation rate ($1/T_1$) versus Gd-DTPA concentration for free Gd-DTPA in water and for HA-NPs at different polymer concentrations loaded with Gd-DTPA. (c) T1-weighted images of Gd-DTPA, unloaded (used as control) and HA-NPs at different polymer concentrations loaded with Gd-DTPA. All samples are imaged at 3T, 25°C, using standard spin echo (SE) sequence. (d) Distribution of longitudinal relaxation times of (T_1) of 200 μ M Gd-DTPA in water (squares), unloaded 0.25% HA-NPs (circles) and 0.25% HA-NPs loaded with 200 μ M Gd-DTPA (triangles).

3.6 Modeling of NMR dispersion: NMRD profile

The NMRD profiles as function of the static magnetic field of the aqueous solutions of Gd-DTPA and loaded and unloaded NPs (Figure 12) are set up in order to establish the effects caused by Hydrodentcity functionalities on the parameters that determine the observed relaxivities. The longitudinal relaxation rates are recorded at 37°C as a function of resonance frequency and according to NP Gd-loading obtained by ICP-MS. The NMRD experimental curve for free Gd-DTPA shows a plateau in longitudinal relaxivity at low fields and significantly decreases as the applied magnetic field increases starting from 1 MHz. Conversely, longitudinal relaxivity (r_1) for loaded NPs (HA at 0.25% w/v) is characterized by the presence of a low-field plateau and a gradual increase starting from 10 MHz, reaching a “dispersion peak” between 60 and 70 MHz. The same peak and trend in the high field region (20 – 70 MHz) is observed for both at 25°C and 37°C. As a control, unloaded NPs do not exhibit increase in relaxivity in this field region, confirming that the nanohydrogel structure containing Gd-DTPA contributes to slowing the chelator's tumbling motion and allows water exchange thanks to its hydrophilic properties, as hypothesized in the concept of Hydrodentcity.

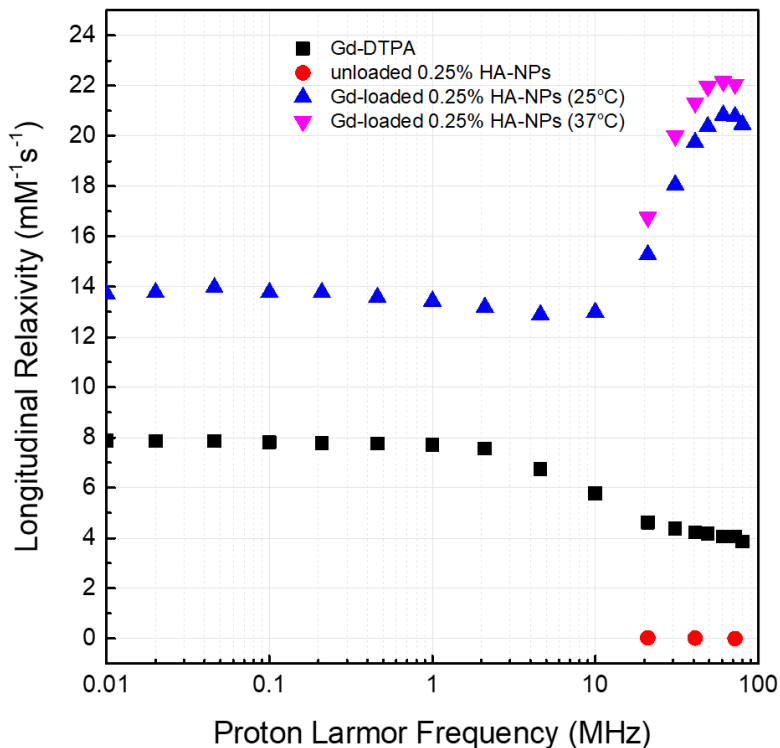


Figure 12. NMRD profiles showing relaxivity of Gd-DTPA in water (squares), unloaded 0.25% HA-NPs (circles), Gd-loaded 0.25% HA-NPs at 25°C (triangles) and 37°C (flipped triangles).

3.7 In vivo analysis and cytotoxicity evaluation of HA NPs

In vivo MRI analysis has been conducted on 3T MRI instrumentation for all subjects before the injection protocol as reported in the experimental section.

Figure 13 and 14 show the coronal view MRI images of a mouse (C57 - Balb/c murine model) injected with CA (Gd-DTPA, 800 μ M) and loaded HA NPs (99 μ M) respectively.

It is no observed adverse effects during the experiments and, considering the renal excretion of the CA, the kidney appear lighter than other tissues. In particular, the bladder becomes lighter after 6 min from injection and remains high to 1 h. After this time, the signal strength of the whole mice body tends to the normality.

In the case of loaded HA NPs injection, the signal intensity in the kidney immediately increases. The enhanced signal intensity is detectable after 3 min and remains visible to 1 h after intravenous injection.

It is also important to notice that MRI signal in the kidneys, in the case of loaded HA NPs compared to the free CA, has the higher persistence (Figure 15).

The accumulation of the metal within the organs is measured by ICP-MS, after homogenization and digestion as reported in the Experimental Section of this chapter. Further evaluations are under investigation. These preliminary in vivo tests show there is an enhancement of the MRI signal and confirm the stability of HA NPs.

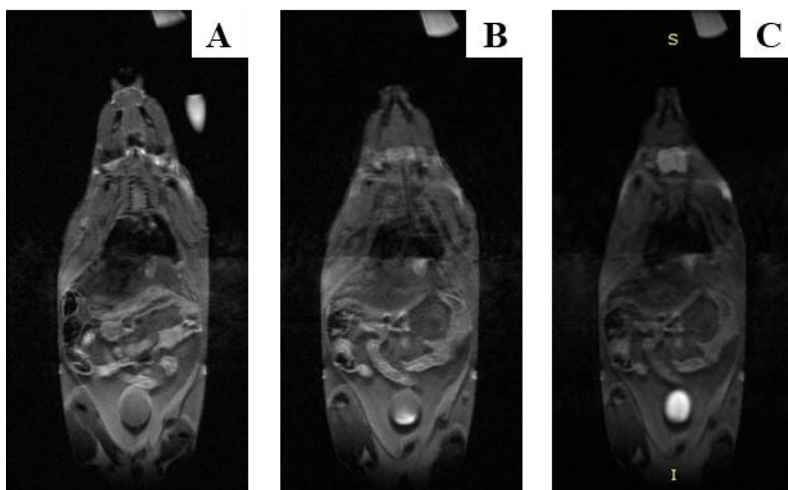


Figure 13. In vivo coronal view MRI images of a mouse after intravenous injection of Gd-DTPA (800 μ M). Qualitative Image Analysis for bladder at different time intervals: **A)** before injection of Gd-DTPA; **B)** after 6 minutes and **C)** after 30 minutes from injection of Gd-DTPA.

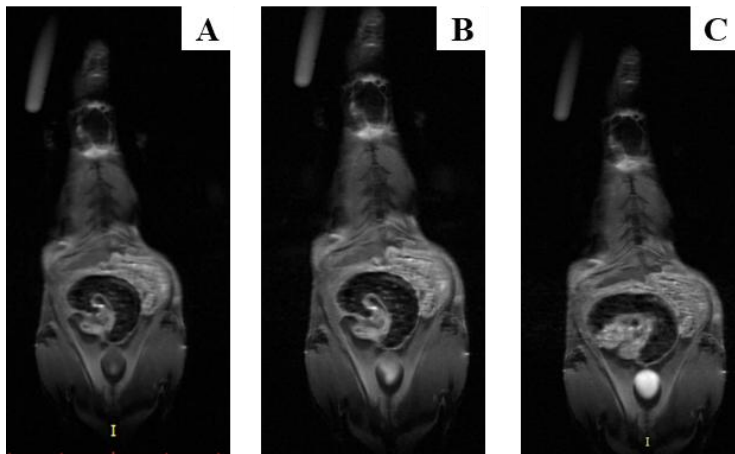
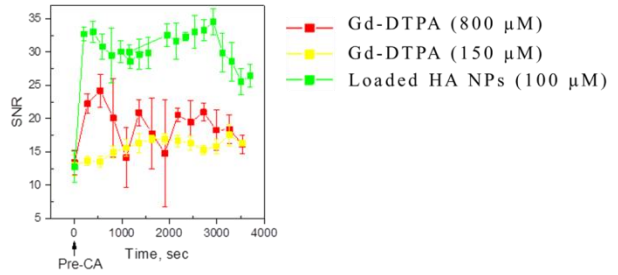
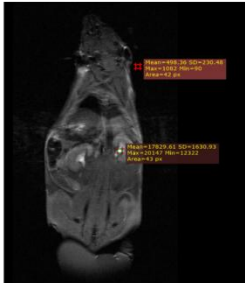


Figure 14. In vivo coronal view MRI images of a mouse after intravenous injection of loaded HA NPs ($99 \mu\text{M}$). Qualitative Image Analysis for bladder at different time intervals: **A)** before injection of loaded HA NPs; **B)** after 6 minutes and **C)** after 60 minutes from injection of loaded HA NPs.

Kidney



Bladder

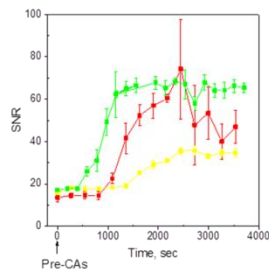
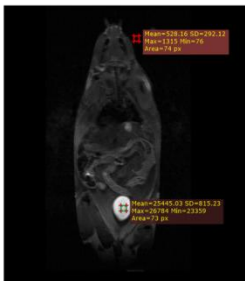


Figure 15. Biodistribution for kidney and bladder of CA and loaded HA NPs at different concentration after 1 h from injection.

4. Conclusion

The optimal conditions to combine a CA with a hydrophilic biopolymer are identified and applied to the nanoscale in order to produce nanostructures of biomedical interest with high relaxivity. In particular, stable crosslinked HA NPs encapsulating Gd-DTPA are successfully prepared using a method that exploits the use of W/O nanoemulsions as templates. The aqueous emulsion droplets are shown to provide a good environment for the formation of the NPs and seemed to limit efficiently their size. NPs collected from the emulsion droplets using a purification procedure showed a size of about 200 nm and spherical shape. The conditions of the herein presented protocol to produce these biocompatible NPs offer advantages for the encapsulation of a broad-spectrum of biomolecules and provide a potential synthetic route to design a wide range of highly efficient nanostructured MRI CAs, letting the surface available for possible functionalization. In conclusion, this work proves that a new generation of more efficient CAs can be developed. It can be done using biocompatible and clinical relevant CAs without their chemical modification as approved in the clinical practice. Furthermore, the size of the resulting NPs is in a range that makes them suitable for delivery to cells and certain tissues and further increase in relaxivity can be potentially achieved by tuning the system to the most efficient structure by choosing the correct biopolymer-CA combination and optimizing concentration and crosslinking degree of the structure. From a biomedical point of view, the possibility to tune relaxometric properties of CAs by controlling hydrogel structural parameters can pave the way to new advancements in the design of nanovectors for diagnosis and therapy. In addition, preliminary studies about toxicity, in vivo biodistribution and MRI acquisition highlight the powerful effect of the produced nanostructures for application in clinical imaging.

Despite the promising achievements, further studies are needed to carry out a deeper investigation and a full validation our intriguing hypothesis.

CHAPTER III

Functionalized HA NPs: the case study of a B-cell lymphoma.

1. Introduction

Cancer is the most common cause of death in industrialized countries¹⁷³ and, in certain cases, the patient remains asymptomatic. Actually, the choice of the right therapeutic approach is subject to an accurate and reliable diagnosis in order to identify the primary site of tumour and potential dissemination of the disease to distant sites in the body¹⁷⁴. In this context, diagnostic radiology and nuclear medicine studies play important roles in clinical management of cancer¹⁷⁵.

In particular, in the case of lymphoma neoplasms, which expression is variable, the diagnose from imaging is difficult¹⁷⁶.

In particular, lymphomas are lymphoproliferative diseases composed by malignant B and T cells, which arise predominantly in the lymphoid tissues during the course of normal development¹⁷⁷. The most common form of lymphomas, Non-Hodgkin Lymphomas (NHLs), can originate from T cells, or more frequently, very distinct malignancies like classical Hodgkin lymphoma (cHL) and multiple myeloma (MM) arise from B lymphocytes with various stages of differentiation. Therefore, the early detection of this pathology affects the therapy of patients¹⁷⁸.

The pivotal role of techniques such as CT and MRI are undoubtedly first-line modalities to be employed in patients affected by cancer. However, they rely on anatomical landmarks (i.e. morphological alterations due to the tumour) to identify tumour involvement and this leaves the clinicians with a grey area of cases that require further investigations (i.e. PET imaging)¹⁷⁹.

Conventional imaging with CT⁵, in the case of lymphoma, shows the technical limits of CT are: (1) limited accuracy at initial staging for assessing lymphoma in small nodes (< to 1.5 cm), bone marrow, or various extranodal sites; (2) inability to differentiate active disease within a residual mass; and (3) limited ability to assess early response to treatment although more aggressive, but also potentially more toxic treatment^{5, 180}. As a result of these limitations, several lesions seen on PET images may not be visible on CT examinations and, overall, PET examinations are more sensitive in these evaluation. In fact, unlike CT, which shows anatomic details, ¹⁸F-FDG PET

can play a significant role in the staging of patients with lymphoma¹⁸¹. In fact, high-grade tumours demonstrate greater metabolic activity (and greater ¹⁸F-FDG accumulation) than low grade tumours. Unfortunately, variable aggressiveness and makes it difficult to diagnose them from imaging. In addition, the future goal of imaging consists of optimal staging method for non-invasively lymphoma detection.

In this scenario, MRI is recently emerged for monitoring of pathological progression and evaluation efficacy of treatments^{3, 4, 182, 183}. MRI's susceptibility to artifacts of motion and organ pulsation means that it has certain limitations for the detection, for example, of lymph node metastases, particularly in the thorax and diaphragm region, leading to reduced diagnostic accuracy (79% to 82%). In addition, the lack of metabolic information in borderline large lesions ≤ 1 cm in diameter constitutes a disadvantage versus multimodal imaging in dignity assessment¹⁸⁴.

An interesting strategy to increase the degree of information resulting from the MRI analysis could be to associate CAs with nanovectors for diagnostic purpose. In fact, if designed appropriately, these nanovectors may act as a drug vehicle able to target tumor cells protecting the active molecules from inactivation during their transport. The physico-chemical characteristics (particle size, surface charge, surface coating, stability) of the NPs allow the redirection and the concentration of the marker at the site of interest. Indeed, nanovectors with ligand-decorated surface enhance selective cellular uptake ('active targeting')¹⁸⁵.

Currently, even if *in vitro* studies has received considerable attention in recent years the clinical translation of NPs remain laborious. In particular, MNPs functionalized with anti-CD20 antibodies, are made and tested on two murine cell lines. The results indicate that receptor recognition ability of the antibody (< 95%) is retained after conjugation with MNPs proving that anti-CD20-MNPs can be used for sensitive detection of cancer cells.

Kozłowska et al.¹⁸⁶, instead, synthesize liposomes loaded with Gd ions using different membrane-incorporated chelating lipids and functionalized with monoclonal anti-CD138 (syndecan-1) antibody for multiple myeloma and non Hodgkin's lymphoma diagnosis. In this case, the use of the polychelating amphiphilic polymer increases both

the Gd content and the longitudinal relaxivity of the Gd-loaded liposomes as compared to commercial CA (Gd-DTPA).

To selectively target site-specific markers, several approaches have been used, and among these, mimotopes are particularly interesting. Mimotopes are amino-acidic sequences that are able to mimic the three-dimensional structure of the original antigenic epitope¹⁸⁷. In addition, these molecules can be conjugated to a variety of nanostructures, as recently reported by Torino et al.¹⁸⁸, and act as vehicles for therapeutic and/or diagnostic agents with extreme specificity.

An example of mimotope is represented by peptide A20-36 (pA20-36) that binds the Ig-BCR of B-cell lymphoma (A20) cells¹⁸⁹.

In this context, the current section reports the use of biocompatible HA-based NPs, produced as indicated in Chapter II, that are conjugated with pA20-36 for in vitro and in vivo evaluations. In vivo experiments are performed in accordance with the European guidelines of the 2010/63/EU Directive on the protection of animals used in scientific studies, after Italian Ministry of Health approval, Protocol no. 49/2015-PR e n° 50/201.

2. Experimental Section

2.1 Materials

EDC (N-(3-Dimethylaminopropyl)-N'-ethylcarbodiimide, MW=191.70), NHS (N-Hydroxysuccinimide, MW=115.09), Streptavidin (1mg/ml), QuantiPro™ BCA assay kit, the WST-1 assay and Plasma from human P953 are purchased from Sigma Aldrich Co. Cy7-PEG1KDa-NH₂, and Fitc-PEG1KDa-NH₂ are purchased from Nanocs Inc. Peptide pA20-36 (amino acids sequence: EYVNCNLDLVGNCVIRG, MW=1922, 1 mg/ml) and peptide pA20-S (amino acids sequence: DQEWCKTISFEPCLN, MW=1067, 1 mg/ml) are purchased from CASLO ApS.

Polystyrene NPs are purchased by Thermo and used for PEG-FITC quantification.

2.2 Functionalization of HA NPs

The strategy of NPs functionalization provides the following steps: 1) chemical modification of HA NPs; 2) covalent binding of proteins (**Indirect Conjugation**) and/or peptides (**Direct Conjugation**); 3) formation of “HA NPs-Protein-Peptide” or “HA NPs-Peptide” conjugates; 4) characterization of the products and analysis of critical control points.

The reactions are schematically represented in figure 16.

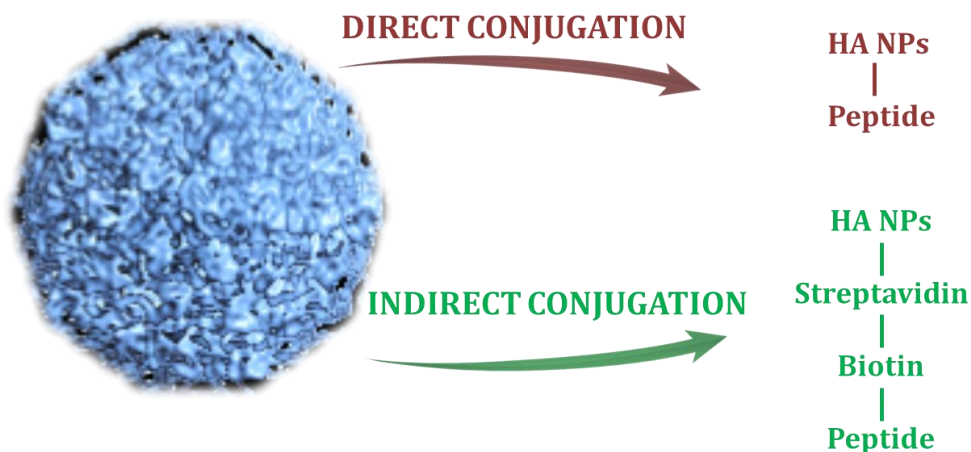


Figure 16. Representation of strategy to conjugate the NPs with selected peptides.

2.2.1 Quantification of carboxyl groups on the surface of crosslinked HA NPs

Back titration method is performed to directly quantify carboxylic groups on the surface of particles. 0.1 mg/ml of NPs are dispersed in NaOH solution (20 ml of 0.01 M) and HCl is used as the tritant agent. The molar concentration of carboxylic sites are obtained from difference in concentration at equivalent point between HCl and NaOH.

2.2.2 Direct conjugation of HA NPs

Unloaded and loaded NPs, produced as indicated in Chapter III, are centrifuged, collected and characterised by SEM analysis. The surface of the NPs has been activated using an amidation reaction with EDC (0.02 M) and NHS (0.01 M) for 10 minutes in water solution on rotary shaker¹⁴⁵. The peptides, pA20-S and pA20-36 (500µl), previously deactivated with TEA, is added directly to the reaction. Reactions are kept in agitation by a rotating shaker for 4 hours and, finally a further purification is carried out to remove the excess of peptides. The collected material is resuspended in PBS solution.

2.2.3 Indirect conjugation streptavidin-biotin-peptide

The surface of the NPs has been activated using an amidation reaction with EDC (0.02 M) and NHS (0.01 M) for 10 minutes in water solution on rotary shaker¹⁴⁵. Then, the samples are centrifuged at 70,000 rpm, 15° C, 10 minutes and the resulting pellets are resuspended in PBS solution.

Subsequently, the STR protein (1.5 mg/ml) is added and allowed to react overnight on rotary shaker. After removal of the excess reagents by ultracentrifugation method, the pA20-36 (150 µg/mL) to be conjugated is added to the resulting pellets. In addition, it is also tested the peptide A20-S as negative control and pA20-36 at the same concentration reported above of. The reaction is conducted for 4 hours on rotary shaker, and finally a further purification is carried out to remove the excess of peptides. The collected material is resuspended in PBS solution.

2.2.4 Bicinchoninic Acid Assay

The bicinchoninic acid assay (BCA assay, sensitivity: 0.5 µg/ml), also known as the Smith assay, is used for quantitation of total protein in a sample, in this case allows to measure the concentration of the peptide on the surface of the HA NPs. It is based on the principle that under alkaline conditions the copper Cu^{+2} ions form a complex with peptide bonds of proteins and are reduced to Cu^{+1} . In addition, the presence of a specific chemical compound (purple colour) allows to quantify the amount of protein present in the sample of interest. The intensity variation is determined by absorbance

spectrophotometer measurement at 562 nm (enspire Multimode Plate Reader PerkinElmer). 150 μ L of the HA NPs suspension are reacted with equal amount of working reagent solution and the mixture is incubated at 37°C for 2 h. The results are compared with a bovine serum albumin (BSA) calibration curve and the concentration value is then extrapolated by a straight line of calibration built using BSA samples of known concentration (0 - 40 μ g/mL). All measurements are performed in triplicate.

2.2.5 Cell Lines

A20 is a murine cell line derived from a spontaneously arising tumor in an aged BALB/c mouse. It pathologically mimics the characteristics of human diffuse large B-cell lymphoma²¹¹. The 5T33 murine myeloma (5T33MM) cells are used as control.

The cell lines are kindly provided by Prof C. Palmieri (University of Catanzaro, Italy). The cell lines are grown in suspension culture with Roswell Park Memorial Institute (RPMI) 1640 medium (Gibco), supplemented with 10% fetal bovine serum (FBS; Gibco), 50 units/mL penicillin, 50 μ g/mL streptomycin and 2 mM L-glutamine at 37°C in a 5% CO₂ atmosphere.

2.2.6 PEGylation

Moreover, direct PEGylation of NPs surface is obtained by the formation of an amide bond between the their -COOH groups and the -NH₂ end groups of the PEG, which is labeled with various fluorophores (ie. Cy7 or FITC). In particular, PEG1kDa or PEG2kDa labeled are used for these experiments.

The first step of process provides the activation of the carboxylic groups due to the contact between sample (500 μ L) and a solution of EDC (0.02 M) and NHS (0.01 M) for 10 minutes in water solution on rotary shaker. After this, a NH₂ -PEG-Dye (1 mg/ml) is added (4h, at RT, slight rotation). Two washing are carried out by ultracentrifugation (70,000 rpm, 15°C, 10 min) and, finally, the pellet is resuspended in a phosphate buffer (pH 6.8). The amount of PEG conjugated to NPs is determined by spectrofluorimetric (enspire Multimode Plate Reader PerkinElmer). All measurements are performed in triplicate.

3. Results and Discussion

3.1 Functionalization of HA NPs

Nanomedicine govern the ways in which engineered nanomaterials interact with human environment. In particular, the surface modification of the NPs play a key role in biomedical sciences. Several clinical results have suggested that the presence of specific recognition chemical moieties reduces not only the side effect, especially in oncological field, but also enhances the efficacy of nanovectors.

For this reason, here, it is reported an example of functionalization of loaded HA NPs with specific biomarker (pA20-36) for lymphoma target. In addition, a further bioconjugation, mediated by PEG, is explored.

3.1.1 Quantification of carboxyl groups on the surface of crosslinked HA NPs

The first step for the NPs functionalization is represented by evaluation of the number of -COOH groups presented on the surface of the NPs through the application of back titration.

In Figure 17 is showed the graphical representation of the equivalence point obtained by titration (HCl-NaOH). The results report that the presence of -COOH groups is about 26 nmol/ml of NPs solution.

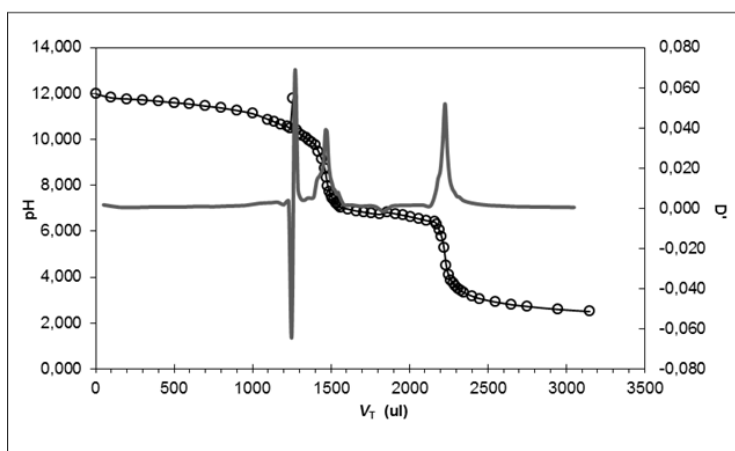


Figure 17. Representation of the equivalence point obtained by back titration.

3.1.2 Direct conjugation with peptide pA20-36 and pA20-S

In the case of direct conjugation with pA20-36 and pA20-S, the results show that HA NPs have maintained their stable morphology post reaction.

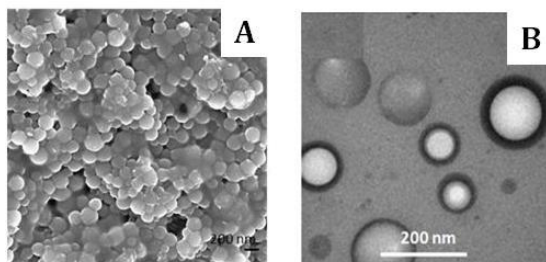


Figure 18. Morphological and Optical characterization of pA20-S-HA NPs. **A)** SEM characterization and **B)** TEM image.

3.1.3 Indirect conjugation with peptide pA20-36

HA NPs are subjected also to indirect conjugation. Also in this case, the results show that the morphology of nanovectors is preserved. Here, it is reported SEM analysis of intermediate of reaction mediated by STR protein (Figure 19). As it is showed in figure 19 C, after only 12 h of reaction the presence of STR coating is visible. Moreover, it is possible to notice the presence of outer coating, in particular by TEM analysis (Figure 19 D).

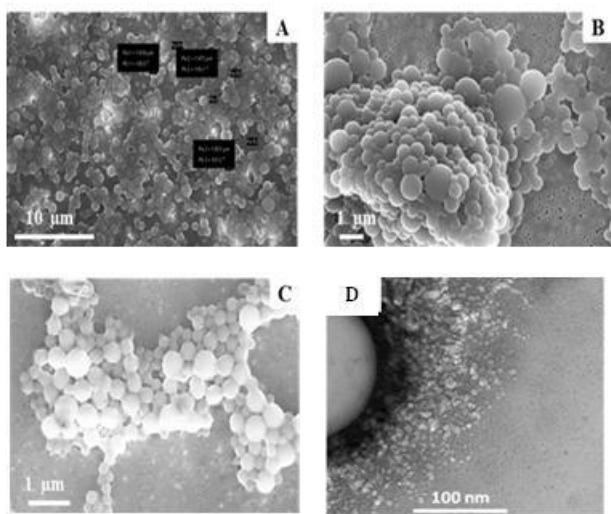


Figure 19. SEM images of indirect conjugation with STR protein. **A)** uncoated HA NPs (control); **B)** HA NPs after 1 h of STR reaction; **C)** HA NPs after 12 h of STR reaction; **D)** TEM image post indirect conjuguation.

The concentration of pA20-36 on the surface of the HA NPs is evaluated by BCA assay (Figure 20). In the case of indirect conjugation, a double quantification is performed (the conjugation with the streptavidin and conjugation with the peptide). In the case of STR conjugation, the yield of process is about 50% while the conjugation of peptide reports a yield of 80%. In the case of direct conjugation, the yield of process is about 70%.

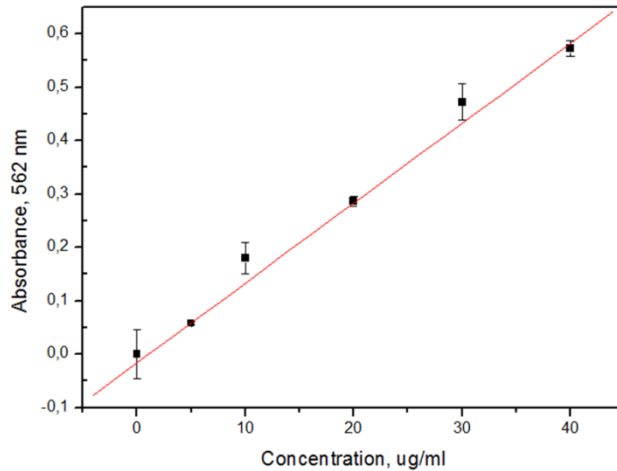


Figure 20. Calibration mediated by BSA (range 0 - 40 $\mu\text{g/ml}$).

3.1.4 PEGylation

In order to reduce interactions between HA NPs and intra/extracellular components, the surface of nanovectors has been coated with PEG, a polymer composed by repeating ethylene ether units. In this way, these nanomaterials are protected from the the attack by immune system and can circulate in the blood vessels for long time allowing their use in drug-delivery and imaging applications.

In this case, after PEGylation reaction, HA NPs have maintained their structural integrity as shown SEM, TEM and STED images (Figura 21) .

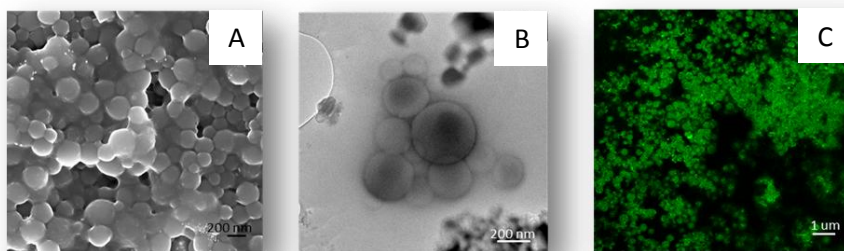


Figure 21. Morphological and Optical characterization of HA NPs after their functionalization with NH₂-PEG(2kDa)-FITC: **A)** SEM image; **B)** TEM image and **C)** Confocal microscope image.

The amount of PEG-FITC conjugated to NPs surface is evaluated by the spectrofluorimeter. Polystyrene NPs are used as model (concentration range: 1-150 μg/ml). The calibration curve for Polystyrene NPs is reported in Figure 22, while in Figure 23 is reported the calibration for NH₂-PEG(2kDa)-FITC.

The results obtained by the spectrofluorimeter analysis show that the final yield of the PEGylation process is about 65% w/v. This value can be explained on the basis of volumetric and steric effects of this polymer.

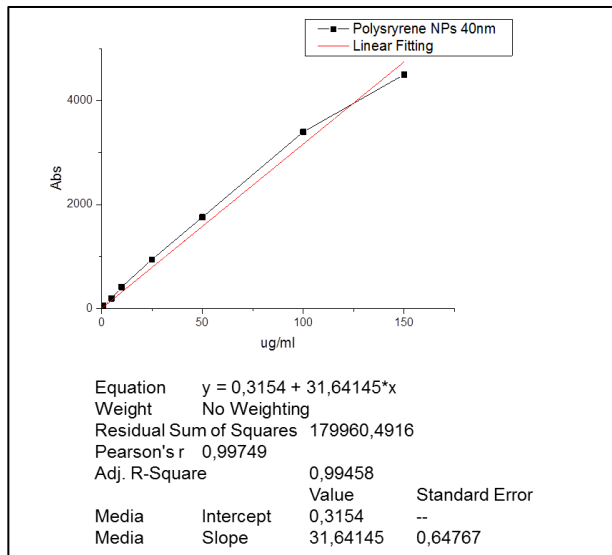


Figure 22. Calibration mediated by Polystyrene NPs (range 0-150 $\mu\text{g/ml}$).

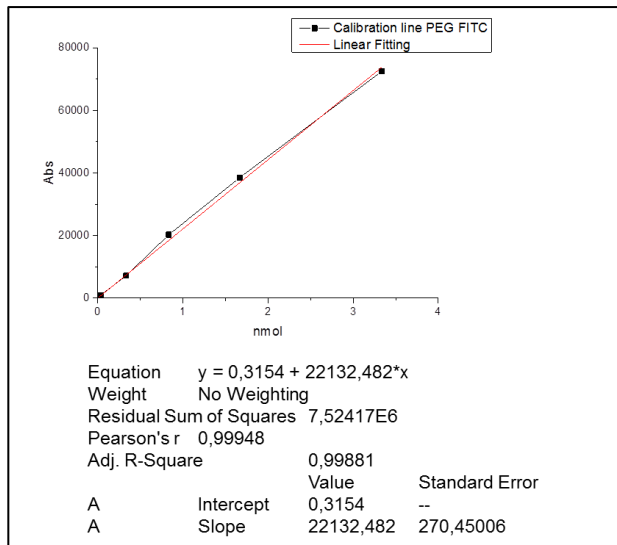


Figure 23. NH₂-PEG(2kDa)-FITC: Calibration line in the range 0-80 nmol/ml.

4. Conclusions

In this section, it is proved that the HA NPs can be successfully functionalized and PEGylated without compromising their structure and stability. In fact, the presence of carboxylic group on the the surface allows to functionalize these nanovectors with suitable biomarkers in order to ensure the tissue specificity and the action of CA. In conclusion, the new nanoprobe allows to detect in vivo a specific pathology, as lymphoma, leveraging on active targeting. Further analysis about these nanovectors are under investigation, in particular for MRI applications.

CHAPTER IV

Emerging use of nanoparticles in diagnosis of atherosclerosis disease

1. Introduction

Cardiovascular disease continues to be the leading cause of death in the Western world¹⁹² and it is caused mainly by atherosclerosis. It is a multifactorial systemic disease characterized by arterial wall thickening and rigidity and the formation of the characteristic plaques that developed simultaneously in medium and large-sized arteries, inducing a blood flow reduction with different complications¹⁹³.

This inflammatory pathology that has origins in childhood and occurs decades before the disease becomes clinically apparent (cardiac arrest, acute myocardial infarction or stroke)^{194, 195}. The pathogenesis of atherosclerosis has been the subject of many scientific works and the major players involved in this process are endothelial cells, inflammatory and immune cells (mainly macrophages and T cells), and intimal smooth muscle cells (SMCs)^{196, 197}. For many years it was believed that the disease was only characterized by a passive accumulation of cholesterol in the vessel wall, but, nowadays, it is known that the evolution of the lesion is much more complex and not fully clarified. In addition, the degree of luminal stenosis is only indirect indicator of atherosclerotic process¹⁹⁸. At the beginning, our understanding of the atherosclerotic pathology is mainly based on postmortem examinations of human coronary arteries or analysis of resected surgical specimens from patients who underwent carotid endarterectomy.

In recent years, several imaging techniques, invasive and noninvasive, are available to detect and display different characteristics of atherosclerotic lesions of clinical interest⁵. The choice and applicability of each imaging technique depend not only on its diagnostic efficacy but also on the type of questions being asked. Unfortunately, these imaging modalities, neither characterize nor correlate the image parameters with histopathological lesion types, which are more clinically relevant. Most of the standard imaging modalities characterize some of the morphological and functional features of the vascular lesion, but a quantitative evaluation of atherosclerotic disease during its natural history and following therapeutic interventions are necessary for understanding

the stabilization or progression of the disease and for selecting suitable medical or surgical interventions.

In addition, current therapeutic approaches treat atherosclerosis systemically, not locally, which is often associated with decreased efficacy and increased side effects. Nanoparticle mediated, targeted delivery of diagnostic agents or therapeutic compounds to specific molecules, cells, or tissues represents an innovative approach for the diagnosis and treatment of atherosclerosis. Nanoencapsulation in combination with targeted delivery may enhance stability and bioavailability of pharmaceutical agents, improve their pharmacokinetics, increase detection sensitivity and therapeutic efficacy.

2. Advances in targeting strategies for nanoparticles in atherosclerosis imaging

As described previously, MRI represents the unique technique that combines excellent soft tissue discrimination with high spatial resolution without the use of ionizing radiation. Nevertheless, this imaging modality is limited by its low sensitivity and requires the use of CAs to display the damaged site clearly. This restriction may be overcome with a noninvasive molecular imaging approach, considered an in vivo equivalent to immunohistochemical techniques and based on a signal imaging element encapsulated or conjugated to a carrier that transports a ligand that is then recognized by the target molecule. In fact, this strategy can facilitate early diagnosis, has the potential to image the pathophysiological process of the disease before the onset of symptoms and can be applied to follow the efficacy of therapy. In this scenario, the advantage of MRI resides in its ability to provide not only anatomical but also functional information quantifying specific biological processes within a single imaging modality.

A variety of molecular targets has so far been successfully employed in preclinical models of CVD to identify typical features associated with plaques that are prone to rupture. Actually, plaque rupture represents a key process in the initiation of cardiac arrest, acute myocardial infarction or stroke syndrome, but given the complexity and

heterogeneous nature of the plaques, it could not be identified a biomarker that is able to discriminate between patient that needs monitoring (stable plaque) and patient at risk of clinical events (unstable plaque).

Examples of biomarkers are shown below: cell adhesion molecules (VCAM 1 or E-selectin)¹⁹⁹, extracellular matrix, lipoproteins, smooth muscle cells, macrophages, phosphatidylserine and $\alpha V\beta 3$ integrin^{200, 201}.

At first, the CAs were conjugated with monoclonal antibodies or specific peptides, but excellent results are then obtained with NPs that combine a high binding affinity for the target zone with the capacity to transport a sufficient amount of a CA. The most widely employed NPs are: superparamagnetic iron oxide (SPIO), micelles, liposomes dendrimers and polymeric nanoparticles²⁰¹⁻²⁰³. In this section will discuss the recent progress in targeting strategies for nanoparticles focused on the recent innovative works for nanomedicine.

2.1 Superparamagnetic Iron Oxide Nanoparticles (SPIONs)

Several MRI strategies to display the atherosclerotic lesions were successfully developed using NPs platform^{204, 205}. In effect, their chemical, physical and pharmacokinetic characteristics and the ability to transport high payloads make them highly suited to cellular and molecular imaging of atherosclerotic lesions.

Generally, two categories of contrast agents are used for molecular MR imaging of atherosclerotic plaques: superparamagnetic iron oxide nanoparticles (SPIONs) and nanoparticles that incorporate gadolinium (Gd) chelates^{202, 206}. SPIONs represent the main platform used and are composed of an iron oxide core formed by magnetite (Fe_3O_4) and/or maghemite (γFe_2O_3) and coated with a polysaccharide, synthetic polymer, or monomer, which make them water soluble, prevent their aggregation and improve biocompatibility²⁰⁷. Moreover, the combination “core-shell” influences the pharmacodynamic and pharmacokinetic features of the final product. Passive targeting of these nanocarriers dependent on the control of parameters such as the surface charge and hydrodynamic radius that affect circulation time of the nanoparticles, accessibility to tissues, opsonization, and so on. Differently, active targeting takes advantage of

nanoparticle' surface modifications with monoclonal antibodies or peptides²⁰⁷. Generally, the term SPIO can be used to refer to: standard SPIO (SSPIO, 60-150 nm), ultrasmall SPIO (USPIO, <50 nm), monocrystalline iron oxide nanoparticles (MION, ~30 nm) and cross-linked iron oxide (CLIO)²⁰⁸. Phagocytic cells of reticuloendothelial system (RES) take up injected SPIONs spontaneously by

endocytosis or phagocytosis allowing a rapid accumulation of these particles at the level of the lesion of interest²⁰⁹. This system have been characterized as MRI contrast agents for the imaging of the plaque inflammation, which represents one the most of the features of high-risk atherosclerotic plaques²⁰⁴. In particular, Ruehm and coworkers²⁰⁹ demonstrated that in hyperlipidemic rabbits there is an accumulation of USPIOs in plaques with high macrophage content and that this phenomenon induced MR signal changes. For this reason, Kooi and colleagues²¹⁰ investigated the detection of macrophages in human atherosclerotic plaque. The results showed that the use of a USPIO agent, Sinerem® (Guerbet; Ferumoxtran-10), accumulated mainly in macrophages in human atherosclerotic lesions prone to rupture, it induced significant decrease of signal T2* images obtained 24 hours after intravenous administration but not in the images obtained after 72 hours (washout phenomenon). This information suggested that USPIO-enhanced MRI is as a promising method for the in vivo differentiation between low- and high-risk plaques and additional studies conducted by Trivedi et al.²¹¹ confirmed these preliminary results, suggesting furthermore that there is a process of accumulation and excretion of USPIOs. A representative example of a study, in which MRI is used to monitor the target site accumulation of USPIOs, is published by Tang and colleagues²¹². In summary, the researchers explored whether there is a difference in the degree of inflammation between asymptomatic and symptomatic patients. The results suggested that one inflamed symptomatic vascular bed can be increase the risk of other arterial vessels to become inflamed. Finally, preclinical (atheromatous rabbits and ApoE knockout mice) and clinical studies of Sinerem® for noninvasive MRI assessment of atherosclerotic plaque inflammation are summarized by Tang et al.²¹³.

An example of active targeting, for development of a non-invasive method to detect vulnerable plaque prior rupture in vivo, is reported by Smith et al.²¹⁴. In this investigation SPIONs consisting of an iron oxide core coated with dextran and conjugated to a cellular protein, Annexin V, that recognizes apoptotic cells by specific molecular interaction with Phosphatidyl Serine (PS). They tested in two rabbit models of atherosclerosis and MRI was performed with a 4.7 T small animal MRI system. The

results were confirmed by further histological investigation and vascular targeting by the system, SPIONs-Annexin V, was atheroma-specific. In addition, the administered dose was significantly lower than the particles without target in the same animal model. Therefore, the presence of a biomarker, as Annexin V, can provide additional support for the diagnosis of vulnerable plaque.

Nahrendorf et al.¹⁹⁹, instead, functionalized MION with linear peptide (VHPKQHR) for targeting of the vascular cell adhesion molecule-1 (VCAM-1), which is a biomarker expressed at early stages and progression of atherosclerotic lesions. Even in this case, the conducted studies in animal models showed that the anatomical area of interest became dark (hypointense signal) after the injection of the nanoparticles. Kang and colleagues²¹⁵ prepared similar system using CLIO nanoparticles with E-selectin antibody fragments to detect E-selectin in endothelial cells. The expression of this molecule is induced by an inflammatory cytokine (interleukin-1 β) and, as expected, a high decrease in T2* signal is present in the treated mice with interleukin-1 β compared to mice not treated.

Many research groups have long studied the use of these carriers based on the models mentioned above in atherosclerosis detection and several scientific works are reported in the literature²¹⁶, but none is currently approved for clinical diagnostic evaluation and there are not others in clinical development.

2.2 Polymeric Nanoparticles

The strategy to prepare PNs with imaging functionality is to incorporate materials or functional groups with some characteristic that makes them a new promising tool for the diagnostic. Generally, the CA can be covalently conjugated or physically encapsulated within polymeric matrix^{41, 43, 49, 217}. In the first case, the molecules with imaging properties are connected to polymeric backbone and there may be nonhomogeneous distribution and poor loading efficiency of CA on the polymer surface. Conversely, in the latter case, the system offers high loading efficiency and homogenous distribution of contrast media within the polymeric matrix. Initial characterization of polymeric nanoparticles containing gadolinium chelate (Gd-DTPA)

as CA for enhanced MRI is reported by Doiron et al.²¹⁸. In this work a water-in-oil-in-oil double emulsion solvent evaporation technique was used to encapsulate the CA in a poly(lactide-co-glycolide) (PLGA) or polylactide-poly(ethylene glycol) (PLA-PEG) particle for the transport of MRI agent for the detection of staged atherosclerosis. PLGA particles showed negative zeta potentials, while PLA-PEG particles had neutral zeta potentials. In vitro experiment showed that cytotoxicity of these particles on human umbilical vein endothelial cells (HUVEC) was minimal, while MRI in vitro experiment demonstrated that the relaxivity of the PLGA particles is similar to that of unencapsulated Gd-DTPA. Recently, Zhang and colleagues²¹⁹ have successfully synthesized using water in oil in water method and characterized a new type of delivery system based on PLGA. In this case, (Gd)-loaded PLGA nanoparticles show on the surface a specific peptide sequence (Arg-GlyAsp-Ser, RGDS) for the detection of thrombus at the molecular level. The results of in vitro experiments suggest that these molecular probes can be used for detection of thrombus with a longitudinal relaxation similar to commercial CAs.

Recently, our group is focused on the use of biomaterials to improve the healthcare services in the field of atherosclerosis diagnosis. Russo et al.⁴¹, for example, report a new Hyaluronic Acid (HA) nanoprobe (35 nm), obtained by a controlled and continuous microfluidic process, which entraps CAs for MRI. In a subsequent work, the impact that hydrophilic biopolymer networks have on the relaxivity of Gd-based CAs has been analysed and the concept of “Hydrodenticity” has been defined to describe the ability of these biopolymers to enhance the properties of the metal chelate, as reported by Russo et al.⁴³. Vecchione et al.⁴⁹, instead, describe a core-shell architecture for multimodal imaging applications obtained by a modified complex coacervation. The relaxivity of Gd-DTPA nanoconstructs is more than four times higher than the relaxivity measured for free Gd-DTPA in solution.

2.3 Micelles

Micelles are self-assembled nanostructures composed by amphiphilic molecules (lipid or polymer). They can be made mainly by a hydrophobic core and externally a

hydrophilic surface, characteristics that allow encapsulating therapeutic or diagnostic agents within the micelles. A first in vitro study is conducted by Lipinski et al.²²⁰ that evaluated the uptake of micelles linked to specific antibody (immunomicelles) for macrophages and containing Gd-DTPA micelles, and a murine model of Apolipoprotein E knockout (ApoE KO) is used for ex vivo imaging of lesions. The micelles (size <100 nm) are made by lipid monolayers and the results of the experiments demonstrated that the immunomicelles are taken up by the macrophages compared to untargeted micelle and both micelles and immunomicelles are superior CAs compared to the others used in clinical practice. This enhancement is related to the content of macrophages, which is associated with plaques vulnerable to rupture. A limitation for this study is represented by long acquisition time. A similar approach was published by Mulder and coworkers²²¹. The obtained results in this work are consistent with previously findings that show uptake of immunomicelles in cultured macrophages and in ex vivo atherosclerotic aorta²²⁰. Subsequently, Briley-Saebo et al.²²² conducted a study using micelles containing Gd and antibody (murine or human) that bind oxidation-specific epitopes (OSE). The aim of this work was to obtain a non-invasive in vivo imaging of atherosclerotic plaques rich of OSE by the use of MRI. Also in this case, the results show that the active targeting allows to obtain a significant signal enhancement using micelles containing a specific antibody and a good identification of atherosclerotic lesions. In another work²²³, the same authors changed the model previously adopted in order to evaluate the in vivo MRI efficacy of manganese (Mn(II)) as molecular imaging probe for OSE. Mn is a paramagnetic metal ion, endogenous, and bio-compatible and DTPA is used as the chelating agent. The intracellular accumulation in intraplaque macrophages of targeted bio-compatible Mn-micelles and de-metallation resulting in free Mn resulted in significant efficacy of contrast-enhanced MR imaging, allowing the visualization of atherosclerotic lesion through a non-invasive method.

2.4 Liposomes

Two approaches have been used to prepare liposome-based CAs: (1) encapsulation of

the contrast agent into the liposome and (2) chemical conjugation of the MRI probe to the liposome membrane. An example of liposomes used for delivery to atherosclerotic tissue has been reported by Maiseyeu et al.²²⁴, where Gd-decorated liposomes enriched with phosphatidylserine (PS) were used for imaging of accumulated macrophages at atherosclerotic site in ApoE *-/-* knockout mouse models. This approach allowed a significant enhancement of atherosclerotic plaque *in vivo* for molecular characterization of high-risk plaques. Based on similar rationale of macrophage activity in atherosclerotic lesions, Resen et al.²²⁵ and Mulder and coworkers²²⁶ have reported the development and contrast-enhanced targeted MR imaging of vascular disease associated inflammation using Gd-liposomes.

Kozłowska et al.¹⁸⁶, instead, synthesize liposomes loaded with Gd ions using different membrane-incorporated chelating lipids and functionalized with monoclonal anti-CD138 (syndecan-1) antibody for multiple myeloma and non Hodgkin's lymphoma diagnosis. In this case, the use of the polychelating amphiphilic polymer increases both the Gd content and the longitudinal relaxivity of the Gd-loaded liposomes as compared to commercial CA (Gd-DTPA).

2.5 Dendrimers

Dendrimers are a highly significant class of nanosystems that exhibits many attractive characteristics and plays an important roles not only as drug delivery carriers, but also as imaging agents²²⁷. In more detail, they are nano-sized structures characterized by a controllable multibranching three-dimensional arrangement, globular shape, high functionality, small size and low polydispersity²²⁸. These structures offer three points for modification with diagnostic agents: the core, the branching zone and the branch extremities²²⁹. Therefore, active molecules may be encapsulated into the interior area or chemically/physically linked onto the nanovector surface.²³⁰ Their pharmacokinetics and pharmacodynamics features are not very clear and thus remain to be explored for their bioapplication²²⁸. In addition, the composition and size of dendrimer-based MR imaging agents influences their behavior. The pioneers in this field are Kobayashi et al.²³¹ that conducted a study about optimization of the

performance of dendrimer-based MRI agents *in vivo* in comparison to Gd-[DTPA] using the poly (amido amine) (PAMAM) and diaminobutane core polyaminoamine (DAB) for the preparation of MRI contrast agents. They observed that dendrimer-based MRI contrast agents are quickly excreted by the kidneys and also able to visualize vascular structures better than Gd-DTPA due to less extravasation. Therefore, these structures are retained in the body for a prolonged time. Recently, Nguyen and colleagues²³² have synthesized, characterized, and evaluated the MR efficacy of manganese (Mn) dendrimers targeted to OSE in murine models. Considering that dendrimers can be easily modified to allow for the addition of contrast agents and antibodies for targeted delivery, PAMAM-based dendrimers were chosen for their ability to load large amounts of Mn and DTPA is chosen as chelating agent. The results demonstrated that the administration of the targeted dendrimers allow to obtain a significant enhancement of vascular lesions in comparison to untargeted dendrimers. The analysis was only qualitative because the observed MR imaging signal did not correlate with the histological presence of OSE.

3. Conclusion

Despite the progress in primary and secondary prevention and the growth of the knowledge base of atherosclerosis pathology, the incidence of myocardial infarction and stroke continues to remain high. Nowadays, the nanotechnology and the design of nanoscale devices seem to be a promising avenue for improving cardiovascular outcomes. The examples reported in this work include the use of NPs for MRI as tool for non-invasively evaluating atherosclerotic plaques, but their application in atherosclerotic field is very limited so far. A future goal in this field is represented by the combination of disease-specific biomarkers linked to the suitable carriers with MRI imaging modality in order to improve diagnosis and therapy of the atherosclerotic lesion. Therefore, it is essential to broaden our current understanding of distinct stages of pathological process for the development of novel diagnostic approaches based on

these concepts. In the end, potentially harmful effects of these new methodologies must be borne in mind.

CHAPTER V

Application of HA NPs in
atherosclerosis field: preliminary
results

1. Introduction

In contrast with conventional imaging approaches, molecular imaging allows to evaluate biological features of atherosclerotic plaques *in vivo* by ensuring prevention, screening, diagnosis, and treatment of vascular disorders .

Nowadays, as explained in the Chapter IV, imaging tools for early detection of clinical atheroma based on the plaque biology are lacking. In fact, despite there is a wide knowledge concerning the use of nanotechnologies in cardiovascular disease, the use of nanovectors for imaging applications in clinical practice remains limited, not only for safety iussess, but also for the heterogeneous nature of atherosclerotic plaques which does not allow for a proper segregation the different types of patients. In addition, it is known that the old generation of NPs is nonspecific and, actually there is no commercialized product, without considering that several studies conducted in murine models have significantly highlight that there are different anatomies of vascular disease compared to humans.

In this context, therefore, the combination of specific peptides and nanostructures becomes a key factor to interact and/or overcome the biological barriers.

Unlike other macromolecules, peptides are small entity with higher specificity and affinity for target sites and with limited steric constraints. In addition, they can be synthesized in the laboratory using different methods, thereby supporting the early detection of pathology, moreover due to the high surface area to volume ratio of nanovectors, several copies of the ligands can be conjugated. Not for nothing, recently, the use of phage display tecnology is under investigation in order to identify new and specific peptides ligand for pathology process^{1,2}.

This technique allows to the synthesized more libraries of heterogenous bacteriophage, (viruses that infect bacterial cells) using recombinant DNA technology. The advantage of phage display consists principally of binding partner of the peptide sequence that is known.

Here, it is reported the development of a new probe for molecular imaging investigation of cardiovascular disease through the biological knowledge that drive plaque progression.

The experimental design and preliminary studies performed on human atherosclerotic plaque and HA NPs are given below.

2. Experimental design

The ability to functionalize the surface of nanovectors with targeting ligands play a key role in real-time diagnosis of vascular diseases. A variety of targeting peptides for atheroma have been already tested preclinically, but the search of new and performing biomarkers is necessary in order to discriminate a patient at risk from a patient which instead only needs to be monitored over time. For this reason, it is decided to test the versatility of HA NPs, selecting a suitable peptide, for MRI imaging of cardiovascular disease.

From a bioengineering perspective, the first step of experimental design (see Figure 24 for schematic representation) of new probe consists of selection an appropriate peptide, took from random peptide libraries selected based on interaction with specific epitopes, able to recognise the site of interest. This process provides for the application of phage display technology³, introduced by Smith and Parmley. Phage-panning procedure for selection of peptides with vascular endothelium cellular binding specificity uses an M13 random peptide phage display library. After this procedure, different clones are chosen for further characterizations. ELISA test are made to confirm specific binding between cell line and peptide in vitro. Then, the lead clone with the highest specificity is selected, expanded and sequenced to determine the targeting peptide sequence.

The second part of strategy (Figure 25) provides that loaded HA NPs, synthesized as reported in the Chapter III, are conjugated with identified peptide using conventional functionalization strategy (amidation reaction). After this step, chemical-physical characterizations, relaxation measurements and in vitro/in vivo evaluations are

performed in order to establish not only safety but also potential diagnostic effectiveness of new probe.

Finally, the probe is tested for ex-vivo experiments using human carotid endarterectomy (CEA) specimen in order to evaluate diagnostic efficacy and at the same time the immunohistochemistry of biological sample.

The effective binding between tissue and probe is also evaluated by electron microscope analysis. Special attention is given to the ultrastructural morphology of these tissue.

It is already known, the phage display technology is a laborious method and time-consuming and, actually, the process of peptide selection is under development.

For this reason, in this chapter, it is possible to report only preliminary studies concerning the manipulation of ex-vivo human tissues for electron microscope analysis (Figure 26).

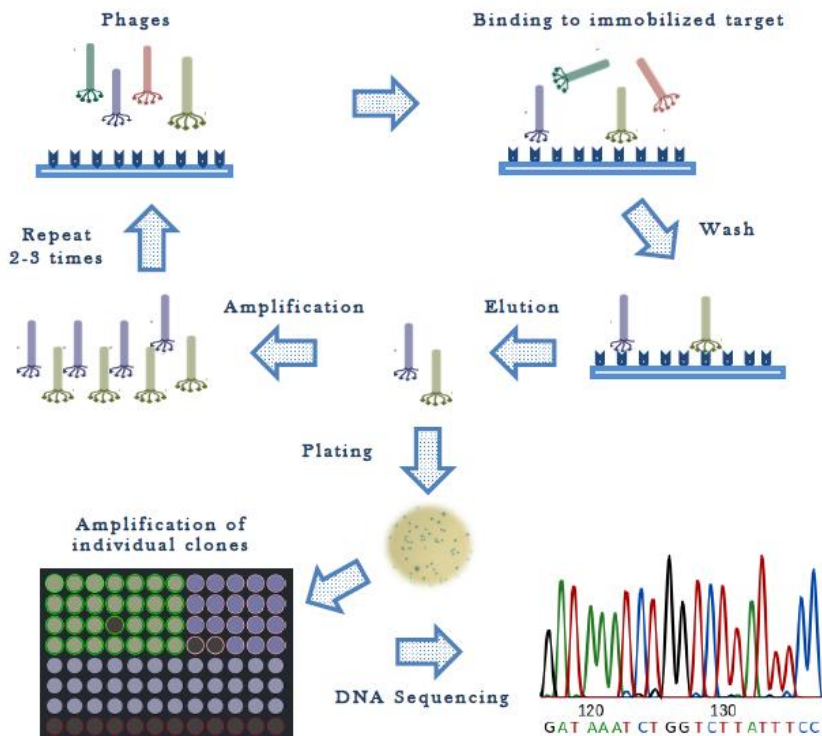


Figure 24. Phage display. Principles of protocol used for selecting sequences that have affinity to specific biomarker.

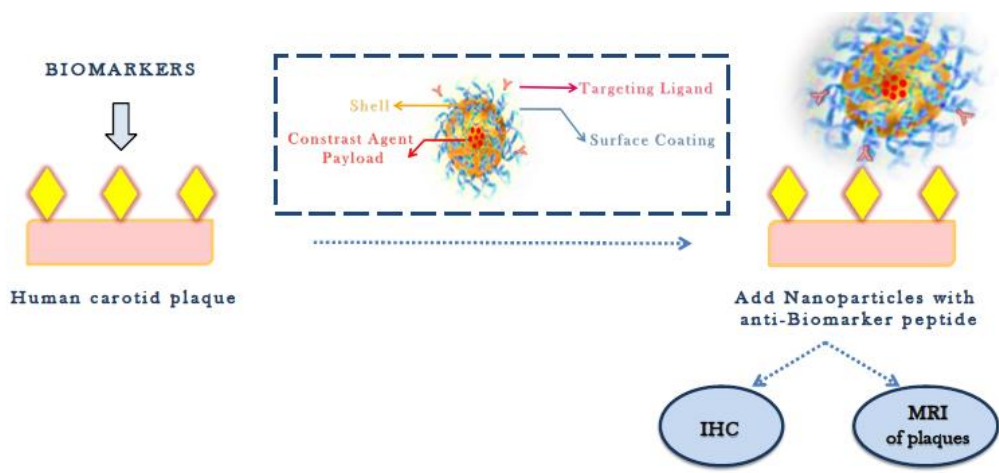


Figure 25. Experimental design of ex-vivo human plaque stage. The markers on human carotid plaque are detected by peptide, which are bound to the HA NPs, thereby making these plaques “MRI visible. Concomitant immunohistochemistry is performed.

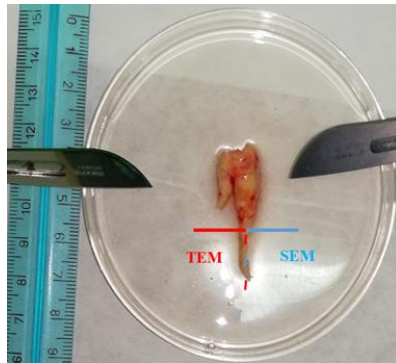


Figure 26. Human carotid endarterectomy (CEA) specimen before electron microscopy analysis.

3. Experimental section

3.1 Materials and methods

Fibrous and atheromatous plaques are selected from human carotid obtained after endarterectomy. This surgical procedure is used to reduce the risk of stroke by correcting stenosis in the carotid artery. The surface area of these plaques appears yellowish. All the samples (postoperatively) are immediately immersed in physiological solution (4°C, 2 hours) and, then tissue slices fixed following the protocols reported below.

On the basis of analysis, different thickness of cross-sectional slices are cut from each lesion.

All investigated subjects are men (average age of 65 years).

All procedures are carried out according to EU directives and reviewed by local ethical committee.

3.2 Electron Microscopy analysis

For transmission electron microscopy (TEM), all tissue slices (1 mm x 1 mm) are fixed in 0,5% of glutaraldehyde and 4% of paraformaldehyde in 0.1 M Na cacodylate buffer, pH 7.4, overnight at 4°C, followed by rinsing in buffer (3 washes, 4°C, 10 minutes). Samples are postfixed in osmium tetroxide (4%) and potassium ferrocyanide (2%) for 1 h at 4°C. This step is followed by three quick changes of 0.1 M Na cacodylate buffer over a total of 5 minutes and three quick washes with water solution (4°C, 5 minutes). Addition of uranyl acetate (4%) for over-night at 4°C. Three quick washes with water solution (4°C, 5 minutes). Treatment with 0.15% tannic acid in water for 3 minutes at 4°C. Three quick washes with water solution (4°C, 5 minutes). After this, the samples are dehydrated and embedded schedule generally

employed is as follows: 30, 50 and 70%, 1 hour at 4°C; 95% (twice) and 100% (three times) EtOH, 1 hour at 4°C; 1:2 Epon:EtOH, 2 hour; 1:1 Epon:EtOH overnight, 2:1 Epon:EtOH, Epon and two further changes (3 hours), Epon overnight, Epon further changes (3 hours), before embedding. The polymerization process is performed at

70°C for 72 hours. Ultrathin Cryo-ultramicrotome (Leica) sections (80nm) are obtained using a diamond knife and collected on copper grids (300 Meshes). All sections are analyzed with a TEM (TECNAI G²20 FEI).

For scanning electron microscopy (Field Emission, FE SEM, Ultraplus Zeiss), small tissue blocks of the region of interest are analyzed. All samples are treated according to the same protocol reported above for TEM analysis. Here, after the dehydration steps, critical point drying (CPD Leica) procedure is applied in order to preserve the surface structure of samples for next analysis. Finally, the samples are coated with 20 nm of gold using sputter coater and visualized at SEM.

3.3 Nanoparticles investigation

Different chemical reagents, used during protocols preparation for electron microscopy analysis, are tested on unloaded HA NPs in order to establish if their morphology and stability are preserved during the ex-vivo experiments.

In particular, 5 aliquots (500 µl) of unloaded HA NPs in water solution are incubated for 1 hour with the following substances: sodium cacodylate (0.1 M), Gluteraldehyde (2,5% v/v), osmium tetroxide (1% v/v) and paraformaldehyde (4% v/v).

Then, three quick washes with water solution (RT, 5 minutes) are performed.

The resulting samples are filtered, coating with 10 nm of gold and observed at SEM.

4. Results and discussion

Atherosclerotic process is activated by alterations of endothelial cells. Thus, it is necessary the use of the microscopy in order to visualize the whole intimal surface and for better understanding the physiopathology of this disease.

In this work, scanning microscopy analysis is performed on the luminal surface of the human carotid vessel wall (Figure 27). The examination shows that endothelial layer is preserved even if it is possible to notice non regular architecture. Several platelets and leukocytes adhering to endothelium (Figure 28) and collagen fibrils (Figure 29) are visible in all samples.

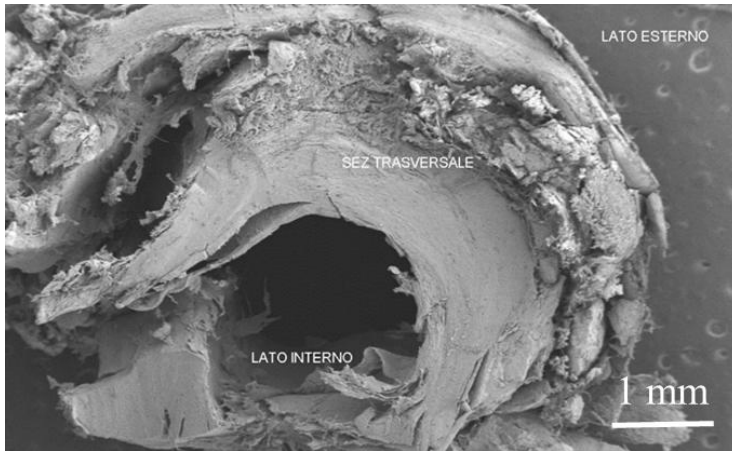


Figure 27. Scanning electron image of trasversal section of human carotid artery shows how the wall thickness varies in the same tissue.

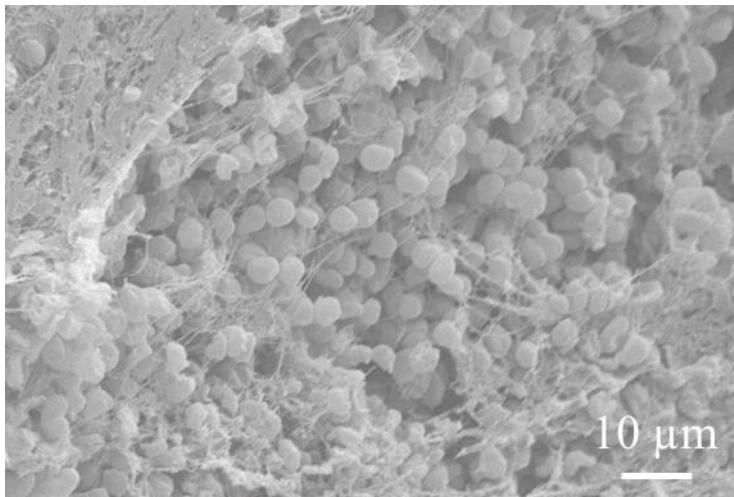


Figure 28. Scanning electron image of the surface of endothelium. Platellets and leukocytes adhering to endothelium are visible.

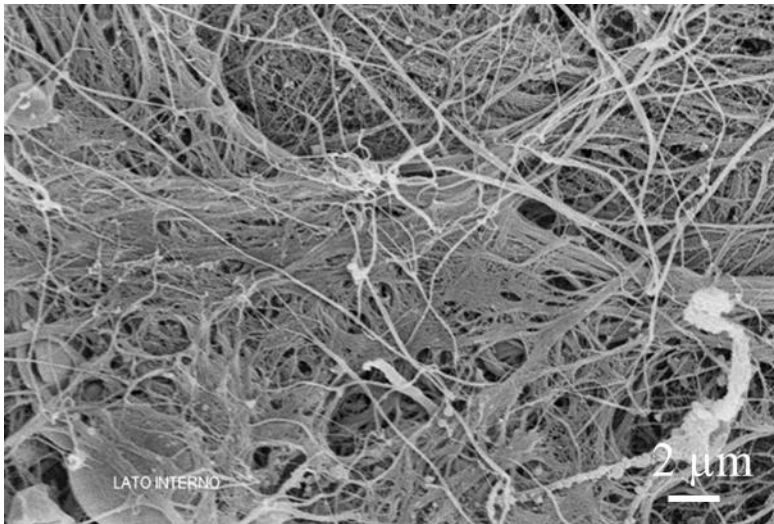


Figure 29. Scanning electron image of subendothelial surface. Fibrous cap formed by fibrin proteins and collagen fibrils are visible.

TEM analysis, instead, show the presence of a high number of macrophage foam cell and lipid droplets in all samples investigated (Figure 30).

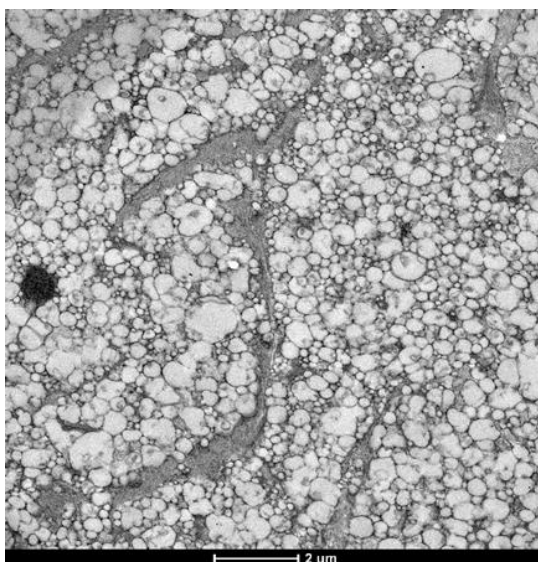


Figure 30. Transmission electron microscopy showing a macrophage foam cell and lipid droplets.

There are no morphologic alterations of unloaded HA NPs after treatment with the principal chemical reagents used during preparation process for microscopy analysis (Figure 31).

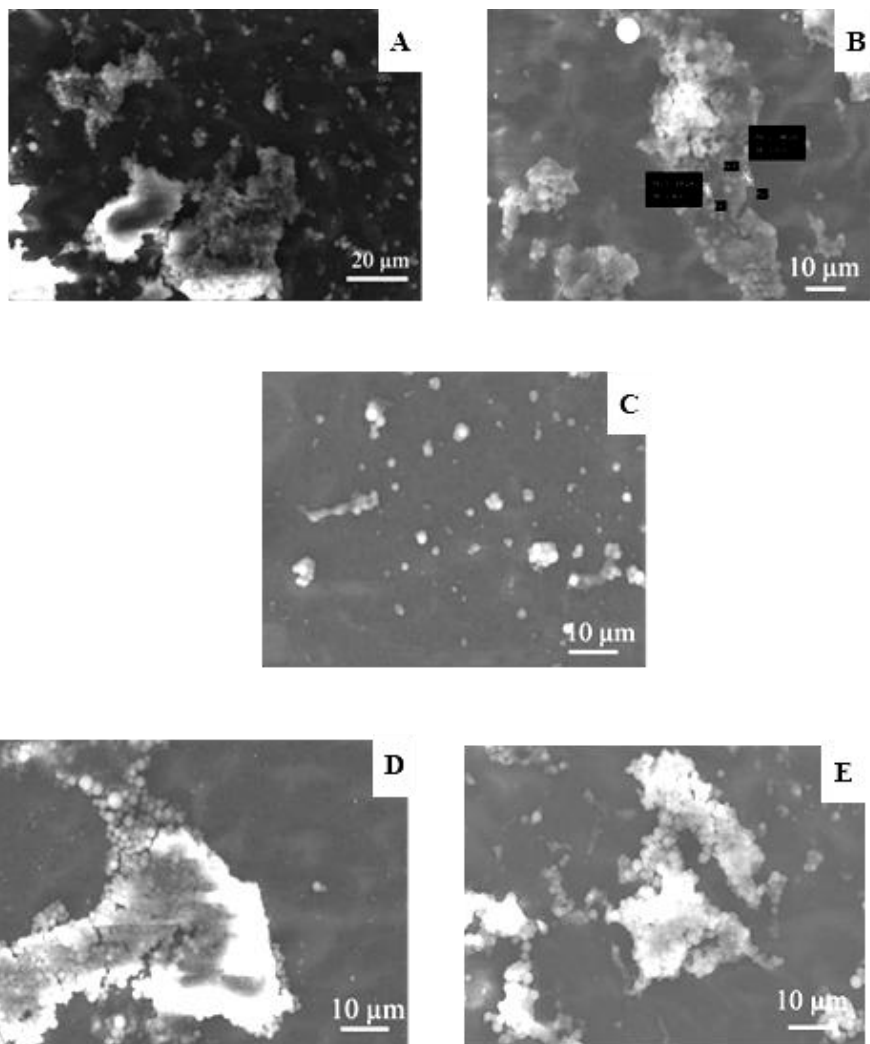


Figure 31. Scanning electron image of unloaded HA NPs tested with chemical reagents for 1 hour at RT: A) HA NPs control; B) Paraformaldehyde (4% v/v); C) Glutaraldehyde (2,5% v/v); D) osmium tetroxide (1% v/v) and E) sodyum cacodylate (0.1 M).

5. Conclusion

In conclusion, here, it is report the use of phage display technology to identify peptides specific able to target vascular endothelial cells, in particular unstable plaques. Further chracterization studies are needed to find and investigate the binding specificity of lead peptide to human atherosclerotic tissue and the future application of a new probe in the clinical practice.

Actually, the experimental design has been defined and preliminary tests on biological sample and nanovectors are performed. The correlation between the ultrastructural of vessel wall and endothelial dysfunction remains to be established.

Main Conclusions and Future Perspectives

Despite the progress in primary and secondary prevention and the growth of the knowledge base of pathological processes, the incidence of many diseases to remain high. The use of CAs is enormously increased in the diagnostic practice because they contribute to better disease detection and characterization, monitoring and thus guidance of disease management.

Although pharmaceutical compounds are widely used in clinical practice, they have certain limitations for which have received special attention in the last year. Nowadays, the nanotechnology and the design of nanoscale devices seem to be a promising avenue for improving clinical outcomes.

Contrast media specifically designed for MRI applications are still under development and there is a number of technologies involved in the development of nanocarrier including in its chemical, physical and biological properties. Despite several efforts towards nanocarriers, to choose the most adequate nanocarrier is not obvious for a variety of reasons that can simultaneously affect the biodistribution and target of nanocarriers. However, there remains a gap between technological advances and clinical applications. In this sense, the future prospects of nanotechnology and nanomedicine are very promising.

However, as stated above, the major challenge consists of development of an appropriate paramagnetic CA which shows the following properties: low toxicity, high relaxivity and long half-lives, high availability, chemical stability, high magnetic moment, and capability for binding the ligands to NPs. In this context, biopolymer-based CAs can satisfy the required properties. The biological properties of HA, for example, make it an ideal candidate to create nanovectors for medical applications, although, in order to achieve this, the nanosystems need to be refined to allow an enhanced longevity in the physiological environment.

In particular, in this work is proved that a new generation of more efficient MRI CAs can be developed. It can be done using biocompatible and clinical relevant CAs without their chemical modification as approved in the clinical practice. The optimal conditions to combine a CA with a hydrophilic biopolymer are identified and applied to the nanoscale in order to produce nanostructures of biomedical interest with high

relaxivity. In particular, stable crosslinked HA NPs encapsulating Gd-DTPA are successfully prepared using a method that exploits the use of W/O nanoemulsions as templates.

The aqueous emulsion droplets are shown to provide a good environment for the formation of the NPs and seemed to limit efficiently their size. NPs collected from the emulsion droplets using a purification procedure show a size of about 200 nm and spherical shape. In addition, WST-1 assay is successfully carried out, proving their non-cytotoxicity for murine fibroblast cells.

Thus, the conditions of the herein presented protocol to produce these biocompatible NPs offer advantages for the encapsulation of a broad-spectrum of biomolecules and provide a potential synthetic route to design a wide range of highly efficient nanostructured MRI CAs, letting the surface available for possible functionalization. Development of biomarkers for early detection of the most common illnesses (from oncology to cardiology) is another important topic for research using nanotechnology. A future goal in this field is represented by the combination of disease-specific biomarkers linked to the suitable carriers with MRI imaging modality in order to improve diagnosis of specific body lesions. Therefore, it is essential to broaden our current understanding of distinct stages of pathological process for the development of novel diagnostic approaches based on these concepts.

In particular, the development of the nanovectors reported in this work includes their use for MRI as tool for non-invasively evaluating lymphoma and atherosclerotic plaques, but their application in their respective fields is very limited so far.

However, from a biomedical point of view, the possibility to tune relaxometric properties of CAs by controlling hydrogel structural parameters can pave the way to new advancements in the design of nanovectors for diagnosis and therapy. In addition, this approach can be easily applied to other types of hydrophilic polysaccharides and further used to design biocompatible NPs with a potential application as drug delivery carriers in MRI applications. In the end, potentially harmful effects of these new methodologies must be borne in mind. This involves detailed risk assessment of products before their use.

References

1. Laal, M., Innovation Process in Medical Imaging. *World Congress on Administrative and Political Sciences* **2013**, *81*, 60-64.
2. Frangioni, J. V., New technologies for human cancer imaging. *Journal of Clinical Oncology* **2008**, *26* (24), 4012-4021.
3. Mansfield, P., Snapshot magnetic resonance imaging (nobel lecture). *Angewandte Chemie-International Edition* **2004**, *43* (41), 5456-5464.
4. Caravan, P.; Ellison, J. J.; McMurry, T. J.; Lauffer, R. B., Gadolinium(III) chelates as MRI contrast agents: Structure, dynamics, and applications. *Chemical Reviews* **1999**, *99* (9), 2293-2352.
5. Sandfort, V.; Lima, J. A. C.; Bluemke, D. A., Noninvasive Imaging of Atherosclerotic Plaque Progression: Status of Coronary Computed Tomography Angiography. *Circulation. Cardiovascular imaging* **2015**, *8* (7), e003316-e003316.
6. Wilson, G. T.; Gopalakrishnan, P.; Tak, T., Noninvasive cardiac imaging with computed tomography. *Clinical medicine & research* **2007**, *5* (3), 165-71.
7. Barsanti, C.; Lenzarini, F.; Kusmic, C., Diagnostic and prognostic utility of non-invasive imaging in diabetes management. *World Journal of Diabetes* **2015**, *6* (6), 792-806.
8. Griffeth, L. K., Use of PET/CT scanning in cancer patients: technical and practical considerations. *Proceedings (Baylor University. Medical Center)* **2005**, *18* (4), 321-30.
9. Yun, M. J.; Jang, S.; Cucchiara, A.; Newberg, A. B.; Alavi, A., F-18 FDG uptake in the large arteries: A correlation study with the atherogenic risk factors. *Seminars in Nuclear Medicine* **2002**, *32* (1), 70-76.
10. Sun, Z.-H.; Rashmizal, H.; Xu, L., Molecular imaging of plaques in coronary arteries with PET and SPECT. *Journal of Geriatric Cardiology* **2014**, *11* (3), 259-273.
11. Adak, S.; Bhalla, R.; Raj, K. K. V.; Mandal, S.; Pickett, R.; Luthra, S. K., Radiotracers for SPECT imaging: current scenario and future prospects. *Radiochimica Acta* **2012**, *100* (2), 95-107.
12. Sogbein, O. O.; Pelletier-Galarneau, M.; Schindler, T. H.; Wei, L. H.; Wells, R. G.; Ruddy, T. D., New SPECT and PET Radiopharmaceuticals for Imaging Cardiovascular Disease. *Biomed Research International* **2014**.
13. Zhou, Z. X.; Lu, Z. R., Gadolinium-based contrast agents for magnetic resonance cancer imaging (vol 5, pg 1, 2013). *Wiley Interdisciplinary Reviews-Nanomedicine and Nanobiotechnology* **2013**, *5* (2), 190-190.
14. Bellin, M. F., MR contrast agents, the old and the new. *European Journal of Radiology* **2006**, *60* (3), 314-323.
15. Shellock, F. G.; Kanal, E., Safety of magnetic resonance imaging contrast agents. *Jmri-Journal of Magnetic Resonance Imaging* **1999**, *10* (3), 477-484.

16. Mathurdevre, R.; Lemort, M., BIOPHYSICAL PROPERTIES AND CLINICAL-APPLICATIONS OF MAGNETIC-RESONANCE-IMAGING CONTRAST AGENTS. *British Journal of Radiology* **1995**, *68* (807), 225-247.
17. Tweedle, M. F.; Wedeking, P.; Kumar, K., BIODISTRIBUTION OF RADIOLABELED, FORMULATED GADOPENTETATE, GADOTERIDOL, GADOTERATE, AND GADODIAMIDE IN MICE AND RATS. *Investigative Radiology* **1995**, *30* (6), 372-380.
18. Chang, C. A., MAGNETIC-RESONANCE-IMAGING CONTRAST AGENTS - DESIGN AND PHYSICO-CHEMICAL PROPERTIES OF GADODIAMIDE. *Investigative Radiology* **1993**, *28*, S21-S27.
19. Oliveira, I. S.; Hedgire, S. S.; Li, W. E.; Ganguli, S.; Prabhakar, A. M., Blood pool contrast agents for venous magnetic resonance imaging. *Cardiovascular Diagnosis and Therapy* **2016**, *6* (6), 508-518.
20. Geraldes, C.; Laurent, S., Classification and basic properties of contrast agents for magnetic resonance imaging. *Contrast Media & Molecular Imaging* **2009**, *4* (1), 1-23.
21. Pierre, V. C.; Allen, M. J.; Caravan, P., Contrast agents for MRI: 30+years and where are we going? *Journal of Biological Inorganic Chemistry* **2014**, *19* (2), 127-131.
22. Xiao, Y. D.; Paudel, R.; Liu, J.; Ma, C.; Zhang, Z. S.; Zhou, S. K., MRI contrast agents: Classification and application (Review). *International Journal of Molecular Medicine* **2016**, *38* (5), 1319-1326.
23. Toth, E.; Helm, L.; Merbach, A. E., Relaxivity of MRI contrast agents. *Contrast Agents I: Magnetic Resonance Imaging* **2002**, *221*, 61-101.
24. Bloembergen, N.; Purcell, E. M.; Pound, R. V., RELAXATION EFFECTS IN NUCLEAR-MAGNETIC-RESONANCE ABSORPTION. *Resonances: a Volume in Honor of the 70th Birthday of Nicolaas Bloembergen* **1990**, 411-444.
25. Rogosnitzky, M.; Branch, S., Gadolinium-based contrast agent toxicity: a review of known and proposed mechanisms. *Biometals* **2016**, *29* (3), 365-376.
26. Weller, A.; Barber, J. L.; Olsen, O. E., Gadolinium and nephrogenic systemic fibrosis: an update. *Pediatric Nephrology* **2014**, *29* (10), 1927-1937.
27. Do, C.; Barnes, J. L.; Tan, C.; Wagner, B., Type of MRI contrast, tissue gadolinium, and fibrosis. *American journal of physiology. Renal physiology* **2014**, *307* (7), F844-55.
28. McDonald, R. J.; McDonald, J. S.; Kallmes, D. F.; Jentoft, M. E.; Murray, D. L.; Thielen, K. R.; Williamson, E. E.; Eckel, L. J., Intracranial Gadolinium Deposition after Contrast-enhanced MR Imaging. *Radiology* **2015**, *275* (3), 772-782.
29. Kanda, T.; Ishii, K.; Kawaguchi, H.; Kitajima, K.; Takenaka, D., High Signal Intensity in the Dentate Nucleus and Globus Pallidus on Unenhanced T1-weighted MR Images: Relationship with Increasing Cumulative Dose of a Gadolinium-based Contrast Material. *Radiology* **2014**, *270* (3), 834-841.
30. Raymond, K. N., Next generation, high relaxivity gadolinium MRI agents. *Abstracts of Papers of the American Chemical Society* **2004**, *227*, U145-U146.

31. Acharya, A., A Prospective Combination of Nanotechnology and Medicine: Nanomedicine. *International Journal of Advanced Biotechnology and Research* **2017**, *8* (2), 915-920.
32. Sen Gupta, A., Role of particle size, shape, and stiffness in design of intravascular drug delivery systems: insights from computations, experiments, and nature. *Wiley Interdisciplinary Reviews-Nanomedicine and Nanobiotechnology* **2016**, *8* (2), 255-270.
33. Vieira, D. B.; Gamarra, L. F., Advances in the use of nanocarriers for cancer diagnosis and treatment. *Einstein-Sao Paulo* **2016**, *14* (1), 99-103.
34. Din, F. U.; Aman, W.; Ullah, I.; Qureshi, O. S.; Mustapha, O.; Shafique, S.; Zeb, A., Effective use of nanocarriers as drug delivery systems for the treatment of selected tumors. *International Journal of Nanomedicine* **2017**, *12*, 7291-7309.
35. Biffi, S.; Voltan, R.; Rampazzo, E.; Prodi, L.; Zauli, G.; Secchiero, P., Applications of nanoparticles in cancer medicine and beyond: optical and multimodal in vivo imaging, tissue targeting and drug delivery. *Expert Opinion on Drug Delivery* **2015**, *12* (12), 1837-1849.
36. Patel, T.; Zhou, J. B.; Piepmeier, J. M.; Saltzman, W. M., Polymeric nanoparticles for drug delivery to the central nervous system. *Advanced Drug Delivery Reviews* **2012**, *64* (7), 701-705.
37. Zhong, Y. A.; Meng, F. H.; Deng, C.; Zhong, Z. Y., Ligand-Directed Active Tumor-Targeting Polymeric Nanoparticles for Cancer Chemotherapy. *Biomacromolecules* **2014**, *15* (6), 1955-1969.
38. Tripodo, G.; Trapani, A.; Torre, M. L.; Giammona, G.; Trapani, G.; Mandracchia, D., Hyaluronic acid and its derivatives in drug delivery and imaging: recent advances and challenges. *Eur. J. Pharm. Biopharm.* **2015**, *97*, 400-416.
39. Chen, H. Y.; Qi, B.; Moore, T.; Wang, F. L.; Colvin, D. C.; Sanjeeva, L. D.; Gore, J. C.; Hwu, S. J.; Mefford, O. T.; Alexis, F.; Anker, J. N., Multifunctional Yolk-in-Shell Nanoparticles for pH-triggered Drug Release and Imaging. *Small* **2014**, *10* (16), 3364-3370.
40. Courant, T.; Roullin, V. G.; Cadiou, C.; Callewaert, M.; Andry, M. C.; Portefaix, C.; Hoeffel, C.; de Goltstein, M. C.; Port, M.; Laurent, S.; Vander Elst, L.; Muller, R.; Molinari, M.; Chuburu, F., Hydrogels Incorporating GdDOTA: Towards Highly Efficient Dual T1/T2 MRI Contrast Agents. *Angewandte Chemie-International Edition* **2012**, *51* (36), 9119-9122.
41. Russo, M.; Bevilacqua, P.; Netti, P. A.; Torino, E., A Microfluidic Platform to design crosslinked Hyaluronic Acid Nanoparticles (CHANPs) for enhanced MRI. *Scientific Reports* **2016**, *6*.
42. Russo, M.; Grimaldi, A. M.; Bevilacqua, P.; Tammaro, O.; Netti, P. A.; Torino, E., PEGylated crosslinked hyaluronic acid nanoparticles designed through a microfluidic platform for nanomedicine. *Nanomedicine* **2017**, *12* (18), 2211-2222.

43. Russo, M.; Ponsiglione, A. M.; Forte, E.; Netti, P. A.; Torino, E., Hydrodenticity to enhance relaxivity of gadolinium-DTPA within crosslinked hyaluronic acid nanoparticles. *Nanomedicine* **2017**, *12* (18), 2199-2210.
44. Ponsiglione, A. M.; Russo, M.; Netti, P. A.; Torino, E., Impact of biopolymer matrices on relaxometric properties of contrast agents. *Interface Focus* **2016**, *6* (6).
45. Srinivas, M.; Heerschap, A.; Ahrens, E. T.; Figdor, C. G.; de Vries, I. J. M., F-19 MRI for quantitative in vivo cell tracking. *Trends in Biotechnology* **2010**, *28* (7), 363-370.
46. Wang, K. W.; Peng, H.; Thurecht, K. J.; Whittaker, A. K., Fluorinated POSS-Star Polymers for F-19 MRI. *Macromolecular Chemistry and Physics* **2016**, *217* (20), 2262-2274.
47. Gizzatov, A.; Stigliano, C.; Ananta, J. S.; Sethi, R.; Xu, R.; Guven, A.; Ramirez, M.; Shen, H. F.; Sood, A.; Ferrari, M.; Wilson, L. J.; Liu, X. W.; Decuzzi, P., Geometrical confinement of Gd(DOTA) molecules within mesoporous silicon nanoconstructs for MR imaging of cancer. *Cancer Lett.* **2014**, *352* (1), 97-101.
48. Vecchione, D.; Grimaldi, A. M.; Forte, E.; Bevilacqua, P.; Netti, P. A.; Torino, E., Hybrid Core-Shell (HyCoS) Nanoparticles produced by Complex Coacervation for Multimodal Applications. *Scientific Reports* **2017**, *7*.
49. Vecchione, D.; Aiello, M.; Cavaliere, C.; Nicolai, E.; Netti, P. A.; Torino, E., Hybrid core shell nanoparticles entrapping Gd-DTPA and F-18-FDG for simultaneous PET/MRI acquisitions. *Nanomedicine* **2017**, *12* (18), 2223-2231.
50. Tsitsilianis, C.; Gotzamanis, G.; Iatridi, Z., Design of "smart" segmented polymers by incorporating random copolymers as building blocks. *European Polymer Journal* **2011**, *47* (4), 497-510.
51. van Nostrum, C. F., Covalently cross-linked amphiphilic block copolymer micelles. *Soft Matter* **2011**, *7* (7), 3246-3259.
52. Epps, T. H.; O'Reilly, R. K., Block copolymers: controlling nanostructure to generate functional materials - synthesis, characterization, and engineering. *Chemical Science* **2016**, *7* (3), 1674-1689.
53. Feng, H. B.; Lu, X. Y.; Wang, W. Y.; Kang, N. G.; Mays, J. W., Block Copolymers: Synthesis, Self-Assembly, and Applications. *Polymers* **2017**, *9* (10).
54. Xiao, Y.; Xue, R.; You, T. Y.; Li, X. J.; Pei, F. K., A new biodegradable and biocompatible gadolinium (III) -polymer for liver magnetic resonance imaging contrast agent. *Magnetic Resonance Imaging* **2015**, *33* (6), 822-828.
55. Hou, S. J.; Tong, S.; Zhou, J.; Bao, G., Block copolymer-based gadolinium nanoparticles as MRI contrast agents with high T-1 relaxivity. *Nanomedicine* **2012**, *7* (2), 211-218.
56. Cao, Y.; Liu, M.; Kuang, Y.; Zu, G. Y.; Xiong, D. S.; Pei, R. J., A poly(epsilon-caprolactone)-poly(glycerol)-poly(epsilon-caprolactone) triblock copolymer for designing a polymeric micelle as a tumor targeted magnetic resonance imaging contrast agent. *Journal of Materials Chemistry B* **2017**, *5* (42), 8408-8416.

57. Luo, B. H.; Wang, S. Q.; Rao, R.; Liu, X. H.; Xu, H. B.; Wu, Y.; Yang, X. L.; Liu, W., Conjugation Magnetic PAEEP-PLLA Nanoparticles with Lactoferrin as a Specific Targeting MRI Contrast Agent for Detection of Brain Glioma in Rats. *Nanoscale Research Letters* **2016**, *11*.
58. Jeong, S. Y.; Kim, H. J.; Kwak, B. K.; Lee, H. Y.; Seong, H.; Shin, B. C.; Yuk, S. H.; Hwang, S. J.; Cho, S. H., Biocompatible Polyhydroxyethylaspartamide-based Micelles with Gadolinium for MRI Contrast Agents. *Nanoscale Research Letters* **2010**, *5* (12), 1970-1976.
59. Ge, Z. S.; Liu, S. Y., Functional block copolymer assemblies responsive to tumor and intracellular microenvironments for site-specific drug delivery and enhanced imaging performance. *Chemical Society Reviews* **2013**, *42* (17), 7289-7325.
60. Kato, Y.; Ozawa, S.; Miyamoto, C.; Maehata, Y.; Suzuki, A.; Maeda, T.; Baba, Y., Acidic extracellular microenvironment and cancer. *Cancer Cell International* **2013**, *13*.
61. Gao, G. H.; Im, G. H.; Kim, M. S.; Lee, J. W.; Yang, J.; Jeon, H.; Lee, J. H.; Lee, D. S., Magnetite-Nanoparticle-Encapsulated pH-Responsive Polymeric Micelle as an MRI Probe for Detecting Acidic Pathologic Areas. *Small* **2010**, *6* (11), 1201-1204.
62. Okada, S.; Mizukami, S.; Kikuchi, K., Application of a Stimuli-Responsive Polymer to the Development of Novel MRI Probes. *ChemBiochem* **2010**, *11* (6), 785-787.
63. Zhu, L. P.; Yang, Y.; Farquhar, K.; Wang, J. J.; Tian, C. X.; Ranville, J.; Boyes, S. G., Surface Modification of Gd Nanoparticles with pH-Responsive Block Copolymers for Use As Smart MRI Contrast Agents. *Acs Applied Materials & Interfaces* **2016**, *8* (7), 5040-5050.
64. Hu, J. M.; Liu, T.; Zhang, G. Y.; Jin, F.; Liu, S. Y., Synergistically Enhance Magnetic Resonance/Fluorescence Imaging Performance of Responsive Polymeric Nanoparticles Under Mildly Acidic Biological Milieu. *Macromolecular Rapid Communications* **2013**, *34* (9), 749-758.
65. Hu, X. L.; Liu, G. H.; Li, Y.; Wang, X. R.; Liu, S. Y., Cell-Penetrating Hyperbranched Polyprodrug Amphiphiles for Synergistic Reductive Milieu-Triggered Drug Release and Enhanced Magnetic Resonance Signals. *Journal of the American Chemical Society* **2015**, *137* (1), 362-368.
66. Mouffouk, F.; Simao, T.; Dornelles, D. F.; Lopes, A. D.; Sau, P.; Martins, J.; Abu-Salah, K. M.; Alrokayan, S. A.; da Costa, A. M. R.; dos Santos, N. R., Self-assembled polymeric nanoparticles as new, smart contrast agents for cancer early detection using magnetic resonance imaging. *International Journal of Nanomedicine* **2015**, *10*, 63-76.
67. Tsai, H. C.; Chang, W. H.; Lo, C. L.; Tsai, C. H.; Chang, C. H.; Ou, T. W.; Yen, T. C.; Hsiue, G. H., Graft and diblock copolymer multifunctional micelles for cancer chemotherapy and imaging. *Biomaterials* **2010**, *31* (8), 2293-2301.
68. Locatelli, E.; Gil, L.; Israel, L. L.; Passoni, L.; Naddaka, M.; Pucci, A.; Reese, T.; Gomez-Vallejo, V.; Milani, P.; Matteoli, M.; Llop, J.; Lellouche, J. P.; Franchini, M.

- C., Biocompatible nanocomposite for PET/MRI hybrid imaging. *International Journal of Nanomedicine* **2012**, *7*, 6021-6033.
69. Zhang, P.; Guo, Z. D.; Zhang, D. L.; Liu, C.; Chen, G. B.; Zhuang, R. Q.; Song, M. L.; Wu, H.; Zhang, X. Z., A Novel Copolymer-Based Functional SPECT/MR Imaging Agent for Asialoglycoprotein Receptor Targeting. *Molecular Imaging* **2016**, *15*.
70. Porsch, C.; Zhang, Y. N.; Ostlund, A.; Damberg, P.; Ducani, C.; Malmstrom, E.; Nystrom, A. M., In Vitro Evaluation of Non-Protein Adsorbing Breast Cancer Theranostics Based on ¹⁹F-Polymer Containing Nanoparticles. *Particle & Particle Systems Characterization* **2013**, *30* (4), 381-390.
71. Koziolova, E.; Goel, S.; Chytil, P.; Janouskova, O.; Barnhart, T. E.; Cai, W. B.; Etrych, T., A tumor-targeted polymer theranostics platform for positron emission tomography and fluorescence imaging. *Nanoscale* **2017**, *9* (30), 10906-10918.
72. Kamaly, N.; Miller, A. D., Paramagnetic Liposome Nanoparticles for Cellular and Tumour Imaging. *International Journal of Molecular Sciences* **2010**, *11* (4), 1759-1776.
73. Zou, J.; Sood, R.; Ranjan, S.; Poe, D.; Ramadan, U. A.; Kinnunen, P. K. J.; Pyykko, I., Manufacturing and in vivo inner ear visualization of MRI traceable liposome nanoparticles encapsulating gadolinium. *Journal of Nanobiotechnology* **2010**, *8*.
74. Bui, T.; Stevenson, J.; Hoekman, J.; Zhang, S. R.; Maravilla, K.; Ho, R. J. Y., Novel Gd Nanoparticles Enhance Vascular Contrast for High-Resolution Magnetic Resonance Imaging. *Plos One* **2010**, *5* (9).
75. Kono, K.; Nakashima, S.; Kokuryo, D.; Aoki, I.; Shimomoto, H.; Aoshima, S.; Maruyama, K.; Yuba, E.; Kojima, C.; Harada, A.; Ishizaka, Y., Multi-functional liposomes having temperature-triggered release and magnetic resonance imaging for tumor-specific chemotherapy. *Biomaterials* **2011**, *32* (5), 1387-1395.
76. Na, K.; Lee, S. A.; Jung, S. H.; Shin, B. C., Gadolinium-based cancer therapeutic liposomes for chemotherapeutics and diagnostics. *Colloids and Surfaces B-Biointerfaces* **2011**, *84* (1), 82-87.
77. Li, W.; Su, B.; Meng, S. Y.; Ju, L. X.; Yan, L. H.; Ding, Y. M.; Song, Y.; Zhou, W.; Li, H. Y.; Tang, L.; Zhao, Y. M.; Zhou, C. C., RGD-targeted paramagnetic liposomes for early detection of tumor: In vitro and in vivo studies. *European Journal of Radiology* **2011**, *80* (2), 598-606.
78. Liao, Z. Y.; Wang, H. J.; Wang, X. D.; Zhao, P. Q.; Wang, S.; Su, W. Y.; Chang, J., Multifunctional Nanoparticles Composed of A Poly(DL-lactide-coglycolide) Core and A Paramagnetic Liposome Shell for Simultaneous Magnetic Resonance Imaging and Targeted Therapeutics. *Advanced Functional Materials* **2011**, *21* (6), 1179-1186.
79. Gianolio, E.; Porto, S.; Napolitano, R.; Baroni, S.; Giovenzana, G. B.; Aime, S., Relaxometric Investigations and MRI Evaluation of a Liposome-Loaded pH-Responsive Gadolinium(III) Complex. *Inorganic Chemistry* **2012**, *51* (13), 7210-7217.
80. Hossann, M.; Wang, T. T.; Syunyaeva, Z.; Wiggerhorn, M.; Zengerle, A.; Issels, R. D.; Reiser, M.; Lindner, L. H.; Peller, M., Non-ionic Gd-based MRI contrast

- agents are optimal for encapsulation into phosphatidylglycerol-based thermosensitive liposomes. *Journal of Controlled Release* **2013**, *166* (1), 22-29.
81. Thomsen, H. S.; Morcos, S. K.; Almen, T.; Bellin, M. F.; Bertolotto, M.; Bongartz, G.; Clement, O.; Leander, P.; Heinz-Peer, G.; Reimer, P.; Stacul, F.; van der Molen, A.; Webb, J. A. W., Nephrogenic systemic fibrosis and gadolinium-based contrast media: updated ESUR Contrast Medium Safety Committee guidelines. *European Radiology* **2013**, *23* (2), 307-318.
82. Cheng, Z. L.; Al Zaki, A.; Jones, I. W.; Hall, H. K.; Aspinwall, C. A.; Tsourkas, A., Stabilized porous liposomes with encapsulated Gd-labeled dextran as a highly efficient MRI contrast agent. *Chemical Communications* **2014**, *50* (19), 2502-2504.
83. Park, J. H.; Cho, H. J.; Yoon, H. Y.; Yoon, I. S.; Ko, S. H.; Shim, J. S.; Cho, J. H.; Kim, K.; Kwon, I. C.; Kim, D. D., Hyaluronic acid derivative-coated nanohybrid liposomes for cancer imaging and drug delivery. *Journal of Controlled Release* **2014**, *174*, 98-108.
84. Smith, C. E.; Shkumatov, A.; Withers, S. G.; Yang, B. X.; Glockner, J. F.; Misra, S.; Roy, E. J.; Wong, C. H.; Zimmerman, S. C.; Kong, H., A Polymeric Fastener Can Easily Functionalize Liposome Surfaces with Gadolinium for Enhanced Magnetic Resonance Imaging. *Acs Nano* **2013**, *7* (11), 9599-9610.
85. Gu, M. J.; Li, K. F.; Zhang, L. X.; Wang, H.; Liu, L. S.; Zheng, Z. Z.; Han, N. Y.; Yang, Z. J.; Fan, T. Y., In vitro study of novel gadolinium-loaded liposomes guided by GBI-10 aptamer for promising tumor targeting and tumor diagnosis by magnetic resonance imaging. *International Journal of Nanomedicine* **2015**, *10*, 5187-5204.
86. Silva, S. R.; Duarte, E. C.; Ramos, G. S.; Kock, F. V. C.; Andrade, F. D.; Frezard, F.; Colnago, L. A.; Demicheli, C., Gadolinium(III) Complexes with N-Alkyl-N-methylglucamine Surfactants Incorporated into Liposomes as Potential MRI Contrast Agents. *Bioinorganic Chemistry and Applications* **2015**.
87. Xiao, Y. A.; Liu, Y. J.; Yang, S. M.; Zhang, B.; Wang, T. Q.; Jiang, D. D.; Zhang, J.; Yu, D. X.; Zhang, N., Sorafenib and gadolinium co-loaded liposomes for drug delivery and MRI-guided HCC treatment. *Colloids and Surfaces B-Biointerfaces* **2016**, *141*, 83-92.
88. Necas, J.; Bartosikova, L.; Brauner, P.; Kolar, J., Hyaluronic acid (hyaluronan): a review. *Veterinarni Medicina* **2008**, *53* (8), 397-411.
89. Port, M.; Raynal, I.; Elst, L. V.; Muller, R. N.; Dioury, F.; Ferroud, C.; Guy, A., Impact of rigidification on relaxometric properties of a tricyclic tetraazatriacetic gadolinium chelate. *Contrast Media & Molecular Imaging* **2006**, *1* (3), 121-127.
90. Jaszberenyi, Z.; Sour, A.; Toth, E.; Benmelouka, M.; Merbach, A. E., Fine-tuning water exchange on Gd-III poly(amino carboxylates) by modulation of steric crowding. *Dalton Transactions* **2005**, (16), 2713-2719.
91. Ruloff, R.; Toth, E.; Scopelliti, R.; Tripier, R.; Handel, H.; Merbach, A. E., Accelerating water exchange for Gd-III chelates by steric compression around the water binding site. *Chemical Communications* **2002**, (22), 2630-2631.

92. Ananta, J. S.; Godin, B.; Sethi, R.; Moriggi, L.; Liu, X.; Serda, R. E.; Krishnamurthy, R.; Muthupillai, R.; Bolskar, R. D.; Helm, L.; Ferrari, M.; Wilson, L. J.; Decuzzi, P., Geometrical confinement of gadolinium-based contrast agents in nanoporous particles enhances T-1 contrast. *Nature Nanotechnology* **2010**, *5* (11), 815-821.
93. Sethi, R.; Ananta, J. S.; Karmonik, C.; Zhong, M.; Fung, S. H.; Liu, X.; Li, K.; Ferrari, M.; Wilson, L. J.; Decuzzi, P., Enhanced MRI relaxivity of Gd³⁺-based contrast agents geometrically confined within porous nanoconstructs. *Contrast Media & Molecular Imaging* **2012**, *7* (6), 501-508.
94. Callewaert, M.; Roullin, V. G.; Cadiou, C.; Millart, E.; Van Gulik, L.; Andry, M. C.; Portefaix, C.; Hoeffel, C.; Laurent, S.; Vander Elst, L.; Muller, R.; Molinari, M.; Chuburu, F., Tuning the composition of biocompatible Gd nanohydrogels to achieve hypersensitive dual T-1/T-2 MRI contrast agents. *Journal of Materials Chemistry B* **2014**, *2* (37), 6397-6405.
95. Berezin, M. Y., *Nanotechnology for Biomedical Imaging and Diagnostics: From Nanoparticle Design to Clinical Applications*. Wiley: 2015.
96. Zhu, W.; Artemov, D., Biocompatible blood pool MRI contrast agents based on hyaluronan. *Contrast Media & Molecular Imaging* **2011**, *6* (2), 61-68.
97. Dash, M.; Chiellini, F.; Ottenbrite, R. M.; Chiellini, E., Chitosan-A versatile semi-synthetic polymer in biomedical applications. *Progress in Polymer Science* **2011**, *36* (8), 981-1014.
98. Ponsiglione, A. M.; Russo, M.; Netti, P. A.; Torino, E., Impact of biopolymer matrices on relaxometric properties of contrast agents. *Interface Focus* **2016**, *6* (6), 20160061 - 20160061.
99. Russo, M.; Bevilacqua, P.; Netti, P. A.; Torino, E., Commentary on "A Microfluidic Platform to Design Crosslinked Hyaluronic Acid Nanoparticles (cHANPs) for Enhanced MRI". *Molecular Imaging* **2017**, *16*.
100. Okada, S.; Mizukami, S.; Kikuchi, K., Switchable MRI contrast agents based on morphological changes of pH-responsive polymers. *Bioorganic & Medicinal Chemistry* **2012**, *20* (2), 769-774.
101. Vecchione, D.; Grimaldi, A.; Forte, E.; Bevilacqua, P.; Netti, P.; Torino, E., Hybrid Core-Shell (HyCoS) Nanoparticles produced by Complex Coacervation for Multimodal Applications. *Sci. Rep.* **2017**, *7*, 45121.
102. Vecchione, D.; Aiello, M.; Cavaliere, C.; Nicolai, E.; Netti, P. A.; Torino, E., Hybrid core shell nanoparticles entrapping Gd-DTPA and ¹⁸F-FDG for simultaneous PET/MRI acquisitions. *Nanomedicine* **2017**, *12* (18), 2223-2231.
103. Wood, M. L.; Hardy, P. A., Proton relaxation enhancement. *J. Magn. Reson. Imaging* **1993**, *3* (1), 149-156.
104. Li, Y.; Beija, M.; Laurent, S.; vander Elst, L.; Muller, R. N.; Duong, H. T. T.; Lowe, A. B.; Davis, T. P.; Boyer, C., Macromolecular Ligands for Gadolinium MRI Contrast Agents. *Macromolecules* **2012**, *45* (10), 4196-4204.

105. Courant, T.; Roullin, G. V.; Cadiou, C.; Callewaert, M.; Andry, M. C.; Portefaix, C.; Hoeffel, C.; de Goltstein, M. C.; Port, M.; Laurent, S.; Vander Elst, L.; Muller, R. N.; Molinari, M.; Chuburu, F., Biocompatible nanoparticles and gadolinium complexes for MRI applications. *Comptes Rendus Chimie* **2013**, *16* (6), 531-539.
106. Pasqui, D.; De Cagna, M.; Barbucci, R., Polysaccharide-Based Hydrogels: The Key Role of Water in Affecting Mechanical Properties. *Polymers* **2012**, *4* (3), 1517-1534.
107. Sierra-Martin, B.; Fernandez-Barbero, A., Multifunctional hybrid nanogels for theranostic applications. *Soft Matter* **2015**, *11* (42), 8205-8216.
108. Raemdonck, K.; Demeester, J.; De Smedt, S., Advanced nanogel engineering for drug delivery. *Soft Matter* **2009**, *5* (4), 707-715.
109. Pal, K.; Banthia, A. K.; Majumdar, D. K., Polymeric Hydrogels: Characterization and Biomedical Applications. *Designed Monomers and Polymers* **2009**, *12* (3), 197-220.
110. Davies, G.-L.; Kramberger, I.; Davis, J. J., Environmentally responsive MRI contrast agents. *Chemical Communications* **2013**, *49* (84), 9704-9721.
111. Panagopoulou, A.; Vazquez Molina, J.; Kyritsis, A.; Monleon Pradas, M.; Valles Lluch, A.; Gallego Ferrer, G.; Pissis, P., Glass Transition and Water Dynamics in Hyaluronic Acid Hydrogels. *Food Biophysics* **2013**, *8* (3), 192-202.
112. Vázquez, B.; San Roman, J.; Peniche, C.; Cohen, M. E., Polymeric hydrophilic hydrogels with flexible hydrophobic chains. Control of the hydration and interactions with water molecules. *Macromolecules* **1997**, *30* (26), 8440-8446.
113. Budkov, Y. A.; Kolesnikov, A.; Georgi, N.; Kiselev, M., A flexible polymer chain in a critical solvent: Coil or globule? *EPL (Europhysics Letters)* **2015**, *109* (3), 36005.
114. Flory, P. J., Thermodynamics of high polymer solutions. *The Journal of chemical physics* **1942**, *10* (1), 51-61.
115. Martinez, J. C.; Cobos, E. S.; Luque, I.; Murciano-Calles, J.; Ruiz-Sanz, J.; Iglesias-Bexiga, M., *Isothermal titration calorimetry: thermodynamic analysis of the binding thermograms of molecular recognition events by using equilibrium models*. INTECH Open Access Publisher: 2013.
116. Kabiri, M.; Unsworth, L. D., Application of Isothermal Titration Calorimetry for Characterizing Thermodynamic Parameters of Biomolecular Interactions: Peptide Self-Assembly and Protein Adsorption Case Studies. *Biomacromolecules* **2014**, *15* (10), 3463-3473.
117. Gouin, S.; Winnik, F. M., Quantitative assays of the amount of diethylenetriaminepentaacetic acid conjugated to water-soluble polymers using isothermal titration calorimetry and colorimetry. *Bioconjugate Chemistry* **2001**, *12* (3), 372-377.
118. Strain, S. M.; Fesik, S. W.; Armitage, I. M., Structure and metal-binding properties of lipopolysaccharides from heptoseless mutants of Escherichia coli studied by ¹³C and ³¹P nuclear magnetic resonance. *J. Biol. Chem.* **1983**, *258* (22), 13466-13477.

119. Prudencio, M.; Rohovec, J.; Peters, J. A.; Tocheva, E.; Boulanger, M. J.; Murphy, M. E.; Hupkes, H. J.; Kosters, W.; Impagliazzo, A.; Ubbink, M., A caged lanthanide complex as a paramagnetic shift agent for protein NMR. *Chemistry-A European Journal* **2004**, *10* (13), 3252-3260.
120. Yoshida, H.; Hatakeyama, T.; Hatakeyama, H., CHARACTERIZATION OF WATER IN POLYSACCHARIDE HYDROGELS BY DSC. *Journal of Thermal Analysis and Calorimetry* **1993**, *40* (2), 483-489.
121. Yoshida, H.; Hatakeyama, T.; Hatakeyama, H., EFFECT OF WATER ON THE MAIN CHAIN MOTION OF POLYSACCHARIDE HYDROGELS. *Acs Symposium Series* **1992**, *489*, 217-230.
122. Diao, Y.; Whaley, K. E.; Helgeson, M. E.; Woldeyes, M. A.; Doyle, P. S.; Myerson, A. S.; Hatton, T. A.; Trout, B. L., Gel-Induced Selective Crystallization of Polymorphs. *Journal of the American Chemical Society* **2012**, *134* (1), 673-684.
123. Shogbon, C. B.; Brousseau, J.-L.; Zhang, H.; Benicewicz, B. C.; Akpalu, Y. A., Determination of the molecular parameters and studies of the chain conformation of polybenzimidazole in DMAc/LiCl. *Macromolecules* **2006**, *39* (26), 9409-9418.
124. Tao, Z. Molecular Dynamics Simulation Study of PEO-based Polymer Electrolytes in Aqueous Solution. Vanderbilt University, 2008.
125. Teraoka, I., *Polymer solutions: an Introduction to Physical Properties*. 2002.
126. Shetye, S. P.; Godbole, A.; Bhilegaokar, S.; Gajare, P., Hydrogels: Introduction, Preparation, Characterization and Applications. *International Journal of Research Methodologies* **2015**, *1* (1).
127. Tondera, C.; Wieduwild, R.; Röder, E.; Werner, C.; Zhang, Y.; Pietzsch, J., In Vivo Examination of an Injectable Hydrogel System Crosslinked by Peptide–Oligosaccharide Interaction in Immunocompetent Nude Mice. *Advanced Functional Materials* **2017**, *27* (15).
128. Mikhailov, O. V., Molecular nanotechnologies of gelatin-immobilization using macrocyclic metal chelates. *Nano reviews* **2014**, *5*.
129. Riess, G., Micellization of block copolymers. *Progress in Polymer Science* **2003**, *28* (7), 1107-1170.
130. Pomogailo, A. D., Polymer-Immobilised Clusters of the Platinum Group Metals. *Platinum Metals Review* **1994**, *38* (2), 60-70.
131. Aime, S.; Frullano, L.; Crich, S. G., Compartmentalization of a gadolinium complex in the apoferritin cavity: A route to obtain high relaxivity contrast agents for magnetic resonance imaging. *Angewandte Chemie-International Edition* **2002**, *41* (6), 1017-+.
132. Vogler, E. A., Role of water in biomaterials. *Biomaterials Science, 2nd edn.* (Elsevier Academic Press, San Diego, 2004) pp **2004**, 59.
133. Průšová, A.; Šmejkalová, D.; Chytil, M.; Velebný, V.; Kučerík, J., An alternative DSC approach to study hydration of hyaluronan. *Carbohydrate polymers* **2010**, *82* (2), 498-503.

134. Ivanov, D.; Neamtu, A., MOLECULAR DYNAMICS EVALUATION OF HYALURONAN INTERACTIONS WITH DIMETHYLSILANEDIOL IN AQUEOUS SOLUTION. *Revue Roumaine De Chimie* **2013**, *58* (2-3), 229-238.
135. Guillaumie, F.; Furrer, P.; Felt-Baeyens, O.; Fuhlendorff, B. L.; Nymand, S.; Westh, P.; Gurny, R.; Schwach-Abdellaoui, K., Comparative studies of various hyaluronic acids produced by microbial fermentation for potential topical ophthalmic applications. *Journal of Biomedical Materials Research Part A* **2010**, *92A* (4), 1421-1430.
136. Velasco, D.; Tumarkin, E.; Kumacheva, E., Microfluidic Encapsulation of Cells in Polymer Microgels. *Small* **2012**, *8* (11), 1633-1642.
137. Peppas, N. A.; Huang, Y.; Torres-Lugo, M.; Ward, J. H.; Zhang, J., Physicochemical, foundations and structural design of hydrogels in medicine and biology. *Annual Review of Biomedical Engineering* **2000**, *2*, 9-29.
138. Johnson, D. L., Elastodynamics of gels. *The Journal of Chemical Physics* **1982**, *77* (3), 1531-1539.
139. Strom, A.; Larsson, A.; Okay, O., Preparation and physical properties of hyaluronic acid-based cryogels. *Journal of Applied Polymer Science* **2015**, *132* (29).
140. Utech, S.; Boccaccini, A. R., A review of hydrogel-based composites for biomedical applications: enhancement of hydrogel properties by addition of rigid inorganic fillers. *Journal of Materials Science* **2016**, *51* (1), 271-310.
141. Phinikaridou, A.; Andia, M. E.; Protti, A.; Indermuehle, A.; Shah, A.; Smith, A.; Warley, A.; Botnar, R. M., Noninvasive MRI Evaluation of Endothelial Permeability in Murine Atherosclerosis Using an Albumin-Binding Contrast Agent. *Circulation* **2012**, CIRCULATIONAHA.112.092098.
142. Laurent, T. C., The chemistry, biology and medical applications of hyaluronan and its derivatives - Introduction. *Chemistry, Biology and Medical Applications of Hyaluronan and Its Derivatives* **1998**, *72*, 1-2.
143. Sionkowska, A., Current research on the blends of natural and synthetic polymers as new biomaterials: Review. *Progress in Polymer Science* **2011**, *36* (9), 1254-1276.
144. Kogan, G.; Soltes, L.; Stern, R.; Gemeiner, P., Hyaluronic acid: a natural biopolymer with a broad range of biomedical and industrial applications. *Biotechnology Letters* **2007**, *29* (1), 17-25.
145. Schante, C. E.; Zuber, G.; Herlin, C.; Vandamme, T. F., Chemical modifications of hyaluronic acid for the synthesis of derivatives for a broad range of biomedical applications. *Carbohydrate Polymers* **2011**, *85* (3), 469-489.
146. Khunmanee, S.; Jeong, Y.; Park, H., Crosslinking method of hyaluronic-based hydrogel for biomedical applications. *Journal of Tissue Engineering* **2017**, *8*.
147. Sahiner, N.; Ja, X. Q., One-step synthesis of hyaluronic acid-based (sub)micron hydrogel particles: Process optimization and preliminary characterization. *Turkish Journal of Chemistry* **2008**, *32* (4), 397-409.

148. Laurent, T. C.; Fraser, J. R. E., HYALURONAN. *Faseb Journal* **1992**, *6* (7), 2397-2404.
149. Ahmed, E. M., Hydrogel: Preparation, characterization, and applications: A review. *Journal of Advanced Research* **2015**, *6* (2), 105-121.
150. Shimojo, A. A. M.; Pires, A. M. B.; Lichy, R.; Santana, M. H. A., The Performance of Crosslinking with Divinyl Sulfone as Controlled by the Interplay Between the Chemical Modification and Conformation of Hyaluronic Acid. *Journal of the Brazilian Chemical Society* **2015**, *26* (3), 506-512.
151. Ibrahim, S.; Kang, Q. K.; Ramamurthi, A., The impact of hyaluronic acid oligomer content on physical, mechanical, and biologic properties of divinyl sulfone-crosslinked hyaluronic acid hydrogels. *Journal of Biomedical Materials Research Part A* **2010**, *94A* (2), 355-370.
152. Collins, M. N.; Birkinshaw, C., Physical properties of crosslinked hyaluronic acid hydrogels. *Journal of Materials Science-Materials in Medicine* **2008**, *19* (11), 3335-3343.
153. Bibette, J.; Calderon, F. L.; Poulin, P., Emulsions: basic principles. *Reports on Progress in Physics* **1999**, *62* (6), 969-1033.
154. Oh, J. K.; Lee, D. I.; Park, J. M., Biopolymer-based microgels/nanogels for drug delivery applications. *Progress in Polymer Science* **2009**, *34* (12), 1261-1282.
155. Yun, Y. H.; Goetz, D. J.; Yellen, P.; Chen, W. L., Hyaluronan microspheres for sustained gene delivery and site-specific targeting. *Biomaterials* **2004**, *25* (1), 147-157.
156. Sahiner, N., Colloidal nanocomposite hydrogel particles. *Colloid and Polymer Science* **2007**, *285* (4), 413-421.
157. Maroda, M.; Bodnar, M.; Berko, S.; Bako, J.; Eroes, G.; Csanyi, E.; Szabo-Revesz, P.; Hartmann, J. F.; Kemeny, L.; Borbely, J., Preparation and investigation of a cross-linked hyaluronan nanoparticles system. *Carbohydrate Polymers* **2011**, *83* (3), 1322-1329.
158. Bodnar, M.; Daroczi, L.; Batta, G.; Bako, J.; Hartmann, J. F.; Borbely, J., Preparation and characterization of cross-linked hyaluronan nanoparticles. *Colloid and Polymer Science* **2009**, *287* (8), 991-1000.
159. Prata, J. E.; Barth, T. A.; Bencherif, S. A.; Washburn, N. R., Complex Fluids Based on Methacrylated Hyaluronic Acid. *Biomacromolecules* **2010**, *11* (3), 769-775.
160. Lee, H.; Mok, H.; Lee, S.; Oh, Y.-K.; Park, T. G., Target-specific intracellular delivery of siRNA using degradable hyaluronic acid nanogels. *Journal of Controlled Release* **2007**, *119* (2), 245-252.
161. Messenger, L.; Portecop, N.; Hachet, E.; Lapeyre, V.; Pignot-Paintrand, I.; Catargi, B.; Auzely-Velty, R.; Ravaine, V., Photochemical crosslinking of hyaluronic acid confined in nanoemulsions: towards nanogels with a controlled structure. *Journal of Materials Chemistry B* **2013**, *1* (27), 3369-3379.
162. Cho, H.-J.; Yoon, H. Y.; Koo, H.; Ko, S.-H.; Shim, J.-S.; Lee, J.-H.; Kim, K.; Kwon, I. C.; Kim, D.-D., Self-assembled nanoparticles based on hyaluronic acid-

- ceramide (HA-CE) and Pluronic (R) for tumor-targeted delivery of docetaxel. *Biomaterials* **2011**, *32* (29), 7181-7190.
163. Mu, C.-F.; Balakrishnan, P.; Cui, F.-D.; Yin, Y.-M.; Lee, Y.-B.; Choi, H.-G.; Yong, C. S.; Chung, S.-J.; Shim, C.-K.; Kim, D.-D., The effects of mixed MPEG-PLA/Pluronic (R) copolymer micelles on the bioavailability and multidrug resistance of docetaxel. *Biomaterials* **2010**, *31* (8), 2371-2379.
164. Fakhari, A.; Quang, P.; Thakkar, S. V.; Middaugh, C. R.; Berkland, C., Hyaluronic Acid Nanoparticles Titrate the Viscoelastic Properties of Viscosupplements. *Langmuir* **2013**, *29* (17), 5123-5131.
165. Boyken, J.; Frenzel, T.; Lohrke, J.; Jost, G.; Pietsch, H., Gadolinium Accumulation in the Deep Cerebellar Nuclei and Globus Pallidus After Exposure to Linear but Not Macrocyclic Gadolinium-Based Contrast Agents in a Retrospective Pig Study With High Similarity to Clinical Conditions. *Invest. Radiol.* **2018**, *53* (5), 278-285.
166. Jin, Y.-J.; Ubonvan, T.; Kim, D.-D., Hyaluronic acid in drug delivery systems. *Journal of Pharmaceutical Investigation* **2010**, *40* (suppl), 33-43.
167. Mengual, O.; Meunier, G.; Cayre, I.; Puech, K.; Snabre, P., TURBISCAN MA 2000: multiple light scattering measurement for concentrated emulsion and suspension instability analysis. *Talanta* **1999**, *50* (2), 445-456.
168. Balazs, E. A.; Leshchiner, A., Cross-linked gels of hyaluronic acid and products containing such gels. Google Patents: 1987.
169. Sahiner, N.; Jia, X., One-Step Synthesis of Hyaluronic Acid-Based (Sub) micron Hydrogel Particles: Process Optimization and Preliminary Characterization. *Turkish Journal of Chemistry* **2008**, *32* (4).
170. Collins, M. N.; Birkinshaw, C., Investigation of the swelling behavior of crosslinked hyaluronic acid films and hydrogels produced using homogeneous reactions. *Journal of Applied Polymer Science* **2008**, *109* (2), 923-931.
171. Quignard, F.; Di Renzo, F.; Guibal, E., From Natural Polysaccharides to Materials for Catalysis, Adsorption, and Remediation. *Carbohydrates in Sustainable Development I: Renewable Resources for Chemistry and Biotechnology* **2010**, *294*, 165-197.
172. Oh, E. J.; Kang, S.-W.; Kim, B.-S.; Jiang, G.; Cho, I. H.; Hahn, S. K., Control of the molecular degradation of hyaluronic acid hydrogels for tissue augmentation. *Journal of Biomedical Materials Research Part A* **2008**, *86A* (3), 685-693.
173. Jiang, W. G.; Sanders, A. J.; Katoh, M.; Ungefroren, H.; Gieseler, F.; Prince, M.; Thompson, S. K.; Zollo, M.; Spano, D.; Dhawan, P.; Sliva, D.; Subbarayan, P. R.; Sarkar, M.; Honoki, K.; Fujii, H.; Georgakilas, A. G.; Amedei, A.; Niccolai, E.; Amin, A.; Ashraf, S. S.; Ye, L.; Helferich, W. G.; Yang, X.; Boosani, C. S.; Guha, G.; Ciriolo, M. R.; Aquilano, K.; Chen, S.; Azmi, A. S.; Keith, W. N.; Bilsland, A.; Bhakta, D.; Halicka, D.; Nowsheen, S.; Pantano, F.; Santini, D., Tissue invasion and metastasis: Molecular, biological and clinical perspectives. *Seminars in Cancer Biology* **2015**, *35*, S244-S275.

174. Stella, G. M.; Senetta, R.; Cassenti, A.; Ronco, M.; Cassoni, P., Cancers of unknown primary origin: current perspectives and future therapeutic strategies. *Journal of Translational Medicine* **2012**, *10*.
175. Kircher, M. F.; Hricak, H.; Larson, S. M., Molecular imaging for personalized cancer care. *Molecular Oncology* **2012**, *6* (2), 182-195.
176. Frampas, E., Lymphoma: some basic concepts a radiologist should know. *Journal De Radiologie Diagnostique Et Interventionnelle* **2013**, *94* (2), 135-149.
177. Tian, Y. F.; Ahn, H.; Schneider, R. S.; Yang, S. N.; Roman-Gonzalez, L.; Melnick, A. M.; Cerchietti, L.; Singh, A., Integrin-specific hydrogels as adaptable tumor organoids for malignant B and T cells. *Biomaterials* **2015**, *73*, 110-119.
178. van Krieken, J. H., New developments in the pathology of malignant lymphoma: a review of the literature published from January to April 2017. *Journal of Hematopathology* **2017**, *10* (1), 25-33.
179. Johnson, S. A.; Kumar, A.; Matasar, M. J.; Schoder, H.; Rademaker, J., Imaging for Staging and Response Assessment in Lymphoma. *Radiology* **2015**, *276* (2), 322-337.
180. Li, Z.; Tan, S. R.; Li, S.; Shen, Q.; Wang, K. H., Cancer drug delivery in the nano era: An overview and perspectives (Review). *Oncology Reports* **2017**, *38* (2), 611-624.
181. Gallamini, A.; Borra, A., Role of PET in Lymphoma. *Current Treatment Options in Oncology* **2014**, *15* (2), 248-261.
182. Caravan, P., Strategies for increasing the sensitivity of gadolinium based MRI contrast agents. *Chemical Society Reviews* **2006**, *35* (6), 512-523.
183. Tardif, J.-C.; Lesage, F.; Harel, F.; Romeo, P.; Pressacco, J., Imaging Biomarkers in Atherosclerosis Trials. *Circulation-Cardiovascular Imaging* **2011**, *4* (3), 319-333.
184. Schmidt, G.; Dinter, D.; Reiser, M. F.; Schoenberg, S. O., The Uses and Limitations of Whole-Body Magnetic Resonance Imaging. *Deutsches Arzteblatt International* **2010**, *107* (22), 383-389.
185. Shen, Z. Q.; Nieh, M. P.; Li, Y., Decorating Nanoparticle Surface for Targeted Drug Delivery: Opportunities and Challenges. *Polymers* **2016**, *8* (3).
186. Kozłowska, D.; Biswas, S.; Fox, E. K.; Wu, B.; Bolster, F.; Edupuganti, O. P.; Torchilin, V.; Eustace, S.; Botta, M.; O'Kennedy, R.; Brougham, D. F., Gadolinium-loaded polychelating amphiphilic polymer as an enhanced MRI contrast agent for human multiple myeloma and non Hodgkin's lymphoma (human Burkitt's lymphoma). *Rsc Advances* **2014**, *4* (35), 18007-18016.
187. Knittelfelder, R.; Riemer, A. B.; Jensen-Jarolim, E., Mimotope vaccination - from allergy to cancer. *Expert Opinion on Biological Therapy* **2009**, *9* (4), 493-506.
188. Torino, E.; Auletta, L.; Vecchione, D.; Orlandella, F. M.; Salvatore, G.; Iaccino, E.; Fiorenza, D.; Grimaldi, A. M.; Sandomenico, A.; Albanese, S.; Sarnataro, D.; Gramanzini, M.; Palmieri, C.; Scala, G.; Quinto, I.; Netti, P. A.; Salvatore, M.; Greco, A., Multimodal imaging for a theranostic approach in a murine model of B-cell

lymphoma with engineered nanoparticles. *Nanomedicine-Nanotechnology Biology and Medicine* **2018**, *14* (2), 483-491.

189. Palmieri, C.; Falcone, C.; Iaccino, E.; Tuccillo, F. M.; Gaspari, M.; Trimboli, F.; De Laurentiis, A.; Luberto, L.; Pontoriero, M.; Pisano, A.; Vecchio, E.; Fierro, O.; Panico, M. R.; Larobina, M.; Gargiulo, S.; Costa, N.; Dal Piaz, F.; Schiavone, M.; Arra, C.; Giudice, A.; Palma, G.; Barbieri, A.; Quinto, I.; Scala, G., In vivo targeting and growth inhibition of the A20 murine B-cell lymphoma by an idiotype-specific peptide binder. *Blood* **2010**, *116* (2), 226-238.

190. Corbin, I. R.; Li, H.; Chen, J.; Lund-Katz, S.; Zhou, R.; Glickson, J. D.; Zheng, G., Low-density lipoprotein nanoparticles as magnetic resonance imaging contrast agents. *Neoplasia* **2006**, *8* (6), 488-498.

191. Martucci, N. M.; Migliaccio, N.; Ruggiero, I.; Albano, F.; Cali, G.; Romano, S.; Terracciano, M.; Rea, I.; Arcari, P.; Lamberti, A., Nanoparticle-based strategy for personalized B-cell lymphoma therapy. *International Journal of Nanomedicine* **2016**, *11*, 6089-6101.

192. Lloyd-Jones, D. M., Cardiovascular Risk Prediction Basic Concepts, Current Status, and Future Directions. *Circulation* **2010**, *121* (15), 1768-1777.

193. Falk, E., Pathogenesis of atherosclerosis. *Journal of the American College of Cardiology* **2006**, *47* (8), C7-C12.

194. Muntendam, P.; McCall, C.; Sanz, J.; Falk, E.; Fuster, V.; High Risk Plaque, I., The BioImage Study: Novel approaches to risk assessment in the primary prevention of atherosclerotic cardiovascular disease-study design and objectives. *American Heart Journal* **2010**, *160* (1), 49-U73.

195. Davies, J. R.; Rudd, J. H.; Weissberg, P. L., Molecular and metabolic imaging of atherosclerosis. *Journal of Nuclear Medicine* **2004**, *45* (11), 1898-1907.

196. Libby, P.; Ridker, P. M.; Hansson, G. K., Progress and challenges in translating the biology of atherosclerosis. *Nature* **2011**, *473* (7347), 317-325.

197. Moore, K. J.; Tabas, I., Macrophages in the Pathogenesis of Atherosclerosis. *Cell* **2011**, *145* (3), 341-355.

198. Saba, L.; Anzidei, M.; Marincola, B. C.; Piga, M.; Raz, E.; Bassareo, P. P.; Napoli, A.; Mannelli, L.; Catalano, C.; Wintermark, M., Imaging of the Carotid Artery Vulnerable Plaque. *Cardiovascular and Interventional Radiology* **2014**, *37* (3), 572-585.

199. Nahrendorf, M.; Jaffer, F. A.; Kelly, K. A.; Sosnovik, D. E.; Aikawa, E.; Libby, P.; Weissleder, R., Noninvasive vascular cell adhesion molecule-1 imaging identifies inflammatory activation of cells in atherosclerosis. *Circulation* **2006**, *114* (14), 1504-1511.

200. van Tilborg, G. A. F.; Vucic, E.; Strijkers, G. J.; Cormode, D. P.; Mani, V.; Skajaa, T.; Reutelingsperger, C. P. M.; Fayad, Z. A.; Mulder, W. J. M.; Nicolay, K., Annexin A5-Functionalized Bimodal Nanoparticles for MRI and Fluorescence Imaging of Atherosclerotic Plaques. *Bioconjugate Chemistry* **2010**, *21* (10), 1794-1803.

201. Briley-Saebo, K. C.; Cho, Y. S.; Shaw, P. X.; Ryu, S. K.; Mani, V.; Dickson, S.; Izadmehr, E.; Green, S.; Fayad, Z. A.; Tsimikas, S., Targeted Iron Oxide Particles for In

Vivo Magnetic Resonance Detection of Atherosclerotic Lesions With Antibodies Directed to Oxidation-Specific Epitopes. *Journal of the American College of Cardiology* **2011**, 57 (3), 337-347.

202. Mulder, W. J. M.; Strijkers, G. J.; Van Tilborg, G. A. F.; Cormode, D. P.; Fayad, Z. A.; Nicolay, K., Nanoparticulate Assemblies of Amphiphiles and Diagnostically Active Materials for Multimodality Imaging. *Accounts of Chemical Research* **2009**, 42 (7), 904-914.

203. Weissleder, R.; Nahrendorf, M.; Pittet, M. J., Imaging macrophages with nanoparticles. *Nature Materials* **2014**, 13 (2), 125-138.

204. Sanz, J.; Fayad, Z. A., Imaging of atherosclerotic cardiovascular disease. *Nature* **2008**, 451 (7181), 953-957.

205. Leuschner, F.; Nahrendorf, M., Molecular Imaging of Coronary Atherosclerosis and Myocardial Infarction Considerations for the Bench and Perspectives for the Clinic. *Circulation Research* **2011**, 108 (5), 593-606.

206. Briley-Saebo, K. C.; Mulder, W. J. M.; Mani, V.; Hyafil, F.; Amirbekian, V.; Aguinaldo, J. G. S.; Fisher, E. A.; Fayad, Z. A., Magnetic resonance imaging of vulnerable atherosclerotic plaques: Current imaging strategies and molecular imaging probes. *Journal of Magnetic Resonance Imaging* **2007**, 26 (3), 460-479.

207. Thorek, D. L. J.; Chen, A.; Czupryna, J.; Tsourkas, A., Superparamagnetic iron oxide nanoparticle probes for molecular imaging. *Annals of Biomedical Engineering* **2006**, 34 (1), 23-38.

208. Ma, H. L.; Xu, Y. F.; Qi, X. R.; Maitani, Y.; Nagai, T., Superparamagnetic iron oxide nanoparticles stabilized by alginate: Pharmacokinetics, tissue distribution, and applications in detecting liver cancers. *International Journal of Pharmaceutics* **2008**, 354 (1-2), 217-226.

209. Ruehm, S. G.; Corot, C.; Vogt, P.; Kolb, S.; Debatin, J. F., Magnetic resonance imaging of atherosclerotic plaque with ultrasmall superparamagnetic particles of iron oxide in hyperlipidemic rabbits. *Circulation* **2001**, 103 (3), 415-422.

210. Kooi, M. E.; Cappendijk, V. C.; Cleutjens, K.; Kessels, A. G. H.; Kitslaar, P.; Borgers, M.; Frederik, P. M.; Daemen, M.; van Engelshoven, J. M. A., Accumulation of ultrasmall superparamagnetic particles of iron oxide in human atherosclerotic plaques can be detected by in vivo magnetic resonance imaging. *Circulation* **2003**, 107 (19), 2453-2458.

211. Trivedi, R. A.; Mallawarachi, C.; U-King-Im, J.-M.; Graves, M. J.; Horsley, J.; Goddard, M. J.; Brown, A.; Wang, L.; Kirkpatrick, P. J.; Brown, J.; Gillard, J. H., Identifying inflamed carotid plaques using in vivo USPIO-enhanced MR imaging to label plaque macrophages. *Arteriosclerosis Thrombosis and Vascular Biology* **2006**, 26 (7), 1601-1606.

212. Tang, T. Y.; Howarth, S. P. S.; Miller, S. R.; Graves, M. J.; U-King-Im, J.-M.; Trivedi, R. A.; Li, Z. Y.; Walsh, S. R.; Brown, A. P.; Kirkpatrick, P. J.; Gaunt, M. E.; Gillard, J. H., Comparison of the inflammatory burden of truly asymptomatic carotid atheroma with atherosclerotic plaques contralateral to symptomatic carotid stenosis:

- an ultra small superparamagnetic iron oxide enhanced magnetic resonance study. *Journal of Neurology Neurosurgery and Psychiatry* **2007**, *78* (12), 1337-1343.
213. Tang, T. Y.; Muller, K. H.; Graves, M. J.; Li, Z. Y.; Walsh, S. R.; Young, V.; Sadat, U.; Howarth, S. P. S.; Gillard, J. H., Iron Oxide Particles for Atheroma Imaging. *Arteriosclerosis Thrombosis and Vascular Biology* **2009**, *29* (7), 1001-1008.
214. Smith, B. R.; Heverhagen, J.; Knopp, M.; Schmalbrock, P.; Shapiro, J.; Shiomi, M.; Moldovan, N. I.; Ferrari, M.; Lee, S. C., Localization to atherosclerotic plaque and biodistribution of biochemically derivatized superparamagnetic iron oxide nanoparticles (SPIONs) contrast particles for magnetic resonance imaging (MRI). *Biomedical Microdevices* **2007**, *9* (5), 719-727.
215. Kang, H. W.; Torres, D.; Wald, L.; Weissleder, R.; Bogdanov, A. A., Targeted imaging of human endothelial-specific marker in a model of adoptive cell transfer. *Laboratory Investigation* **2006**, *86* (6), 599-609.
216. Alam, S. R.; Stirrat, C.; Richards, J.; Mirsadraee, S.; Semple, S. I. K.; Tse, G.; Henriksen, P.; Newby, D. E., Vascular and plaque imaging with ultrasmall superparamagnetic particles of iron oxide. *Journal of Cardiovascular Magnetic Resonance* **2015**, *17*.
217. Srikar, R.; Upendran, A.; Kannan, R., Polymeric nanoparticles for molecular imaging. *Wiley Interdisciplinary Reviews-Nanomedicine and Nanobiotechnology* **2014**, *6* (3), 245-267.
218. Doiron, A. L.; Chu, K.; Ali, A.; Brannon-Peppas, L., Preparation and initial characterization of biodegradable particles containing gadolinium-DTPA contrast agent for enhanced MRI. *Proceedings of the National Academy of Sciences of the United States of America* **2008**, *105* (45), 17232-17237.
219. Zhang, Y.; Zhou, J.; Guo, D. J.; Ao, M.; Zheng, Y. Y.; Wang, Z. G., Preparation and characterization of gadolinium-loaded PLGA particles surface modified with RGDS for the detection of thrombus. *International Journal of Nanomedicine* **2013**, *8*, 3745-3756.
220. Lipinski, M. J.; Amirbekian, V.; Frias, J. C.; Aguinaldo, J. G. S.; Mani, V.; Briley-Saebo, K. C.; Fuster, V.; Fallon, J. T.; Fisher, E. A.; Fayad, Z. A., MRI to detect atherosclerosis with gadolinium-containing immunomicelles targeting the macrophage scavenger receptor. *Magnetic Resonance in Medicine* **2006**, *56* (3), 601-610.
221. Mulder, W. J. M.; Strijkers, G. J.; Briley-Saboe, K. C.; Frias, J. C.; Aguinaldo, J. G. S.; Vucic, E.; Amirbekian, V.; Tang, C.; Chin, P. T. K.; Nicolay, K.; Fayad, Z. A., Molecular imaging of macrophages in atherosclerotic plaques using bimodal PEG-micelles. *Magnetic Resonance in Medicine* **2007**, *58* (6), 1164-1170.
222. Briley-Saebo, K. C.; Shaw, P. X.; Mulder, W. J. M.; Choi, S.-H.; Vucic, E.; Aguinaldo, J. G. S.; Witztum, J. L.; Fuster, V.; Tsimikas, S.; Fayad, Z. A., Targeted molecular probes for imaging atherosclerotic lesions with magnetic resonance using antibodies that recognize oxidation-specific epitopes. *Circulation* **2008**, *117* (25), 3206-3215.

223. Briley-Saebo, K. C.; Nguyen, T. H.; Saeboe, A. M.; Volkova, E. R.; Wiesner, P.; Witztum, In Vivo Detection of Oxidation-Specific Epitopes in Atherosclerotic Lesions Using Biocompatible Manganese Molecular Magnetic Imaging Probes (vol 59, pg 616, 2012). *Journal of the American College of Cardiology* **2012**, *59* (11), 1043-1043.
224. Maiseyeu, A.; Mihai, G.; Kampfrath, T.; Simonetti, O. P.; Sen, C. K.; Roy, S.; Rajagopalan, S.; Parthasarathy, S., Gadolinium-containing phosphatidylserine liposomes for molecular imaging of atherosclerosis. *Journal of Lipid Research* **2009**, *50* (11), 2157-2163.
225. Rensen, P. C. N.; Gras, J. C. E.; Lindfors, E. K.; van Dijk, K. W.; Jukema, J. W.; van Berkel, T. J. C.; Biessen, E. A. L., Selective targeting of liposomes to macrophages using a ligand with high affinity for the macrophage scavenger receptor class A. *Current drug discovery technologies* **2006**, *3* (2), 135-44.
226. Mulder, W. J. M.; Douma, K.; Koning, G. A.; Van Zandvoort, M. A.; Lutgens, E.; Daemen, M. J.; Nicolay, K.; Strijkers, G. J., Liposome-enhanced MRI of neointimal lesions in the ApoE-KO mouse. *Magnetic Resonance in Medicine* **2006**, *55* (5), 1170-1174.
227. Severson, S.; Tomalia, D. A., Dendrimers in biomedical applications- reflections on the field. *Advanced Drug Delivery Reviews* **2012**, *64*, 102-115.
228. Yu, M. M.; Jie, X.; Xu, L.; Chen, C.; Shen, W. L.; Cao, Y. N.; Lian, G.; Qi, R., Recent Advances in Dendrimer Research for Cardiovascular Diseases. *Biomacromolecules* **2015**, *16* (9), 2588-2598.
229. Abbasi, E.; Aval, S. F.; Akbarzadeh, A.; Milani, M.; Nasrabadi, H. T.; Joo, S. W.; Hanifehpour, Y.; Nejati-Koshki, K.; Pashaei-Asl, R., Dendrimers: synthesis, applications, and properties. *Nanoscale Research Letters* **2014**, *9*.
230. Hegde, A. R.; Rewatkar, P. V.; Manikkath, J.; Tupally, K.; Parekh, H. S.; Mutalik, S., Peptide dendrimer-conjugates of ketoprofen: Synthesis and ex vivo and in vivo evaluations of passive diffusion, sonophoresis and iontophoresis for skin delivery. *European Journal of Pharmaceutical Sciences* **2017**, *102*, 237-249.
231. Kobayashi, H.; Brechbiel, M. W., Dendrimer-based macromolecular MRI contrast agents: characteristics and application. *Molecular imaging* **2003**, *2* (1), 1-10.
232. Nguyen, T. H.; Bryant, H.; Shapsa, A.; Street, H.; Mani, V.; Fayad, Z. A.; Frank, J. A.; Tsimikas, S.; Briley-Saebo, K. C., Manganese G8 Dendrimers Targeted to Oxidation-Specific Epitopes: In Vivo MR Imaging of Atherosclerosis. *Journal of Magnetic Resonance Imaging* **2015**, *41* (3), 797-805.

Publications along three years

- Chapter

*Enza Torino, Franca De Sarno, Alfonso Maria Ponsiglione. **Bioinspired Materials for Diagnostic Imaging Applications**. Advances in Polymers for Biomedical Applications. ISBN: 978-1-53613-613-5.*

- Abstract

*Franca De Sarno, Anna Maria Grimaldi, Alfonso Maria Ponsiglione, Paolo Antonio Netti, Enza Torino. **Polymer nanostructures based on Hydrodenticity for boosted T 1 relaxivity**. 5th International Conference on Nanotechnology in Medicine (NANOMED 2018), 26-28 June, Manchester, UK.*

*Franca De Sarno, Alfonso Maria Ponsiglione, Enza Torino. **Gadolinium-Based Polymer Nanostructures as Magnetic Resonance Imaging Contrast Agents**. 20th International Conference on Nanomedicine and Nanoscience (ICNN 2018), 3-4 May, Rome, Italy. urn:dai:10.1999/1307-6892/92403*

*Franca De Sarno, Paolo Antonio Netti, Enza Torino **Nanoparticulate Probes for Molecular MRI of Atherosclerosis**. V CONGRESSO GRUPPO NAZIONALE DI BIOINGEGNERIA(GNB 2016), 20-22 June, Naples, Italy.*

- Papers:

*Franca De Sarno, Alfonso Maria Ponsiglione, Enza Torino. **Emerging Use of Nanoparticles in Diagnosis of Atherosclerosis Disease: A Review**. AIP Conference Proceedings (2018).*

*Franca De Sarno, Alfonso Maria Ponsiglione, Anna Maria Grimaldi, Ernesto Forte, Paolo Antonio Netti, Enza Torino. **Water-mediated nanostructures for enhanced MRI: impact of water dynamics on relaxometric properties of Gd-DTPA.** Under submission*

*Franca De Sarno, Alfonso Maria Ponsiglione, Anna Maria Grimaldi, Paolo Antonio Netti, Enza Torino. **Effect of crosslinking agent to design nanostructured hydrogels with improved relaxometric properties.** Under submission*

Communications to Congress/Conferences:

- Poster

*Franca De Sarno, Anna Maria Grimaldi, Alfonso Maria Ponsiglione, Paolo Antonio Netti, Enza Torino. **Polymer nanostructures based on Hydrodenticity for boosted T1 relaxivity.** 5th International Conference on Nanotechnology in Medicine (NANOMED 2018), 26-28 June, Manchester, UK.*

*Yogita Patil-Senl, Vikesh Chhabria, Waqar Ahmed, Tim Mercer, Alfonso Maria Ponsiglione, Franca De Sarno, Enza Torino. **Lipid coated Magnetic Nanoparticles for Targeted Drug Delivery and Hyperthermia.** 3th International Symposium on Nanoparticles/Nanomaterials and Applications (ISN²A 2018), 22-25 January, Caparica, Portugal.*

*Enza Torino, Paolo, Bevilacqua, Franca De Sarno, Ernesto Forte, Anna Maria Grimaldi, Alfonso Maria Ponsiglione, Eugenia Romano, Maria Russo, Donatella Vecchione, Paolo Antonio Netti. **Design of Nanostructures to Improve Properties of Paramagnetic Contrast Agents.** IV International Conference on Nanotechnology in Medicine 7-9 November 2016 Warsaw, Poland.*

*Franca De Sarno, Paolo Antonio Netti, Enza Torino. **Design of nanoparticle probe for MRI detection of atherosclerotic plaque.** V Congresso Gruppo Nazionale di Bioingegneria (GNB 2016), 20-22 June, Naples, Italy.*

- Oral Presentation

*Franca De Sarno, Alfonso Maria Ponsiglione, Enza Torino. **Gadolinium-Based Polymer Nanostructures as Magnetic Resonance Imaging Contrast Agents.** 20th International Conference on Nanomedicine and Nanoscience (ICNN 2018), 3-4 May, Rome, Italy.*

Project Activities

This Research activity has been developed in the framework of the project:

- *“CeSMeMo – PONA3_00173”. This Project focuses on the development of biomedical products, in particular nanosystems for diagnostics and therapy.*

Collaborations

- ***IRCCS SDN** Gianturco Street, 113, 80143, Naples*

SDN, Diagnostics and Nuclear Research Institute, is an integrated group of specialist clinics in diagnostic laboratory and imaging. In vivo MRI analysis are performed in this Diagnostic Center.

Other Activities

- *Award at StartCup Campania with the project “**POP-up**”, 13th October 2017, Naples, Italy.*
- *Premio Nazionale Innovazione (PNI 2017) with the project “**POP-up**”, 12 30th November – 1th December, Naples, Italy*
- *Best Practice with the project “**POP-up**”, 12 – 13th December, Salerno, Italy*

***POP-up** is an entrepreneurial initiative aimed at the production and distribution of a medical device for the Pelvic Organ Prolapse (**POP**) in women. **POP** is a disease that seriously compromises the quality of life of patients and currently the applied therapy is of a surgical type through the insertion of polypropylene mesh, with not always favorable results. The **device**, patented in 2014, is designed for postoperative use and can also be used as urodynamic test prior to surgery to improve clinical outcomes.*